

Hybrid Deflection Prediction for Machining Thin-Wall Titanium Alloy Aerospace Component

A thesis submitted in fulfillment of the requirements for
the award of Doctor of Philosophy

RAJA IZAMSHAH RAJA ABDULLAH

B. Eng., M.Eng.

School of Aerospace, Mechanical and Manufacturing Engineering
RMIT University
August 2011

Declaration

I certify that except where due acknowledgement has been made, the work is that of the author alone; the work has not been submitted previously, in whole or in part, to qualify for any other academic award; the content of the thesis is the result of work which has been carried out since the official commencement date of the approved research program; and, any editorial work, paid or unpaid, carried out by a third party is acknowledged.



Raja Izamshah

20 August 2011

Acknowledgements

Alhamdulillah, all praises to Allah for the strengths and His blessing in completing this thesis. I would like to thank my supervisor Professor John Mo for his steady guidance and tireless dedication. His invaluable input has helped to significantly elevate the quality of this work. I would also like to thank Dr. Songlin Ding for sharing his insight and expertise.

I would like to express my appreciation to my sponsors Universiti Teknikal Malaysia Melaka and Malaysian government.

I greatly appreciated Production Parts Pty. Ltd. Australia for the technical support and materials used in this work. The support of RMIT University technical staffs is also greatly appreciated.

I am most thankful to my wife and daughter, Sarinah and Raja Nurafiqah, for their love, sacrifice, continuous support and understanding during the course of this study. Finally, I would like to thank both of my parents Raja Abdullah and Salmah for their endless love.

Table of Contents

Acknowledgements	iii	
Table of Contents	iv	
List of Figures	ix	
List of Tables	xiii	
Nomenclature	xv	
Abstract	1	
Chapter 1	Introduction	3
1.1	Background	4
1.2	Challenges in Machining Thin-Wall Component	6
1.3	Current Practice in Machining Thin-Wall Component	7
1.4	Research Objectives	9
1.5	Thesis Organisation	10
Chapter 2	Literature Review	13
2.1	Introduction	14
2.2	Definition of Thin-Wall Component	14
2.3	Reviews on Related Work in Machining Thin-Wall Component	15

2.4	Factors Affecting the Magnitude of Wall Deflection	18
2.5	Consideration in Machining Titanium Alloys	21
Chapter 3	Preliminary Investigation on FE Analysis for Modelling	
	Part Deflection in Machining Thin-Wall Component	25
3.1	Introduction	26
3.2	Modelling On DEFORM-3D	29
3.2.1	Mesh Types	31
3.2.2	Failure Criterion	32
3.2.3	Geometry and Mesh	33
3.2.4	Material Properties	36
3.2.5	Boundary Conditions	37
3.2.6	Contact Conditions	39
3.3	Simulations	40
3.3.1	Simulation Parameter	41
3.3.2	Simulation Results	42
3.3.3	Simulation Computational Performance	45
3.3.4	Overall Assessment on Preliminary Investigation with DEFORM-3D	46
3.4	Summary	47
Chapter 4	Overview of the Hybrid Analysis Model	48
4.1	Introduction	49

4.2	Objective of Hybrid Model	49
4.3	Modelling and Simulation System Architecture	50
4.3.1	Machining Load Computational Model	53
4.3.2	Feature Based Geometry Model	55
4.3.3	Material Removal Model	59
4.3.4	Deflection Analysis Model	62
4.3.5	Multiple Regression Analysis Model	64
4.4	Break Down Of Monolithic Component into Standard Features	67
4.5	Cutter Compensation Strategy	70
4.6	Summary	70
Chapter 5	Cutting Forces Prediction for Helical Endmill Tool	72
5.1	Introduction	73
5.2	Mechanistic Modelling of Milling Forces	74
5.3	Determination of Cutting Force Coefficients	79
5.4	Experimental Cutting Force Coefficients	81
5.5	Comparison Between Predicted and Experiment Cutting Forces	83
5.6	Summary	87
Chapter 6	Modelling Part Deflection for Thin-Wall Machining	89
6.1	Introduction	90
6.2	Finite Element Formulation for Deflection Analysis	91

6.3	FEM Solution Procedure	93
6.4	Part Deflection Validation	96
6.4.1	Case 1: T-Shape Component	98
6.4.2	Case 2: L-Shape Component	101
6.4.3	Case 3: Rectangular Pocket Component	104
6.4.4	Case 4: Circular Component	108
6.5	Summary	111
Chapter 7	Multiple Regression Analysis Model	113
7.1	Introduction	114
7.2	Multiple Regression Analysis Model Building	115
7.3	Determination of Multiple Regression Analysis Model for Deflection Prediction	118
7.3.1	Case 1: T-Shape Component	120
7.3.2	Case 2: L-Shape Component	123
7.3.3	Case 3: Rectangular Pocket Component	126
7.3.4	Case 4: Circular Component	130
7.4	Summary	133
Chapter 8	Tool Path Compensation Based On Wall Deflection	134
8.1	Introduction	135
8.2	Mirror Cutter Compensation Method	135

8.3	Cutter Compensation Validation	137
8.4	Summary	141
Chapter 9	Concluding Remarks	143
9.1	Research Contribution	144
9.2	Recommendations for Future Work	147
	Publications	148
	References	150
	Appendix	183
	Appendix I	183

List of Figures

- Figure 1.1: Dimensional surface errors produce in machining thin-wall feature.
- Figure 1.2: Different techniques of step machining approach use in milling thin-wall feature.
- Figure 3.1: CATIA CAD models for endmill and workpiece.
- Figure 3.2: Tetrahedral mesh element constructed for the endmill.
- Figure 3.3: Tetrahedral mesh element constructed for the workpiece shows a high resolution mesh at the machining area.
- Figure 3.4: Initial start condition shows the endmill position with reference to axial and radial depth of cut.
- Figure 3.5: Master and slave object definition for contact conditions in machining simulation.
- Figure 3.6: DEFORM-3D simulation window shows (a) the initial start simulation, Step-1. (b) Chip temperature distribution during the simulation at Step-245.
- Figure 3.7: DEFORM-3D window shows the effective stress and strain values during the simulation at Step-255 and Step-439.
- Figure 3.8: DEFORM-3D window shows the part deflection due to the cutting forces generated between cutting tool and workpiece.
- Figure 3.9: Comparison of part deflection between simulation and experiment for Run-1 shows the maximum values of part deflection occurred at the middle of the wall.
- Figure 4.1: Modelling and simulation system architecture.
- Figure 4.2: Machining loads model.
- Figure 4.3: MATLAB GUI interface sample window for machining loads calculation.
- Figure 4.4: Feature based geometry model

- Figure 4.5: Contextual constraints definition for solid feature generation for T-Shape component geometries.
- Figure 4.6: Sample window shows the GUI input alphanumeric information for T-Shape component geometries.
- Figure 4.7: Material removal model.
- Figure 4.8: Contextual horizontal and vertical constraints for tool diameter, radial and axial depth of cut for the starting cutter location for T-Shape Component.
- Figure 4.9: Cutter profile transformation for modelling the material removal process for T-Shape Component.
- Figure 4.10: Interactive graphical user interface for material removal model parameter for T-Shape Component.
- Figure 4.11: Deflection analysis model.
- Figure 4.12: Transient surface at pre-defined cutting position.
- Figure 4.13: Sample window shows the deflection analysis for T-Shape component geometries.
- Figure 4.14: Multiple regression model.
- Figure 4.15: A generalized unit-element of component features in the aerospace monolithic component.
- Figure 4.16: Sample window shows the developed GUI in CATIA for analysis input graphic information for different type of thin-wall components.
- Figure 4.17: Sample window shows the GUI input alphanumeric information of part creation for different type of thin-wall components as in Section 4.3.2.
- Figure 4.18: Sample window shows the GUI input alphanumeric information of material removal process for different type of thin-wall components as in Section 4.3.3.
- Figure 5.1: Differential milling forces applied on an end mill.
- Figure 5.2: Delay cause by the helical end mill geometry on the cutting edge.
- Figure 5.3: Helical endmill cutting zone contact cases.

- Figure 5.4: Relation between feed per tooth and mean force per revolution for slotting condition.
- Figure 5.5: Comparison between predicted and experimental cutting forces. (Material: Ti6Al4V, 25% immersion up-milling, $ft = 0.06$ mm/tooth, ADOC = 10 mm, $S = 3500$ rpm; tool: 4 flute carbide end mill, $d = 6$ mm)
- Figure 5.6: Comparison between predicted and experimental cutting forces. (Material: Ti6Al4V, 50% immersion up-milling, $ft = 0.06$ mm/tooth, ADOC = 10 mm, $S = 3500$ rpm; tool: 4 flute carbide end mill, $d = 6$ mm)
- Figure 5.7: Comparison between predicted and experimental cutting forces. (Material: Ti6Al4V, 75% immersion up-milling, $ft = 0.04$ mm/tooth, ADOC = 10 mm, $S = 3500$ rpm; tool: 4 flute carbide end mill, $d = 6$ mm)
- Figure 5.8: Comparison between predicted and experimental cutting forces. (Material: Ti6Al4V, 25% immersion down-milling, $ft = 0.06$ mm/tooth, ADOC = 10 mm, $S = 3500$ rpm; tool: 4 flute carbide end mill, $d = 6$ mm)
- Figure 5.9: Comparison between predicted and experimental cutting forces. (Material: Ti6Al4V, 50% immersion down-milling, $ft = 0.06$ mm/tooth, ADOC = 10 mm, $S = 3500$ rpm; tool: 4 flute carbide end mill, $d = 6$ mm)
- Figure 5.10: Comparison between predicted and experimental cutting forces. (Material: Ti6Al4V, 75% immersion down-milling, $ft = 0.04$ mm/tooth, ADOC = 10 mm, $S = 3500$ rpm; tool: 4 flute carbide end mill, $d = 6$ mm)
- Figure 6.1: The pre-defined material removal part file from the material removal model.
- Figure 6.2: OCTREE 3D isoparametric-parabolic tetrahedron mesh associate with the component.
- Figure 6.3: Boundary condition assign to the bottom surface of the component.
- Figure 6.4: Calculated cutting forces from the machining loads model are call and places on the relevant nodes in the transient surface of the component.
- Figure 6.5: Sample window shows the FEA results of the displacement values.
- Figure 6.6: Experimental set-up for model validation.

- Figure 6.7: A sample window of displacement values for the five sensors between simulation and experiment for the T-Shape component. Machining parameter: $S = 3500$ rpm, $ft = 0.05$ mm/tooth, $rdoc = 0.4$ mm. Component attribute: $a = 2.5$ mm, $cI = 20$ mm and $x = 120$ mm.
- Figure 6.8: Deflection analysis result for T-Shape component at the middle of cutter feed location.
- Figure 6.9: A sample window of displacement values for the five sensors between simulation and experiment for the L-Shape component. Machining parameter: $S = 3500$ rpm, $ft = 0.05$ mm/tooth, $rdoc = 0.4$ mm. Component attribute: $a = 2.5$ mm, $cI = 20$ mm and $x = 120$ mm.
- Figure 6.10: Deflection analysis result for L-Shape component at the middle of cutter feed location.
- Figure 6.11: A sample window of displacement values for the five sensors between simulation and experiment for the rectangular pocket component. Machining parameter: $S = 3500$ rpm, $ft = 0.05$ mm/tooth, $rdoc = 0.4$ mm. Component attribute: $a = 2.5$ mm, $cI = 20$ mm and $x = 120$ mm.
- Figure 6.12: Deflection analysis result for the rectangular pocket component at the middle of cutter feed location.
- Figure 6.13: A sample window of displacement values for the five sensors between simulation and experiment for the circular component. Machining parameter: $S = 3500$ rpm, $ft = 0.05$ mm/tooth, $rdoc = 0.4$ mm. Component attribute: $a = 2.5$ mm, $cI = 20$ mm and $\theta = 120$ degree.
- Figure 6.14: Deflection analysis result for the circular component at the middle of cutter feed location.
- Figure 7.1: Normal probability and residual plot for T-shape component.
- Figure 7.2: Normal probability and residual plot for L-shape component.
- Figure 7.3: Normal probability and residual plot for rectangular pocket component.
- Figure 7.4: Normal probability and residual plot for circular component.
- Figure 8.1: Effects of machining surface on cutter path.
- Figure 8.2: Cutter compensation method.

Figure 8.3: Surface error variation between compensated and uncompensated model for all the component cases.

List of Tables

- Table 1.1: Comparison between monolithic and conventional aircraft component.
- Table 3.1: Qualitative comparison between the three finite element software packages.
- Table 3.2: Details of machining parameters and workpiece attributes used in simulation and experiment.
- Table 3.3: DEFORM-3D simulation step and computing time for machining simulation.
- Table 5.1: Estimated cutting constants and edge constants for the milling force prediction.
- Table 5.2: Cutting parameter used for both prediction and experimental cutting force.
- Table 6.1: Cutting parameter and component attribute use in simulation and experiment for the T-Shape Component.
- Table 6.2: Cutting parameter and component attribute use in simulation and experiment for the L-Shape Component.
- Table 6.3: Cutting parameter and component attribute use in simulation and experiment for the rectangular pocket component.
- Table 6.4: Cutting parameter and component attribute use in simulation and experiment for the circular component.
- Table 7.1: Machining parameter and component attribute experimental layout for the prediction of wall deflection.
- Table 7.2: L_{27} orthogonal array experimental layout plan.
- Table 7.3: ANOVA analysis for the T-shape component.
- Table 7.4: The model coefficients for T-shape component.

- Table 7.5: ANOVA analysis for the L-Shape component.
- Table 7.6: The model coefficients for L-shape component.
- Table 7.7: ANOVA analysis for the rectangular pocket component.
- Table 7.8: The model coefficients for rectangular pocket component.
- Table 7.9: ANOVA analysis for the circular component.
- Table 7.10: The model coefficients for circular component.
- Table 7.10: The model coefficients for circular component.

Nomenclature

p	shorter length of two edges in the plate
h	plate thickness
δ	elastic deformation of the wall
T	allowed machining tolerance
$\delta_x, \delta_y, \delta_z$	nodal displacements
S	speed
F	feed rate
C	radial depth of cut
T	wall thickness
H	wall height
L	wall length
D	displacement
dF_t, dF_r	differential tangential and radial cutting force
K_{tc}, K_{rc}	specific cutting force coefficients for tangential and radial direction
K_{te}, K_{re}	specific edge cutting force coefficients for tangential and radial direction
ϕ	tool's immersion angle
R	cutter radius
h_j	chip thickness

f_t	feed per tooth
ψ	helix angle
$\phi(z)$	entry and exit angle for flute j at certain position in the axial direction, z
b	axial depth of cut
F_x, F_y	milling force in feed x and normal y direction
N_t	number of teeth on the cutter
{F}	vector of nodal forces for the structure
[K]	stiffness matrix
{d}	vector of nodal displacement
[B]	strain-displacement matrix
{ σ }	stress vector
[N]	matrix of shape functions
{P}	concentrated forces on the nodes
[E]	elasticity matrix
E	modulus of elasticity
ν	Poisson's ratio
β	coefficient
R^2	coefficient of determination
SS_{ERR}	sum of square of residuals
SS_{TOT}	total sum of square
$C_{initial}$	initial cutter location point
C_{comp}	compensated trajectory of cutter location

ABSTRACT

Machining of aerospace structural components involves several thin-wall rib and flange sections. These thin-wall sections are dictated by design consideration to meet required strength and weight constraints. These components are either forged or cast to the approximate final shape and the end milling process is used to finish machine the parts; or the component is machined from a solid block of material by end milling with roughing and finishing cuts. During machining, the cutting forces cause deflection of the thin-wall section, leading to dimensional form errors that cause the finished part to be out of specification. In this thesis, a new methodology for the prediction of wall deflection during machining thin-wall feature is presented. The new methodology aims to increase the efficiency on modelling the deflection prediction in machining thin-wall component. The prediction methodology is based on a combination of finite element method and statistical analysis. It consists of a feature based approach of parts creation, finite element analysis of material removal and statistical regression analysis of deflection associated with cutting parameters and component attributes. The model is developed to take into account the tool-work geometries on material removal process during machining process. Mathematical models are developed for the wall deflection correlated with cutting parameters and component attributes. The prediction values have been validated by machining tests on titanium alloys parts and show good agreement between simulation model and experimental data. In addition, the cutter compensation method derived from the deflection prediction values can be used to reduce the magnitude of surface error, thus improving the component accuracy for machining thin-wall feature. By adopting the cutter compensation method, only one machining pass is

required to machine the thin-wall feature compared to the current practice in step method which requires few machining passes. All results have been derived for four different cases of typical aerospace component, but it is shown that these results can be applicable for other component shape and materials. A customize computer program has been developed for the proposed model. The developed computer program is an integrated data exchanges between modules upon users input on the design information and machining parameter for automatically generate the solid model, material removal model and FEM analysis. The developed computer program has improved the analysis time and makes the task easier to perform. The proposed method is able to reduce the analysis time from weeks to hours.

CHAPTER 1

INTRODUCTION

1.1 Background

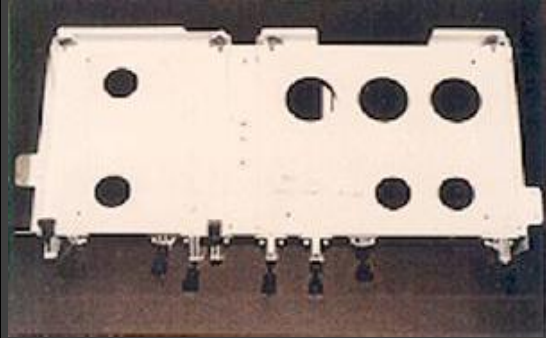

Demand for the next generation, cost effective, high performance aircrafts has motivating the aerospace industry to use non-traditional materials and new aircraft structural design [1]. Generally, most of the aerospace components are machined up to 95% from aluminium and titanium blocks [2]. Due to the low yield stress, aluminium alloys poses a good machinability rating compare to the titanium alloys which are difficult and need special technique for machining process. However, the intrinsic advantage of titanium alloys of better weight to strength ratio makes it more favourable in aerospace application compare to aluminium alloys.

New aircraft are design with one piece flow of monolithic component to replace large number of assembled component. This new monolithic structural components allows for higher quality and reduce the manufacturing times which impact business issues including inventory and Just-In-Time (JIT) manufacturing [3]. On the other hand, these monolithic structural components contains of thin-wall feature that poses some degree of machining technique to achieve the tight dimensional tolerance of aerospace component. Table 1.1 depicted some of the advantages of monolithic component compare to conventional aircraft component.

The milling process of thin-wall monolithic part is studied in this thesis. The project was initiated and collaborated by aerospace component manufacturer, Production Parts Pty. Ltd. The workpiece material is titanium alloys (Ti-6Al-4V) for all

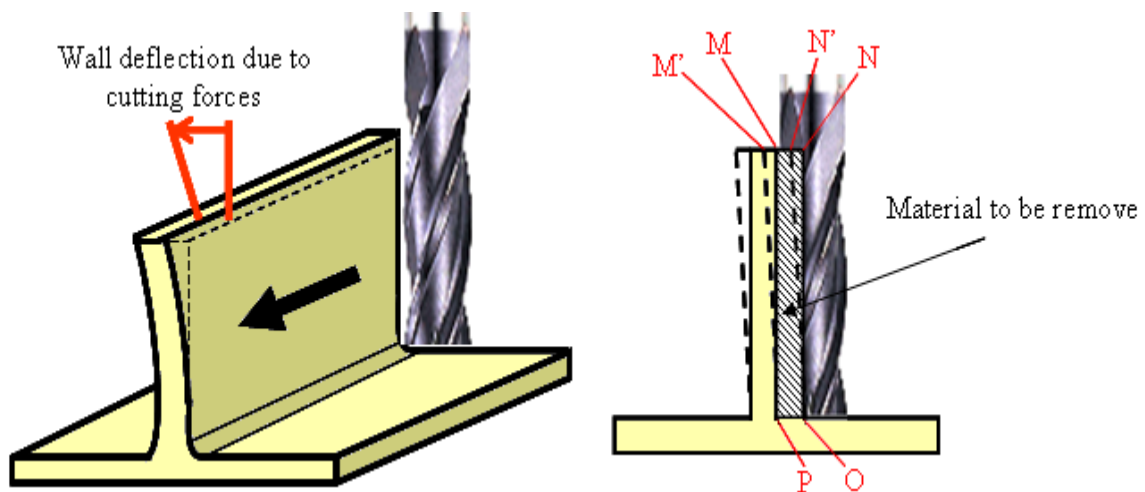
components. The milling process of very flexible component such that contain in monolithic structural components is generally used in aerospace industries. During milling process of this component, large volumes of materials are removed with the risk of instability and tolerance violation. Traditionally, trial-and-error approach is employed to obtain a consistent part shape which tends to lower productivity and raises machining costs.

Table 1.1: Comparison between monolithic and conventional aircraft component [4].

Conventional Part		Monolithic Part	
			
Number of Pieces	= 44	Number of Pieces	= 6
Number of Tools	= 53	Number of Tools	= 5
Design & Manufacturing Time (hrs)	= 965	Design & Manufacturing Time (hrs)	= 30
Machining Time (hrs)	= 13	Machining Time (hrs)	= 8.6
Assembly Man-hours	= 50	Assembly Man-hours	= 5.3
Weight (kg)	= 3.77	Weight (kg)	= 3.37
Overall manufacturing Cost (units)	= 100	Overall manufacturing Cost (units)	= 37

1.2 Challenges in Machining Thin-Wall Component

To remain competitive, manufacturer constantly seeks to improve their product quality by producing ‘right first time’ machined component. The tight dimensional tolerance of aerospace component poses a great challenge for the manufacturer especially for machining a component that contains a thin-wall feature. Because of the poor stiffness of thin-wall feature, deformation is more likely to occur in the machining of thin-wall part which resulting a dimensional surface errors [4, 5, 6]. Figure 1.1 shows the dimensional surface errors produce in machining thin-wall feature. Material in the shaded areas $MNOP$ as depicted in Figure 1.1 (b) is to be removed ideally. However, due to the milling force the wall is deflected which make point M moves to point M' as well as point N to point N' . As a result of the wall deflection, only material $MN'OP$ is removed resulting a dimensional surface errors in NON' areas.



(a) Deflection of wall resulting from cutting force.(b) Machining sketch of thin-wall component.

Figure 1.1: Dimensional surface errors produce in machining thin-wall feature.

1.3 Current Practice in Machining Thin-Wall Component

In current industry practice, the resulting surface errors are usually compensated through one or more of the following techniques: (i) using a repetitive feeding and final ‘float’ cut to bring the machined surface within tolerance; (ii) manual calibration to determine ‘tolerable’ machining conditions; (iii) a lengthy and expensive trial and error numerical control validation process [7]; and (iv) using a step machining approach, which alternately mills each side of the wall as shown in Figure 1.2 [8]. Distinctly all of these existing techniques on machining thin-wall features have a tendency to lower productivity and difficulty in ensuring the component accuracy. The difficulty in machining technique is worsened as the workpiece material is titanium alloys.

To overcome the disadvantages of current industry practice in machining thin-wall components, a finite element method is adopted to model the effect of processing parameters on surface error. There are numerous reports of work claiming the success of employing the finite element method using commercial finite element software for modelling the machining process. Once the surface error is predicted in advance by the finite element method, the surface error compensation strategy can be done. By using the finite element method for predicting the surface error produced in machining, it can eliminate the shop floor trials which are often very costly, time-consuming and labour-intensive [9]. However, the main issue involved in modelling the machining process with the finite element method is the long computational analysis time. Depending on the complexity of the problem, the computational analysis time can be varied up to days or even weeks. This is due to the nature of the FEM calculation which calculates the surface

errors for all over the workpiece at every feed step and every angular increment of cutter. This long computational analysis time limit its application for industry practice which must manufacture parts in a few days. Besides that, the limited design flexibility in FEM software requires transfer of model from other CAD software which can cause problems such as loss of data organization, translation inaccuracies, change in number of entities and excessive file size growth. Therefore, there exist an opportunity to improve the analysis efficiency and machining technique for thin-wall monolithic component in order to increase the part accuracy and productivity.

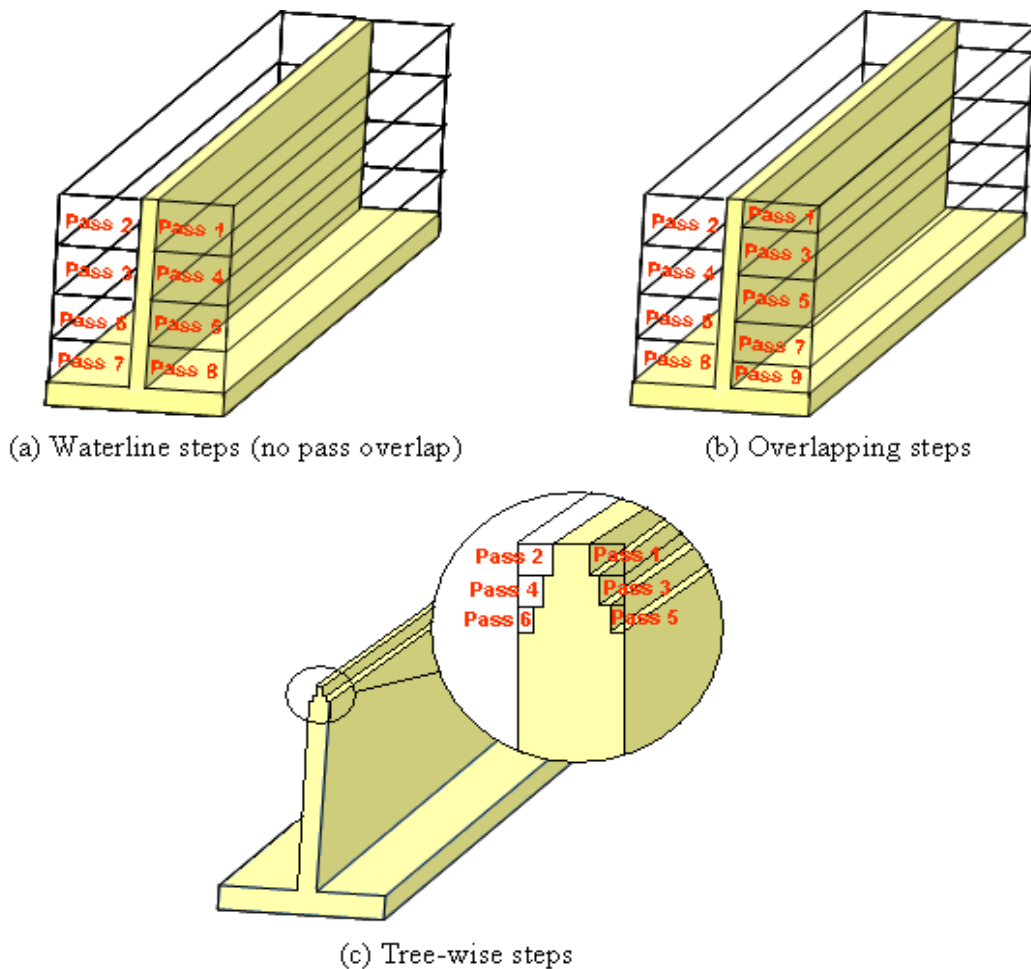


Figure 1.2: Different techniques of step machining approach use in milling thin-wall feature [8].

1.4 Research Objectives

Both the difficulty and the time-consuming nature of the analysis process and machining technique for machining thin-wall monolithic component were cause to initiate this project. The first objective of this thesis is to develop an efficient model for deflection prediction in machining titanium alloys thin-wall monolithic component. The model aims to increase the analysis efficiency from initial part creation to analysis result. In addition, to allow for the prediction of wall deflection that associate with component geometry and machining parameter a mathematical model is develop.

The second objective of this thesis is to apply the developed deflection prediction model for the cutter compensation machining technique. The cutter compensation method aims to increase the part accuracy and machining productivity such that only one machining pass is required to machine the thin-wall feature.

An in-house computer program is developed for the prediction model. Include in the prediction model are the effect of wall deflection on material removal process, the effect of wall deflection on machining parameters and the effect of wall deflection on component attributes. The objectives are achieved through numerical analysis, experiments, statistical analysis and computer programming.

1.5 Thesis Organisation

The chapters of the thesis are organised as follows:

In Chapter 2, the relevant literature on analysing the deflection prediction on machining thin-wall structures are reviewed. They include the existing methods and models for the analysis of machining thin-wall structure, force modelling and factors that affect the magnitude of the force generate in the machining process, factors that affect the magnitude of wall deflection, consideration and technique for machining titanium alloys. The purpose of reviewing these topics is to provide a theoretical base for the remainder of this thesis.

Preliminary scientific studies on technical capability of finite element software DEFORM-3D for modelling the deflection on machining thin-wall workpiece are presented in Chapter 3. Factors like software's capability in handling object geometries, range of material available in the database, its control over process parameters and simulation time were investigated. The study was made on the basis of the efficacy of the software for modelling the deflection on machining thin-wall workpiece and results obtained. Accuracy was checked directly by comparing the results with the experiment.

A methodology for the new hybrid model for deflection prediction on machining thin-wall workpiece is explained in Chapter 4. The hybrid model aims to resolve the disadvantages over the previous research work which includes the procedure from initial part creation to analysis result. The model is developed to take into account the

tool-work geometries on material removal process during the machining process. This chapter will first explain the hybrid model procedures followed by the theory of each model.

In Chapter 5 the mechanistic force model approach and the engagement limits for the helical tool endmill are presented. Then, experimental procedure for the determination of cutting force coefficients using the measure mean cutting force value will be explain. Lastly, the predicted cutting force are validate with the sets of experimental test.

The finite element formulation and procedure to perform the finite element analysis for prediction of wall deflection when machining thin-wall component are explained in Chapter 6. Then, the predicted wall deflections for each component case are validated with the sets of experimental test.

In Chapter 7 the statistical multiple regression analysis model for the deflection prediction are presented. This chapter will first explain the step in building the prediction model via the statistical multiple regression analysis. Then, the develop multiple regression analysis model is verified by confirming the statistical significance of the estimated parameters and the goodness of fit of the model using analysis of variance (ANOVA), coefficient of determination (R^2) and hypothesis testing.

The cutter compensation methods to reduce the surface error produced during machining the thin-wall feature are explain in Chapter 8. The cutter compensation

method is based on the adjustment of cutter path with respect to the magnitude of predicted wall deflection. This chapter will first explain the methodology and step involve for the cutter compensation method. Then, the develop cutter compensation method is verified with the set of experimental test for different case of component.

The thesis concludes with a summary of contributions and suggestions for future work in Chapter 9.

CHAPTER 2

LITERATURE REVIEW

2.1 Introduction

The study on machining of thin-wall component involves many disciplinary areas such as theories and methods of metal cutting, mechanics of machining process and structural mechanics. In this chapter, topics that analyse the deflection prediction on machining thin-wall structures are reviewed. They include the existing methods and models for the analysis of machining thin-wall structure, force modelling and factors that affect the magnitude of the force generated in the machining process, factors that affect the magnitude of wall deflection and consideration and technique for machining titanium alloys. The purpose of reviewing these topics is to provide a theoretical base for the remainder of this thesis.

2.2 Definition of Thin-Wall Component

There are few definitions to characterised thin-wall component. Fitzgerald [10] suggested a guide to differentiate between thin-wall and thick-wall cylinders based on the uniform stress distribution throughout the wall thickness. The theory of thin-wall cylinders and spheres is based on this assumption which indicates a ratio of wall thickness to diameter of about 1/10 represents the dividing line between thin-wall and thick-wall cylinders. Yang [11] gave a guide to differentiate between super-thin plates, thin plates and thick plates for approximation theory of plate bending as;

Super-thin plates	=	$h/p < (1/100)$
Thin plates	=	$(1/100) \leq h/p \leq (1/5)$
Thick plates	=	$h/p > (1/5)$

where p = shorter length of two edges in the plate

h = plate thickness

The above definitions of thin-wall component can be a general guide-line to characterised thin-wall component. However, for the case of this project the thin-wall component is based on whether or not the wall deflects sufficiently to affect machining accuracy. To be specific, a thin-wall component is where elastic deformation of the wall is larger than or equal to the allowed tolerance requirement and can be written as;

$$\delta \geq T$$

where δ = elastic deformation of the wall

T = allowed machining tolerance

2.3 Reviews on Related Work in Machining Thin-Wall Component

Very few research works have been reported in predicting the deformation of thin-wall parts. Budak and Altintas [12] used the beam theory to analyse the form errors

when milling using slender helical endmill for peripheral milling of a cantilever plate structure. The slender helical endmill is divided into a set of equal element to calculate the form errors acting by the cutting forces on both tool and the wall. They developed their own FE code to model the simple cantilever beam problem. Although the proposed beam theory for analysing the form errors provides accurate result, one of the arguments of this model is its ability to model a complex shape, such as an aerospace component. Later in their work [13], they proposed a feed rate scheduling strategy to reduce the surface errors produced in milling flexible workpiece. However, this approach tends to sacrifice the productivity as reducing the feed rate will increase the machining time.

Kline et al. [14] modelled the milling process of thin-wall rectangular plate element clamped on three edges taking the effects of a flexible endmill. The interaction between the milling forces and the structural deformation were neglected on his study. Therefore, their proposed model can only be applied for the case of relatively rigid workpiece. Sagherian et al. [15] improved Kline's model by including the dynamic milling forces and the regeneration mechanism. However, they did not consider the effect of workpiece deflection on the cutting geometry, i.e. the radial depth of cut. They also used a numerical force algorithm and the FE method to simulate cantilever plate displacement.

Later, Tsai and Liao [16] developed an iteration schemes to predict the cutting forces and form error on thin-wall rectangle plate. The cutting force distribution and the system deflections are solved iteratively by modified Newton-Raphson method. They made a few assumptions on the size of the element and their relationship with the

transient surface which restricted its applicability. Dynamic model for milling of low rigidity cantilever plate structure was proposed by Altintas et al. [17]. However, the model did not taken into account the changing of structural properties on the material removal process.

In a series of research works, Ratchev et al. [18, 19, 20, 21, 22, 23 and 24] proposed the modelling and simulation environment for machining low rigidity components. The proposed approach included a module for the integration between force, material removal and the workpiece deflection. However, no direct explanation on the frequency of the update model and the computational efficiency. The validation was performed for a simple cantilever plate and the part geometry is generated from CAD software and fed into a commercial FE package.

The effects of tool deflection on the varying chip thickness were proposed by Sutherland and DeVor [25]. Include in their model is the approximation of instantaneous uncut chip thickness that permit for the tool run-out. However, their proposed model can only be applied for the case of relatively rigid workpiece.

In the literatures, it shows that most of the method employed must calculate the surface errors for all over the workpiece for every feed step and every angular cutter increment. This result in low efficiency as it may take long computational analysis time to obtain the surface error at a certain feed step especially when considering the material removal action. In addition, the analysis is limited to relatively straightforward geometries i.e. simple cantilever plate, which does not represent the practical aerospace

component. Another problem encountered from the existing method, is most of the part geometry is generated from other CAD software and fed into a commercial FE package. The exchanging of data between different platforms can cause problems such as loss of data organization, translation inaccuracies, change in number of entities and excessive file size growth as been reported in [26, 27, 28, 29, 30 and 31].

2.4 Factors Affecting the Magnitude of Wall Deflection

It is important to investigate the factors that affecting the magnitude of wall deflection as it helps to determine which factor that needs to be included in the analysis. In general, the magnitude of wall deflection depends on its stiffness ability that governed by several factors such as cross-sectional size and shape, loading and material properties [32].

The workpiece attribute can be defined as the dimension of the wall thickness, length and height. Liu [33] investigate the effects by varying of each individual factor i.e. wall thickness, wall length and wall height on the elastic deformation of a rectangular plate. In his studies, he concludes that as the wall thickness reduce the magnitude of the deformation increased. In addition, the deformation magnitude of the wall will increase as the wall height increased. Beside that, in his studies he concludes that there is slight effect on the deformation magnitude with wall length. Ning et al. [34] proposed a quantitative analysis and calculation of the deformation of a typical thin-wall structure study. He analyse the effect of varying wall thickness for a rectangular box component. He concludes that the machining deformation is inverse proportional to the thickness of

wall and there is little effect on the deformation from reducing the wall thickness for other three side of the box. Large deflection analysis of axisymmetric circular plates was investigated by Ye [35]. His studies include the analysis with variable thickness using the boundary element method for the deflection at the central location of the plates. His studies show that there is a significant effect on the magnitude of the plate deflection with a variable thickness. Hosseini and Abbas [36] study the deformation of rectangular plates under wedge impact using neural network. Include in their prediction model are the set of parameter from component attributes. Their studies also conclude that there is a significant effect on the magnitude of the plate deflection with component attributes. Other relevant literatures in analysing the magnitude of deflection with the component attribute can be found in [37and 38].

Cutting force produce in the machining process is the dominant factor that contributes to the magnitude of the wall deflection as shown in [39 and 40]. Increasing the cutting forces value will increase the magnitude of wall deflection. Thus, modelling the accurate cutting force in milling is the key factor in predicting the magnitude of wall deflection. The modelling of cutting force in milling can be classified in two approaches namely mechanistic force model and mechanics force model. From literatures it shows that mechanistic force model gives an accurate milling force prediction compare to the mechanics force model. In mechanistic force model approach, the cutting forces are related to average chip thickness by cutting force coefficient calibrated experimentally for a particular workpiece material tool pair [41]. Then, the cutting forces produced by the same cutter with different machining parameters can be predicted analytically by using the calibrated force coefficient.

The cutting forces in the milling process are highly dependent with the machining parameter such as speed, feed rate, radial and depth of cut. William et al. [42] in his studies observed that by increasing the cutting speed will decrease the cutting force. He found that the cutting force dropped to 25–50 % by increasing the cutting speed for machining aluminium, iron and copper. Similar results in decreasing cutting force with increasing cutting speed were also obtained by Lin and Lo [43] and Lin and Yang [44]. Later, Turgut et al. [45] studies the effects of cutting force and surface roughness in milling of Al/Sic metal matrix composites. His studies include the effect of cutting speeds at (300, 350, 400 and 450 m/min), feed rates (0.1, 0.15, 0.20 mm/tooth) and depth of cut (0.5, 1 mm) on cutting forces. He concludes that for coated and uncoated tools, the cutting force increased with increasing feed rate and depth of cut whereas, it is decreased significantly by higher cutting speed. In other reported work, Thomas and Beauchamp [46] statistically analysed cutting force and tool vibration using samples at different speeds, feed rates, depth of cuts, tool lengths and workpiece lengths. Manna and Bhattacharayya [47] studied the machinability of Al/SiC material under different speeds, feed rates and depth of cuts. They both discovered that the cutting force increased with the increase of feed rate which shows that more power is needed to complete the cutting action.

From literatures, it shows that component attribute and cutting force is the critical factor to analyse the magnitude of wall deflection as it reflect the rigidity of the wall. In addition, from the literature it shown that the machining parameters, i.e. speeds, feed rates and depth of cuts are the critical factor for the calculation of the cutting force which redirect to the wall deflection. The cutting speed has a significant effect on the

specific power as the coefficient of friction on the cutter's tooth is speed dependent. By increasing the speed it will decrease the friction, thus decreasing the specific power through the frictional component as noted in [48]. Increasing the feed rate will increase the chip thickness, thus the tangential forces increase as forces are proportional to the chip area [49]. While radial and axial depths of cut affect the width and length of the contact area in the normal and tangential directions. Which, influences the forces directly as the deeper the radial or axial depths of cut, the more flutes will be engaged [50]. Besides that, materials properties are an important factor in determining the magnitude of wall deflection. Materials properties describe the material characteristics such as strength and resistance to the deformation. Materials with low modulus of elasticity tends to severe more deformations and vibrations during the milling of thin parts as shown in [51 and 52].

2.5 Consideration in Machining Titanium Alloys

The high strength, low in weight and outstanding corrosion resistance possessed by titanium alloys have led to a wide range of its applications in aerospace, automotive, medical, chemical plant, power generation, oil and gas extraction, sports, and other major industries. Due to the strong demands of titanium alloys usage, titanium alloys has greatly attracted many researchers. They were numerous of reported work found in the literature involving machining of titanium alloys in many areas. Development of cutting tool for economically machining titanium alloys can be found in [53, 54, 55, 56, 57 and 58], studies on the mechanics of chip formation when machining titanium alloys are reported in [59, 60, 61, 62, 63, 64 and 65], surface integrity and wear mechanism

when machining with titanium alloys are analysed in [66, 67, 68, 69, 70, 71 and 72], cutting forces and stress involved in machining with titanium alloys material are evaluate in [73, 74, 75, 76, 77, 78 and 79], high-speed machining technique to improve material removal rate for machining titanium alloys are investigated in [80, 81, 82, 83, 84, 85 and 86] and finite element simulation for modelling machining process with titanium alloys can be found in [87, 88, 89, 90, 91, 92, 93 and 94]. In addition, non-conventional techniques for machining titanium alloys are explained in [95, 96, 97, 98 and 99].

Generally, titanium alloys are categorised as the type of materials that is difficult to machine [100, 101, 102 and 103]. The machinability rating of titanium alloys is generally considered to be poor due to its several intrinsic metallurgical characteristics that required special technique for machining operation. Titanium alloys have low thermal conductivity and high chemical reactivity [104, 105, 106, 107 and 108]. Its low thermal conductivity increases the temperature at the tool/workpiece interface, which affects the tool life adversely. The chemically reactive of titanium tends to weld the tool during machining, thus leading to chipping and premature tool failure. The low in modulus of elasticity of titanium alloys cause deflection and chatter in the machining process. Even at the elevated temperatures, titanium retains its strength, and this suppresses the plastic deformation needed to form a chip [109]. The high stresses and high temperatures present at the tool/work-piece interface can cause significant surface damage to the titanium alloys [110 and 111]. Contamination and damage of the titanium workpiece via diffusion of tool material and atmospheric constituents can lead to degradation of mechanical properties, especially the fatigue strength [112 and 113].

Based on the problems and difficulties encountered in machining titanium alloys, a special consideration and technique are required to ensure successful result. From literature, there are few general rules for machining titanium alloys that can help in overcoming these factors [114, 115, 116, 117 and 118] such as;

- Low cutting speed is preferable to help to minimise the tool tip temperatures. Tool tip temperatures are greatly affected by cutting speed than by any other single variable. (A change from 20 to 150 sfpm with carbide tools results in a temperature change from about 800°F to 1700°F).
- Sharp cutting tools should be used and replace them at the first sign of wear. However, for titanium the tool wear is not linear. Complete tool failure occurs rather quickly after a small initial amount of wear takes place. A sharp cutting tool helps to minimize the heat build-up and galling.
- Maintain high feed rates consistent with good machining practice as temperature is not affected by feed rate. A change from 0.002 inch to 0.02 inch per revolution (a 10 fold increase) results in a temperature increase of only about 300°F. (Compare this to the temperature increase resulting from only a seven and one half fold increase in cutting speed of 900°F).
- Use rigid setups between tool and workpiece to counter workpiece flexure. The workpiece should be as short as possible and mounted to be vibration-free into the grips of the machine table.

- Never stop feeding when a tool and workpiece are in moving contact. Permitting a tool to dwell in a moving contact causes work hardening and promotes smearing, galling, seizing and total tool breakdown.
- Cutting fluid must be applied when machining titanium alloys. The correct use of coolants during machining operation greatly extends the life of cutting tool. Chemically active cutting fluids transfer heat efficiently and reduce the cutting forces between the tool and the workpiece.
- Hard surface scales should be removed before machining, either by grit blasting or picking in a solution of 2% hydrofluoric acid and 20% nitric acid.

CHAPTER 3

PRELIMINARY INVESTIGATION ON FINITE ELEMENT ANALYSIS FOR MODELLING PART DEFLECTION IN MACHINING THIN-WALL COMPONENT

3.1 Introduction

A reliable prediction on the performance and the influence of the process parameters on the product quality has increased the application of finite element method in modelling the metal forming process [119 and 120]. Finite element method has steadily increased its importance in simulation of manufacturing processes as the benefits of determining the effects of various process parameters on computer has decreased the shop floor trials which are often very costly, time consuming and labour intensive [121].

Based on the success of FEM simulations for bulk forming processes, many researchers developed their own FEM codes to analyze metal cutting processes (Marusich et al. [122 and 123]; Xie et al. [124]; Shet [125]; and Jawahir [126]). However, the non-commercial FEM codes are not designed for end users application and only suitable for particular analysis. In recent years, commercial FE packages such as DEFORM-3D (Ceretti et al. [127 and 128], Özel and Altan [129 and 130], Klocke et al. [131], Bareggi et al. [132]); ABAQUS/Explicit (Guo and Liu [132]; Guo and Liu [133 and 134]; Ng and Aspinwall [135]; Baker et al. [136]; Chuzhoy et al. [137 and 138]; Adibi-Sedeh and Madhavan, [139]; Arrazola et al. [140], and Mabrouki and Rigal [141]) and ADVANTEDGE (Otieno and Clifford [142], Rongdi and Jian [143], Marusich [144], K. Kadirgama et al. [145], Xiao et al. [146]) have been used excessively in both academic and industrial world for metal cutting process analysis. The choice of finite element software for metal cutting analysis is an important criterion in determining the quality and scope of analysis that can be performed as different FE

packages have different capabilities and solver techniques. Gardner et al. [147] made a qualitative comparison between the three finite element software packages (DEFORM-3D, ADVANTEDGE and ABAQUS) on their performances for modelling the machining processes. Some of the issues are highlighted and discussed in Table 3.1.

Table 3.1: Qualitative comparison between the three finite element software packages [147].

Qualitative Factor	ABAQUS	ADVANTEDGE	DEFORM-3D
General overview	General purpose finite element software, not designed for modelling machining analysis. The open-ended of the software present a steep learning curve.	This software designed specifically for modelling machining analysis, but poor solver control and limited flexibility in boundary conditions.	This software designed specifically for modelling machining analysis for three-dimensional (3D) flow of complex metal forming processes.
Simulation setup	This software requires significant time for model setup which requires a lengthy manual input of the simulation parameters.	Rapid simulation setup of the model. Limited flexibility makes it less suitable for specific manufacturing process such as modelling the workpiece deflections.	Requires reasonable amount of time for simulation setup. Good boundary conditions flexibility for modelling the specific manufacturing process.
Machining simulation	Manual design of workpiece and cutting tool. Manual mesh refinement and boundary condition.	Very efficient interface to rapidly configure a model, tool library are provided.	Built in 'machining modules' for easy setup of standard machining process.
Material library	No built in material library, however the materials properties can be define extensively.	Extensive material library.	Extensive material library and comprehensive material models editor.
Remeshing technique	Partial support in adaptive remeshing.	Full adaptive remeshing support. However no controls are allowed.	Full adaptive remeshing support and good controls of meshing parameters for high material deformations.
Solver control	Good control of the solver.	Not suitable for customising control functions.	Uses few solvers with limited control.

From Table 3.1 shows that DEFORM-3D offers a fast and easy setup as well as better control over the simulation process. The effort to model with ADVANTEDGE and ABAQUS was terminated early in this project when it became clear that the time investment for process setup would be significantly larger and unpractical than DEFORM-3D effort. Based on this justification, DEFORM-3D is chosen as the finite element software for the preliminary work to model the deflection in machining thin-wall workpiece. This chapter explains a preliminary scientific study on technical capability of finite element software DEFORM-3D for modelling the deflection on machining thin-wall workpiece. Factors like software's capability in handling object geometries, range of material available in the database, its control over process parameters and simulation time were investigated. The study was made on the basis of the efficacy of the software for modelling the deflection on machining thin-wall workpiece and results obtained. Accuracy was checked directly by comparing the results with the experiment.

3.2 Modelling On DEFORM-3D

DEFORM-3D is a Finite Element Method based system that can be applied to several metal forming processes such as forging, rolling and machining [148]. DEFORM-3D capable of simulating and analysing the three-dimensional (3D) complex flow of metal forming processes. The software has a specific machining module to quickly set up turning, milling, boring and drilling operations which make it a favourable software in both industrial and research area. DEFORM-3D is proved to be a practical and efficient tool to predict the material flow for metal forming operations that

decreased the shop floor trials which are often very costly, time consuming and labour intensive. In addition, the software is built as an 'open system' which offers working flexibility for a range of applications especially in the development and research to the designers and analysts. DEFORM-3D supports user routines and user defined variables.

DEFORM-3D uses the Automatic Mesh Generator (AMG) function generates an optimized mesh system with local element size. The main advantages of the AMG function is to enhanced resolution of part features that can maintain a good control of the overall problem size and computing requirements. In addition, a flexible user-defined control of local mesh density provides a better analysis to meet specific conditions. To resolve the large deformation involves in metal forming process, DEFORM-3D adapt an incremental Lagrangian formulation with an implicit integration method. For good convergence stability in simulation, sparse matrix with a direct integration method was used as a solver.

Application-specific GUIs (graphical user interface) provides for easy setup which simplifies the data input and post-processing. The GUIs is intuitive and provides a fast and easy set-up compare to other finite element packages. The software has an extensive built in material models for elastic, rigid-plastic, thermal elastoplastic, thermal rigid-viscoplastic, porous and rigid.

3.2.1 Mesh Types

Lagrangian mesh is used for the machining simulations in DEFORM-3D. The iterative solvers that are packaged with DEFORM-3D have been optimized for the Lagrangian mesh and, in turn, simulate much faster than other meshes. Although the Lagrangian mesh is not as comprehensive as the Eulerian mesh, however it proves to have much better simulation cycle times. The main advantage of the Lagrangian mesh in simulating milling processes is the ability to know the entire time history of the key variables at every point during the simulation. That means, if a simulation crashes for any reason, a new simulation can start where the crashed simulation stopped. This is particularly useful because nearly every simulation has some sort of problem during the run. This is possible because the Lagrangian mesh is reformulated at nearly every time step, in order to manage the deformation of the material.

One of the biggest strengths of DEFORM-3D is its ability to mesh complex geometries. Significant deformation occurs in machining simulations and this has been historically problematic for the Lagrangian mesh. However, if the geometry is remeshed after each time step, the Lagrangian mesh is a reasonable choice to show burr formation. DEFORM-3D is a leader in creating adaptive meshes and remeshing complex geometry and this makes it a desirable code for milling analysis.

3.2.2 Failure Criterion

In DEFORM-3D machining analysis, the workpiece is modelled as stationary and the cutting tool simultaneously rotates and moves along the feed direction. During the machining process simulation, the cutting edges of the cutting tool are shearing the workpiece material by chip formation. The material separation criterion for machining has been a topic of interest in the development of the theory of finite element modelling of machining. Huang and Black [149] determined that under smooth separation conditions, the chip separation criterion does not greatly affect chip geometry nor stress and strain distributions. Regardless, the maximum plastic strain criterion has been implemented and this has been the most accepted method of failure criteria to model material removal in milling [150].

In DEFORM-3D, a parting line model was assumed to simplify the simulation process. This model assumed a small crack existed in the material and the chip was separated from the workpiece in a predetermined “unzipping” fashion. Eventually, the maximum plastic strain model was proposed and this criterion has been adopted by most FEM models. This maximum plastic strain model assumes that material separation occurs when an element reaches a critical plastic strain for the material model of the workpiece. The element is then split into two elements and a chip is formed.

3.2.3 Geometry and Mesh

The workpiece and endmill geometry of the CATIA CAD files was transferred directly using STL neutral format files. The endmill and workpiece models must contain one surface. No free edges, no invalid edges and no invalid orientations should form the outer boundaries of the model. The workpiece is modelled to include a pre-defined material removal geometry represent the entry location of the endmill which includes the radial and axial depth of cut as shown in Figure 3.1.

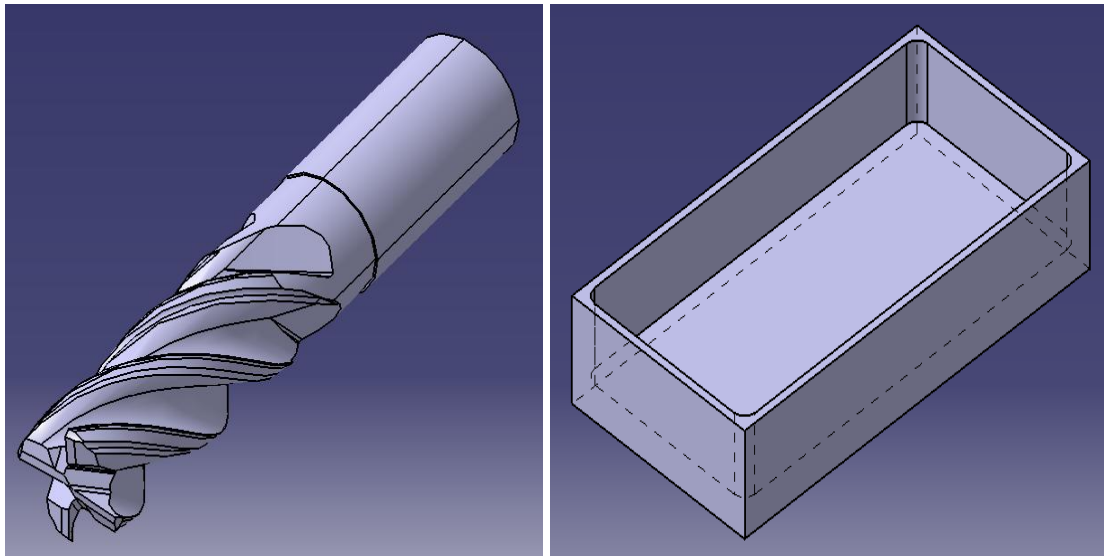


Figure 3.1: CATIA CAD models for endmill and workpiece.

The tool and the workpiece mesh size are very critical in modelling the milling process accurately. A finer mesh generally gives finer accuracy, but the simulation time increases exponentially as the number of elements increases linearly. Tetrahedron solid element is used to mesh the endmill and workpiece because of the complexity of the endmill shape and to capture the change in structural properties of the wall due to material been removed. For the three-dimensional element, each node has three degrees

of freedom of nodal displacements (δ_x , δ_y and δ_z) and the displacements within each element can be obtained by assembling the structural equation and interpolating the nodal values [151]. Using DEFORM's automatic mesh generation (AMG) function, a tetrahedral finite element mesh were constructed for the tool and the workpiece which define the minimum element size and parameters for adaptive remeshing. A minimum element size was specified in the interface area of the workpiece for the adaptive remeshing system. 300,000 total numbers of elements was approximately generated to give an accurate endmill model. The endmill is modeled to be a rigid object that does not deform during the milling process. In the analysis, tool wear and thermal damage of the endmill are not considered to save the computational time. A perfect tools model was considered in all simulations and justified by using a new tool for each run in the experimental work. Figure 3.2 shows the tetrahedral mesh element constructed for the endmill.

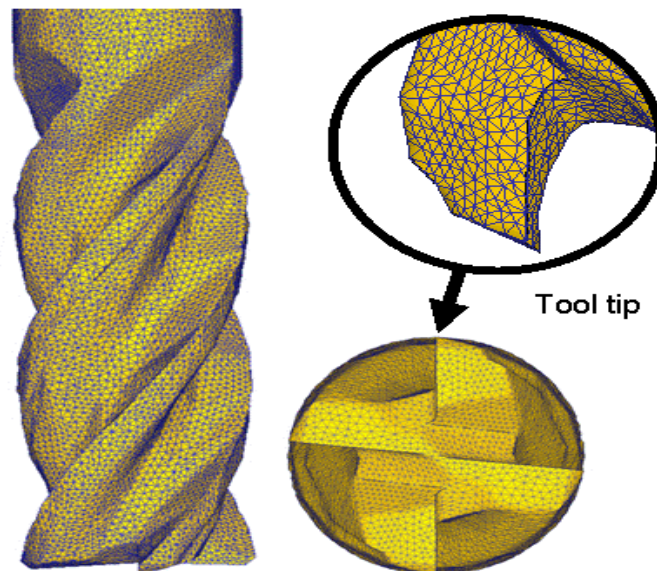


Figure 3.2: Tetrahedral mesh element constructed for the endmill.

Meshing the workpiece is much more complex and problematic than meshing the endmill as only high resolution mesh need to be defined at the machining area on the workpiece for computational efficiency. The workpiece is modeled as a plastic object which means it can be deformed and cut by the endmill. Consequently, when the mesh is deformed it must be regenerated frequently, often at every time step. During the simulation, the mesh helps reconstruction the distorted material as required for a Lagrangian mesh. The workpiece mesh must also be finer than the endmill mesh because the chip geometry can sometimes only be described with very fine elements. The stress, strain, and temperature of the elements all have very high gradients across the workpiece as well. These properties generally vary linearly or, at most, quadratically, from node to node, across an element. To approximate these high gradients accurately, a high resolution mesh is required.

The mesh is weighted to generate more elements in area where there are large strains, large temperatures, large deformations, and large strain rates occur. This option allows the mesh to adapt to the workpiece to optimize the computational time and element allocation. In the simulations that have been performed, the adaptive remeshing is generally weighted toward high strains (~50%), high strain rates (~30%) and the high density mesh window (~20%). The mesh window is placed at one side of the wall where the material to be remove by the endmill edge. An example of an undeformed meshed workpiece is shown in Figure 3.3, showing high mesh density where major deformation will take place. The minimum element size that is specified for the workpiece should be, at most, one half of the feed rate for computational efficiency. Having a fine mesh allows the mesh to deform according to the failure criterion when the endmill advances.

The contact and separation relationships between the endmill and the workpiece are very complex and subject to many errors.

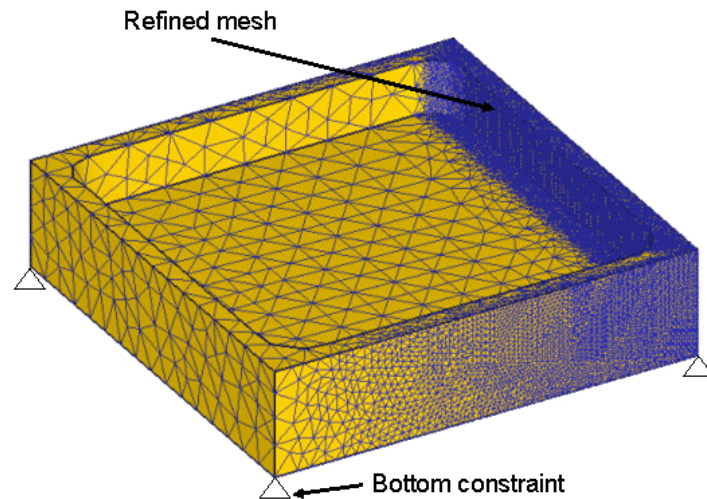


Figure 3.3: Tetrahedral mesh element constructed for the workpiece shows a high resolution mesh at the machining area.

3.2.4 Material Properties

In order to use the equations of the finite element method, extensive material data is needed for the workpiece. The model of the workpiece is subject to severe deformation at very high strain rates and temperatures. In these conditions, there are many variables that control the deformation. DEFORM-3D is prepackaged with a database that includes several metals and alloys. In addition, if the material data are known for a new material, these can be added to the database. The information that is needed to model the material is very difficult to obtain experimentally and many of the material models used are the result of comprehensive testing and modeling. The key relationships to define a new model are:

- Stress vs. strain vs. strain rate vs. temperature model
- Elastic modulus vs. temperature model
- Poisson's ratio
- Thermal expansion, conductivity, heat capacity vs. temperature.

Other information can be added to investigate other phenomenon. For example, to study a TiN coated tool on a titanium workpiece a diffusion coefficient would be needed. Thermal emissivity, hardness, and grain size can also be added to the material model. The material database that DEFORM-3D is equipped with includes (but is not limited to):

- Aluminum alloys
- Tool and die materials (e.g. HSS, WC)
- Stainless steels
- General iron-carbon steels
- Titanium alloys
- Brass

3.2.5 Boundary Conditions

Once the meshing of the workpiece and cutting tool were completed, a boundary condition is assigned to the component. For this case, the bottom surface of the workpiece is fixed in all direction similarly as clamping the component on the machine table. The endmill will have a rotational velocity and a feed rate (process parameters).

Thermal boundary conditions of 20°C were applied to the workpiece and endmill which represent the temperature of the surrounding environment.

Two heat transfer coefficient were used in the simulation, natural convection ($h_{nc} = 20 \text{ W/m}^2/\text{K}$) and forced convection ($h_{fc} = 2000 \text{ W/m}^2/\text{K}$) which represent the maximum that may be achieved according to the work published by O'Donovan [152]. Once the boundary conditions were defined, the tool needs to be positioned manually to the workpiece in accordance to the radial and axial depth of cut for initial start condition (start simulation) as shown in Figure 3.4.

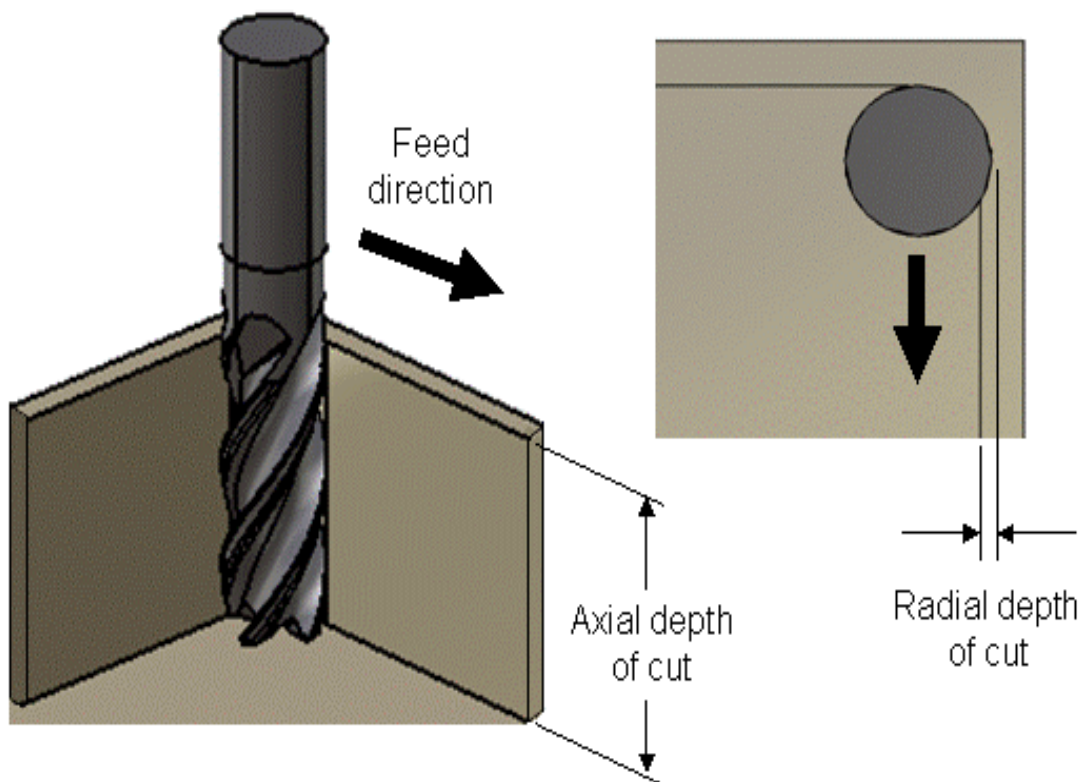


Figure 3.4: Initial start condition shows the endmill position with reference to axial and radial depth of cut.

3.2.6 Contact Conditions

The contact conditions control the friction, heat transfer, and master-slave relationships between the tool and the workpiece. The endmill cutter is set to be the master object and the workpiece is set as the slave object, meaning that the workpiece will deform according to the tool movement. That is, if the workpiece mesh tries to move into the tool, this is not allowable. An additional master-slave relationship is set up between the workpiece and itself. This will ensure that the generated chips will not flow back into the material.

In DEFORM-3D, Coulomb friction law and shear friction law were used to model the frictional contacts along the tool-chip interface. According to the work published by Ozel et al. [153], a mean average friction coefficient of $\mu = 0.6$ are found for machining titanium alloy, Ti-6Al-4V material using uncoated carbide (WC-Co) endmill tool. Figure 3.5 shows the master and slave object definition for contact conditions in machining simulation.

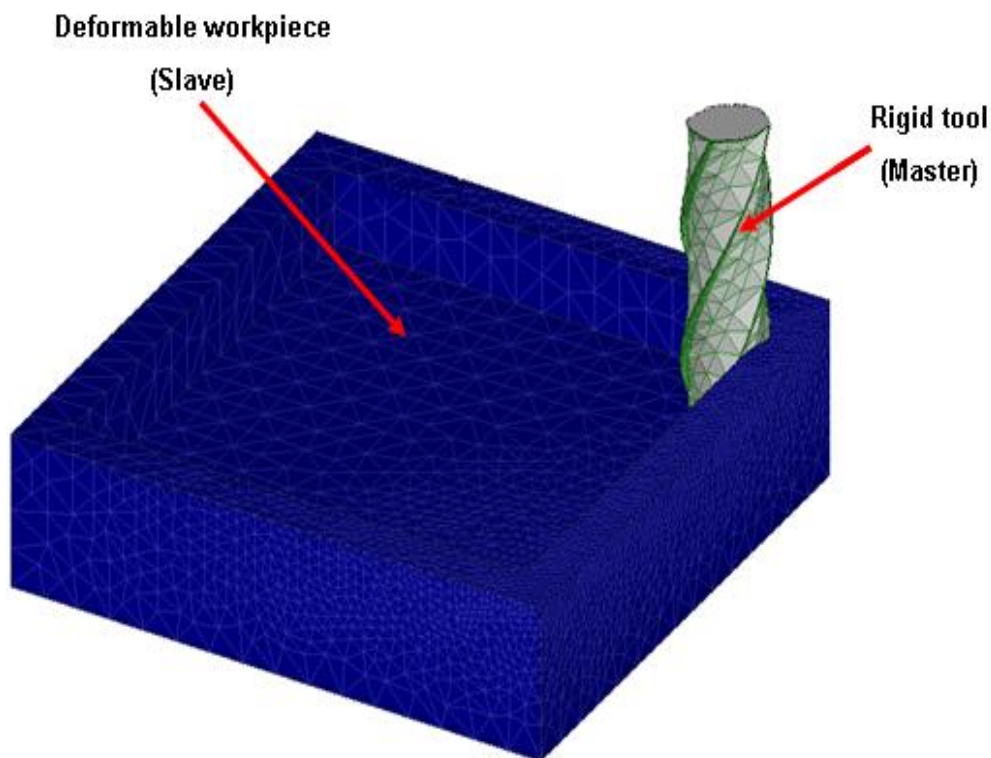


Figure 3.5: Master and slave object definition for contact conditions in machining simulation.

3.3 Simulations

DEFORM-3D has several simulation parameters that can be changed to achieve different objectives. The number and size of time steps can be changed. The number of time steps needs to be only large enough in order for the tool movement goes through the desire machining length. Although the time step can be specified, it is usually determined by the mesh size. Smaller element sizes require smaller time steps. Remeshing criteria and alternative stopping conditions can also be applied, but the default values are usually sufficient. Once all the key parameters setup is complete, a .DB file is created for the analysis and simulation.

3.3.1 Simulation Parameter

The capability of DEFORM-3D is assessed on the basis of technical capability and system performance. Some machining parameters are best obtained by direct measurement, so that the FEM model can be experimentally validated for an identical set of test components. The experimental tests were performed on a HAAS VF1 vertical machining centre. The wall deflection is measured using five Lion Precision ECL 130 inductive displacement sensors and is then analysed using LabVIEW 8.5.1. The sensors are mounted at five different equal locations at the back of the workpiece in which the deflection is occurred. The workpiece is pre-shaped to square pocket which contains of thin-wall with different height and length as in Table 3.2. The workpiece material used in the simulation and experimental is annealed alpha-beta titanium alloy, Ti-6Al-4V. 6 mm four flutes helical fluted carbide flat endmill with 38° helix angle and 5° ramp down angle is used for machining the thin-wall. Total of seven runs were performed for the result validation. The cutting parameters used in the simulation and experiment are listed in Table 3.2.

Table 3.2: Details of machining parameters and workpiece attributes used in simulation and experiment.

Run	Speed (rpm)	Feed (mm/min)	Radial Depth (mm)	Workpiece Thickness (mm)	Workpiece Height (mm)	Workpiece Length (mm)
1	4244	340	0.3	1.8	15	150
2	3850	290	0.5	2.2	15	120
3	4500	420	0.4	2.0	15	100
4	4250	380	0.65	2.2	20	150
5	3700	265	0.2	2.0	20	120
6	4050	410	0.3	1.8	25	100
7	3750	270	0.8	2.2	25	120

3.3.2 Simulation Results

The technical capability assessment for the preliminary study was to measure the results accuracy of the part deflection between simulation and experiment. In addition, the effect of processing parameter and workpiece attributes on the part deflection is observed. Figure 3.6 (a) shows the simulation window at the initial start condition which shows the endmill position at the pre-defined radial and axial depth of cut. The analysis is started as the endmill rotates and moves in the feed direction along the wall, while Figure 3.6 (b) shows the maximum temperature in step-245. It can be observed that the maximum temperature is located at the secondary shear zone due to friction between the chip and the rake face of the endmill. The effective plastic stress and strain analysis for step-255 and step-439 is shown in Figure 3.7 respectively. It can be seen that as an element of the work piece passes through the deformation zones, its magnitude of plastic strains increases. High plastic strain appears in the secondary shear zone where the maximum temperatures are located and it remains constant away from the deformation zone. The effective stress reaches the maximum value at the primary shear zone due to increase in both strain and strain rate. Then it starts to decrease towards the secondary shear zone due to decrease in strain rate and increase in temperature. A maximum value of 1090 MPa is obtained in the primary shear zone and 880 MPa in the secondary shear zone which agreed with the literatures result for machining analysis in [154 and 155].

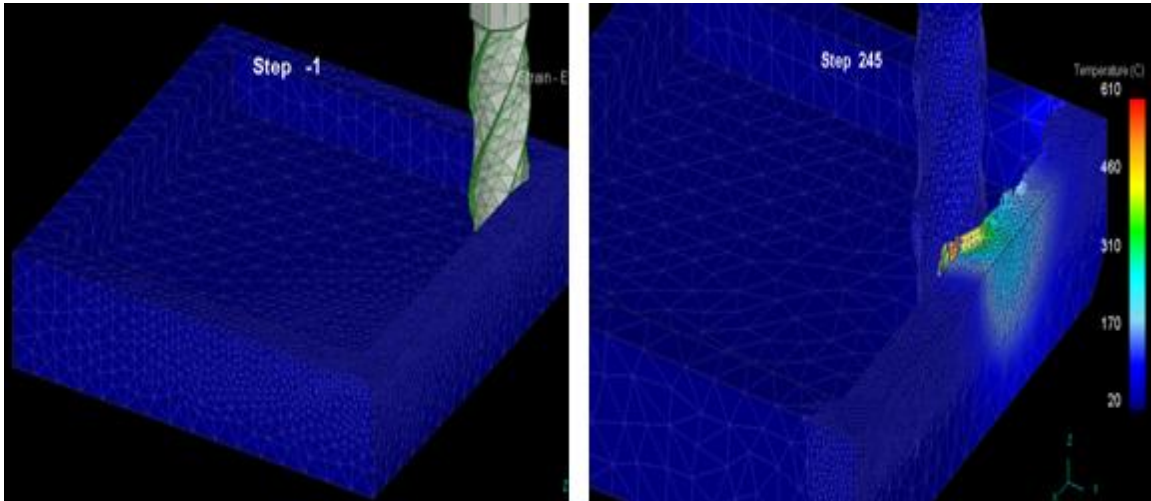


Figure 3.6: DEFORM-3D simulation window shows (a) the initial start simulation, Step-1. (b) Chip temperature distribution during the simulation at Step-245.

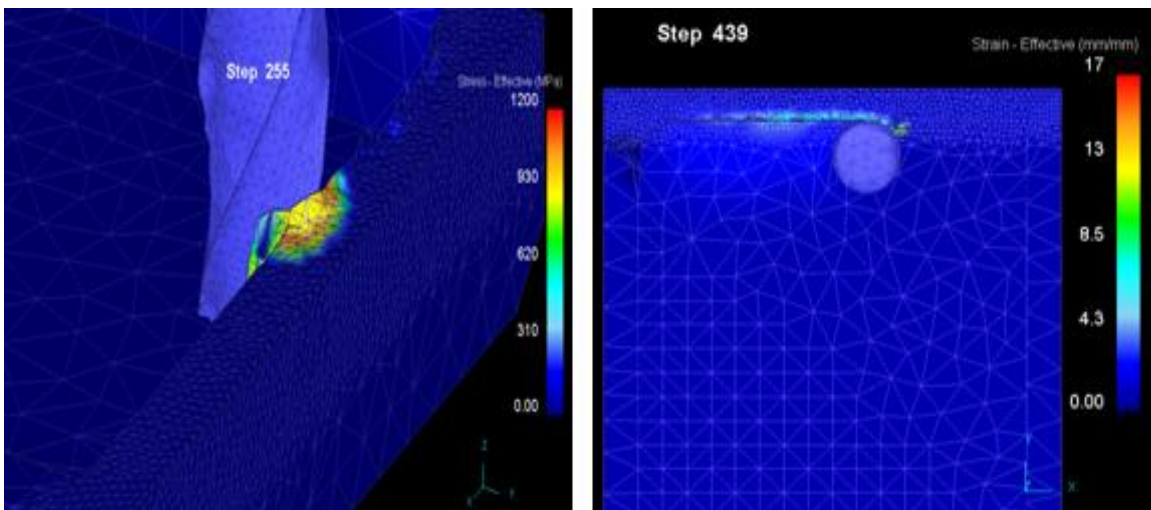


Figure 3.7: DEFORM-3D window shows the effective stress and strain values during the simulation at Step-255 and Step-439.

Figure 3.8 shows the wall displacement in y direction due to the cutting forces distribution between tool and the workpiece. The comparison of part deflection along the workpiece feed direction between simulation and experiment is shown in Figure 3.9 (Run-1). It can be seen that the predicated displacement matches those measured in the

cutting tests very well. The maximum value of the part deflection is obtained at the middle and minimum in at the two ends.

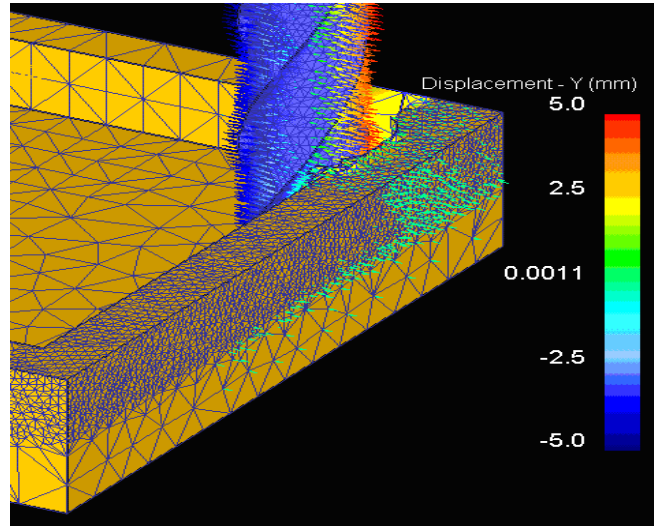


Figure 3.8: DEFORM-3D window shows the part deflection due to the cutting forces generated between cutting tool and workpiece.

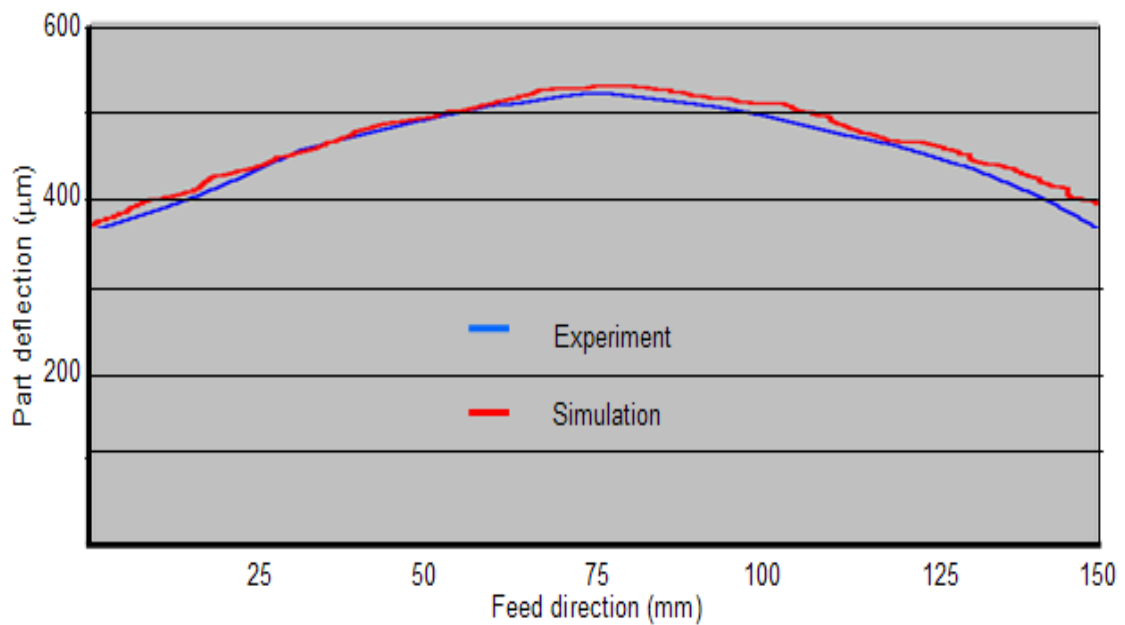


Figure 3.9: Comparison of part deflection between simulation and experiment for Run-1 shows the maximum values of part deflection occurred at the middle of the wall.

3.3.3 Simulation Computational Performance

The second assessment in the preliminary study was the performance in term of computational analysis time. The CPU time were observed at the start of the simulation after the pre-processor setup. The simulation step must take a certain amount of tool rotation per feed step to ensure the machining cycles are complete. The simulation step is dependent to cutting parameter and workpiece length and reflects with the computational time. Table 3.3 lists the simulation step and total CPU time taken for all the runs. It can be observed, apart from the simulation step which dependent to machining length, the processing parameters such as axial and radial depth of cut were a critical factor for determine the speed of the calculation. This is because the axial and radial depth of cut corresponds to the number of elements through the thickness of the workpiece. During the simulation, it can be observed that the simulation tends to stop periodically and the mesh size needs to be adjusted before continuing for the remaining subsequent step.

Table 3.3: DEFORM-3D simulation step and computing time for machining simulation.

Run	Simulation Step	CPU Time (hrs)
1	605	269.4
2	480	208.8
3	401	163.2
4	603	340.8
5	483	199.2
6	405	169.5
7	477	227.4

3.3.4 Overall Assessment on Preliminary Investigation with DEFORM-3D

The preliminary study revealed that DEFORM-3D software offers for a fast and easy setup and are capable in simulating the machining process. However, from the preliminary study there are several issues encountered in using the software for practical use. The main issue in using the software is its long computational analysis time. This is due as the simulation progresses the workpiece tends to demand more and more elements, which causes the simulation to run slower with time that can take several days and even weeks depending on the parameters and hardware resources. In addition, the material removal element separation process tends to create a high element distortion which makes the simulation stop periodically and the mesh size needs to be adjusted by the user. Beside that, the nature of the FEM calculation which calculates the surface errors all over the workpiece for every feed step and every angular increment result in low efficiency.

The simulation also requires a suitable memory size to define the integer and real arrays calculation which requires a significant CPU speedups and special platform to become truly practical, accurate and valuable for the industries which must manufacture parts in a few days. Another disadvantage observed from the preliminary study is most of the component geometry need to be create by other CAD software and transfer to the FEA software. This can increase the pre-processor time for rework the CAD model as exchanging data between different platforms can cause problems such as loss of data

organization, translation inaccuracies, change in number of entities and excessive file size growth.

3.4 Summary

Due to the problems experienced in the preliminary study, a new methodology with good analysis efficiency for modelling the deflection prediction in machining thin-wall workpiece is required. By taking the advantages of FEM and combining it with a statistical analysis can speedup the analysis result for it to become practical and feasible for the industries use. The next chapter will explain the new proposed methodology for modelling the deflection prediction in machining thin-wall workpiece.

CHAPTER 4

OVERVIEW OF THE HYBRID ANALYSIS MODEL

4.1 Introduction

In Chapter 2 and 3, a review on literature and a preliminary scientific study on modelling thin-wall machining were introduced. The drawbacks and disadvantages of the present methodologies on modelling deflection prediction of machining thin-walled have been discussed. In this chapter, a new hybrid model for deflection prediction on machining thin-wall workpiece is developed. The hybrid model aims to resolve the disadvantages over the previous research work which includes the procedure from initial part creation to analysis result. The model is developed to take into account the tool-work geometries on material removal process during machining process. This chapter will first explain the hybrid model procedures and the theory of each model.

4.2 Objective of Hybrid Model

The hybrid methodology aims to analyse the deflection prediction in machining thin-wall monolithic component. The development needs to take accounts on the problems encountered for the modelling process from initial part creation to analysis results for machining the thin-wall components:

- Modelling process is now a lead-time bottleneck and thus needs to be speed up.
- The modelling process should include the adaptation of the machining parameter and the tool-work geometries on material removal process during machining process.

- Besides automation, the software should make the task easier to perform. This will help speeding up the analysis process.
- The modelling software needs to be performed on the same platform to minimise the errors associated with exchanging data.
- The modelling software should give a user fast and better results. This can be achieved by introducing the statistical analysis in the prediction model.

4.3 Modelling and Simulation System Architecture

The proposed modelling and simulation system architecture for machining thin-wall components is shown in Figure 4.1. The system consist of several models, namely, machining load computational model derived from the machining parameter, feature based geometry model, material removal model, deflection analysis model and statistical analysis model. The new proposed hybrid model intends for:

1. Efficient modelling on deflection prediction in machining thin-wall component.
2. Minimizing the analysis time from initial part creation to analysis result.
3. Elimination of time-consuming and error-prone transfer of geometry by integrating between CAD and CAE.
4. A fast and easy set-up using application-specific GUIs (graphical user interface) which simplify data input (machining parameter) and pre-processing.

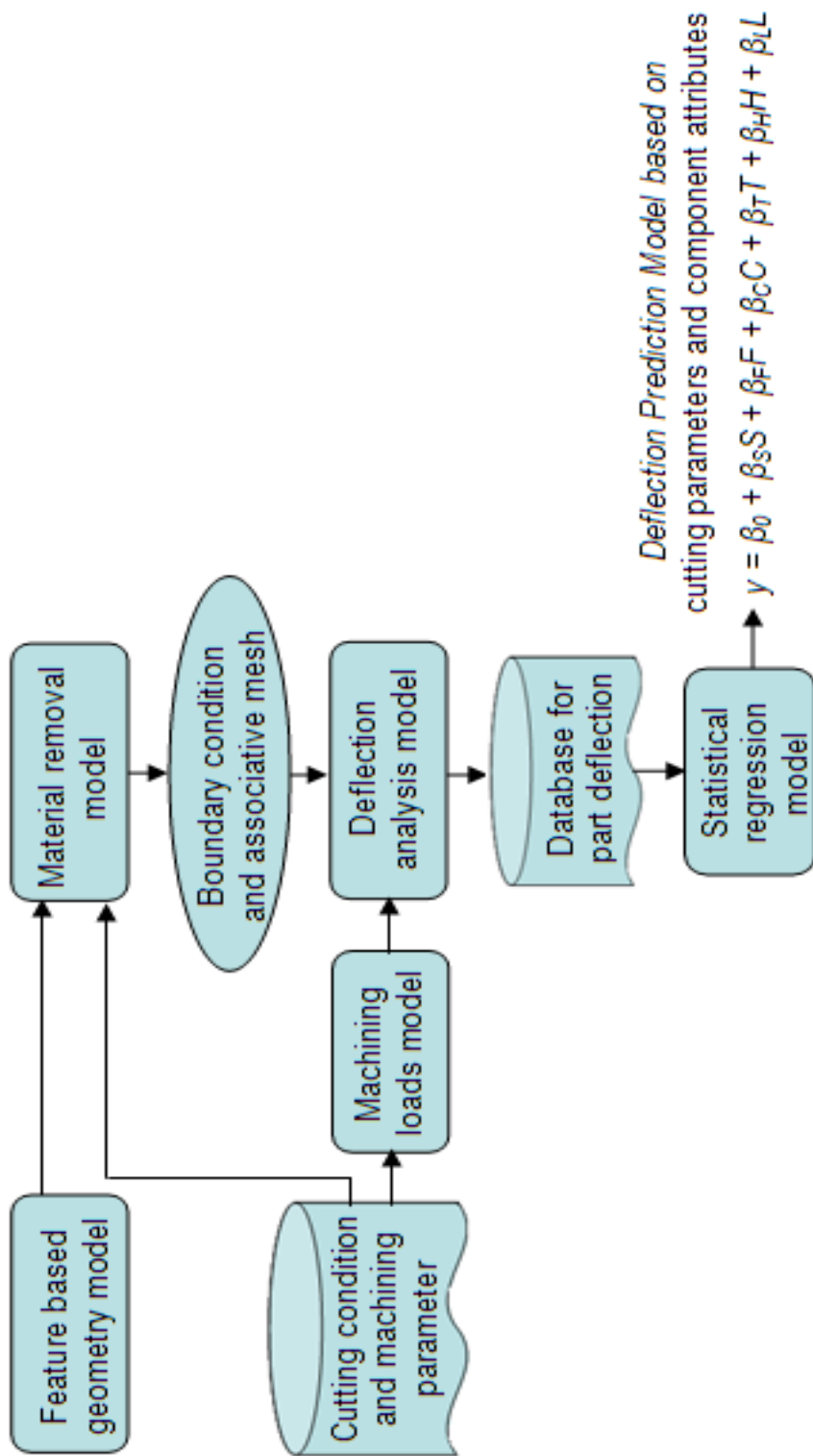


Figure 4.1: Modelling and simulation system architecture.

The proposed hybrid model is based on object oriented approach which creates a separate material removal CAD model for the pre-defined cutter feed step which is contrast with the commercial FEM software process analysis which calculates the surface errors all over the workpiece for every feed step and every angular increment of cutting tool. This, in turn, reduces the computation time. The FE result which contains the part deflection values at the pre-defined feed step will be used to generate the training data set to perform the statistical analysis. The statistical analysis is used to predict the part deflection in associate with the machining parameters and component attributes.

The methodology is performed within the CAD environment and the analysis model is fully associative with the CAD geometry and specification. Unlike most of the FEM software, the part is often generated from CAD software and transferred with a neutral database form such as STL. However, exchanging data between different platforms can cause problems such as loss of data organization, translation inaccuracies, change in number of entities and excessive file size growth. By using a same platform between CAD and FEM those problems associate with the data exchange are eliminated. MATLAB and MINITAB software were used in machining load computational model and statistical analysis respectively. While feature based geometry model, material removal model, deflection analysis model were implemented using CATIAV5 software using Mechanical Design module, Advanced Meshing module and Generative Structural Analysis module. The simulation is performed by automating the task for modelling solids object, material removal and structural analysis with CATIA V5 through the used of macros, with Windows as the operating system and Visual Basic as

the programming language. The proposed task automation is an integrated data exchanges between modules upon users input on the design information and machining parameter for automatically generate the solid model, material removal model and FEM analysis. A details explanation on function of each model is described in the following sections.

4.3.1 Machining Load Computational Model

The purpose of the machining load computational model is to calculate the force generated during the machining process. The prediction of cutting forces during machining is a key component model, as it determines the magnitude of the wall deflection and dependent with the machining parameters [156 and 157]. On the other hand, predictions of cutting forces in milling process are often needed for establishment of automation or optimisation in the cutting process [158]. For a past few decades, there has been extensive research conducted in developing force models for the milling process. The development of force model can be classified in two approaches namely the mechanistic force model [159, 160, 161, 162 and 163] and the mechanics force model [164, 165, 166 and 167]. Investigation on modelling the cutting force from the literatures demonstrate that mechanistic force model prove to give an accurate results compare to the mechanics force model. Hence, the mechanistic force model will be used to calculate the cutting forces for the hybrid model.

In mechanistic force model, the cutting forces are related to average chip thickness by cutting force coefficients calibrated experimentally for a particular tool-

workpiece pair material [168, 169 and 170]. Then, the cutting forces produced by the same cutter can be predicted analytically by using the calibrated cutting force coefficients. Apart from cutting force coefficients, the prediction of cutting forces in machining take into accounts the machining parameters and tool geometry attribute. The machining parameters namely, cutting speed (rpm), radial depth of cut, axial depth of cut, feed rate (mmpt) and tool attributes such as diameter and helix angle (β) are used as an input to calculate the machining loads as shown in Figure 4.2. A details explanation on mechanistic force model calculation and experimental cutting force coefficient are describe later in Chapter 5.

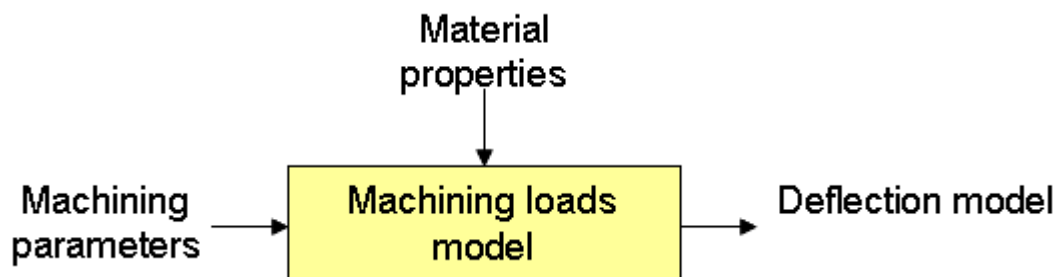


Figure 4.2: Machining loads model.

MATLAB software was used to calculate the machining loads for the machining process. An interactive graphical user interface is developed to make the task easier to perform and execute as shown in Figure 4.3. Once the machining loads is obtain, the values is stored and saved in a native *ASCII file* format and will be used as an input in the deflection analysis model for calculating the magnitude of part deflection.

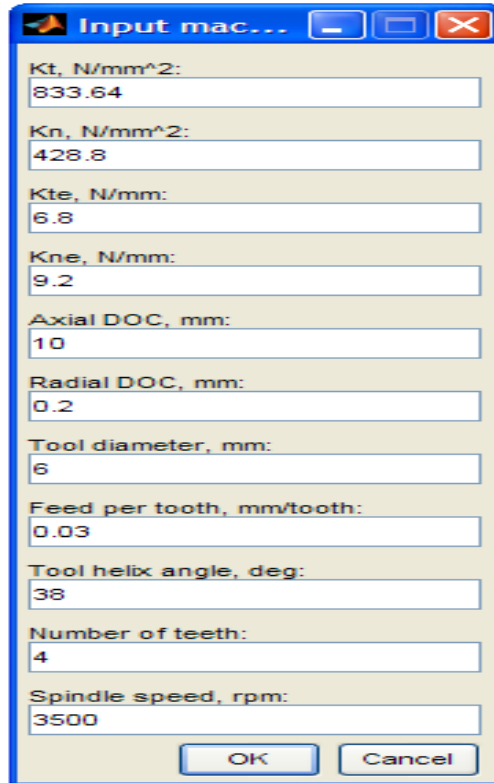


Figure 4.3: MATLAB GUI interface sample window for machining loads calculation.

4.3.2 Feature Based Geometry Model

The main purpose of the Feature based geometry model is for the creation of solid model which acts as an initial master component before the machining. The component feature attributes such as the initial workpiece dimensions and material properties such as density, Young's modulus, Poisson ratio, yield strength, hardness and elongation rate are created in the CATIA Part Design workbench. Once the master component is created, it will be input to material removal model for the subsequent process as shown in Figure 4.4. The component is created by automating the task for modelling solids object with CATIA V5 through the use of MACRO.

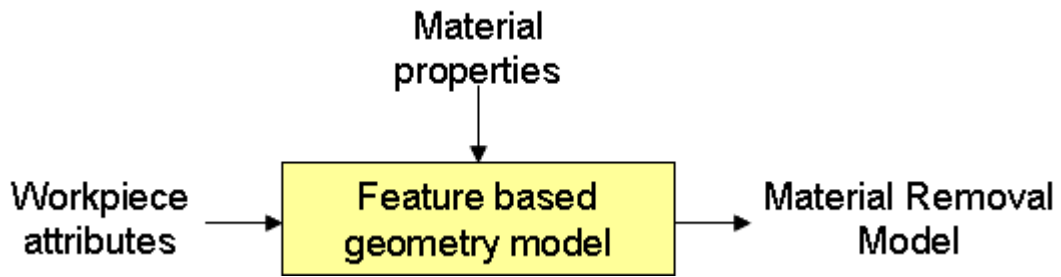


Figure 4.4: Feature based geometry model

A MACRO is a series of functions, writing in scripting languages that group a command to perform task automatically [171]. The MACRO has been developed to generalize the parametric patterns and to allow the user to develop the design features with minimum requirement of expertise in this field. Solid modelling systems are designed with an API (Application Programming Interface) which forms the canvas for writing MACRO. The API provides the entire tool required to write and test the MACRO. The MACRO issues geometric instruction to the solid modeller based on parameter provided by user. The geometric instructions are then used to form a solid model of 3D design. The MACROS has been created with a view of providing simple numeric parameter input which could be given on the window interface [172].

To create a component in Mechanical Design sketcher workbench, a sketch is first created on a 2D plane in 3D space. The geometry is sketched roughly in position on CATIA. Since geometry is roughly sketched, it must be modified to capture design intent. Geometry need to be modified by applying and changing the constraints. Contextual horizontal and vertical constraints are added first follows with parallel, concentric, coincident, etc. Figure 4.5(a) shows the contextual constraints definition for 2D sketch of T-Shape component geometries. Dimensional constraints, similar to

dimensions, are added next and the geometry is automatically updated. To form a solid feature, a pad needs to be create on the sketch and a dimensional constraint are added to define the length of the component as shown in Figure 4.5(b). Once the component was constructed, the generated MACRO instructions step needs to be modified for the development of GUI.

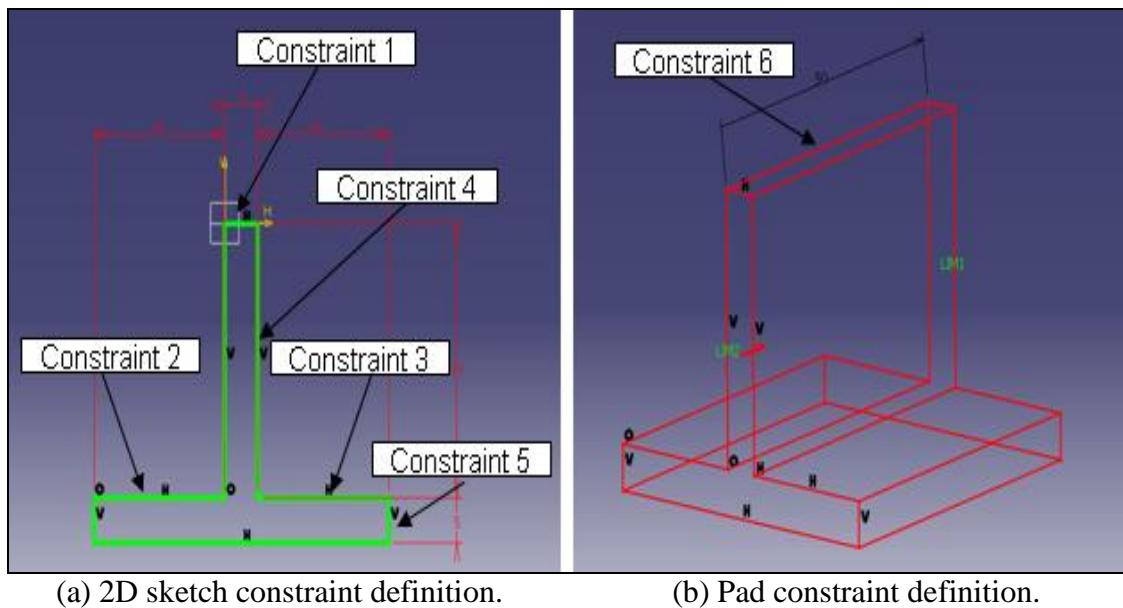


Figure 4.5 (a) and (b): Contextual constraints definition for solid feature generation for T-Shape component geometries.

The developed user interfaces allow users to accomplish the design process in an intuitive and interactive way. The user interfaces make the task easier to perform which help speeding up the pre-processor process. The user interfaces used in the system can be classified into two categories. The first category is for analysis input graphic information and second category is for alphanumeric input information. This set of interfaces is developed in MACRO, which is a built-in function of CATIA V5.

Once the component is selected, it will open a new window to input alphanumeric information for the selected component geometries, as shown in Figure 4.6. By using a simple form, the dimensions are inputs which define the geometry of the part (i.e. length, thickness, height etc.). This application automatically and immediately creates the part compare with the manual process that would require construction of lines and generation of solid model. Once all the information is completed, the system is able to automatically complete the design. The component is saved in *CATPart* file format and work as a master component. Any changes and update of material removal in the next hybrid methodology step need to be done in this master component.

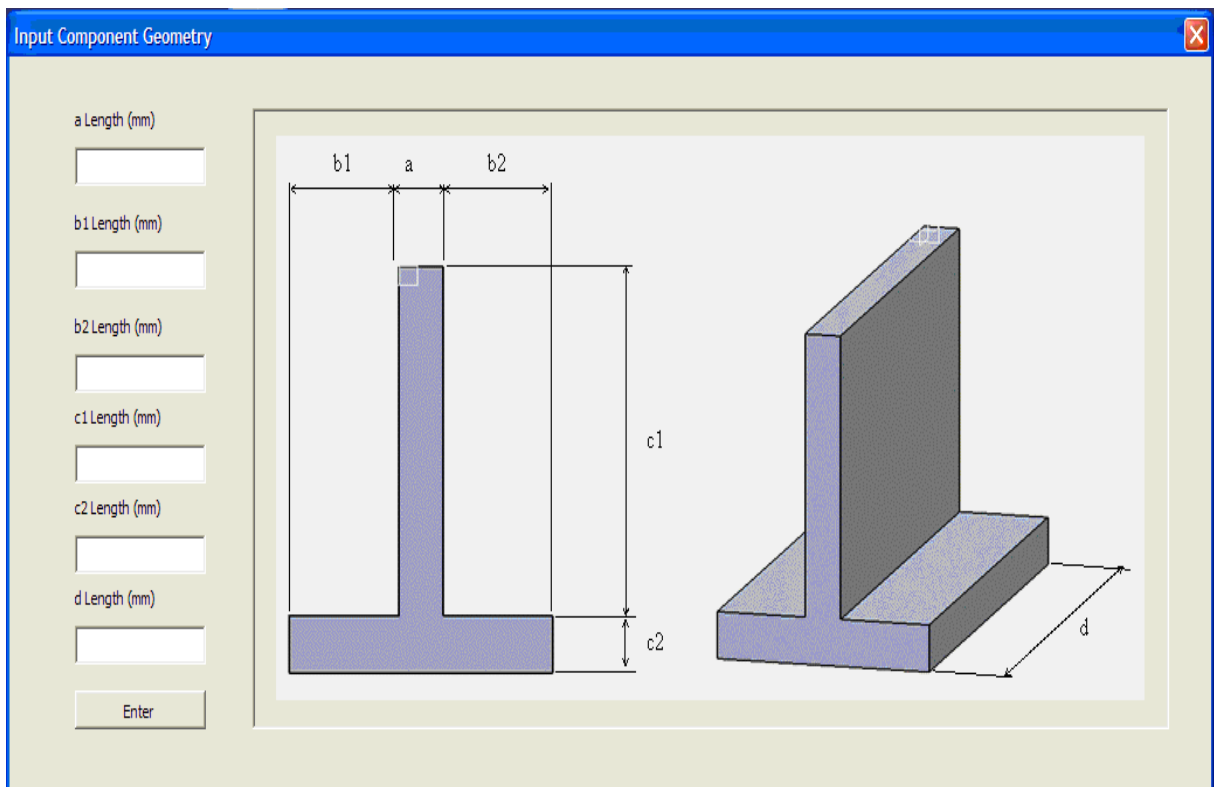


Figure 4.6: Sample window shows the GUI input alphanumeric information for T-Shape component geometries.

4.3.3 Material Removal Model

The objective of material removal model is to model the element deletion for material removal process during machining. When the cutter moves, its path forms the volume of material to be cut. This volume is calculated based on the cutter geometry and its path in the workpiece. The cutter shape and the cutter path that is coincidence with the workpiece material will be removed using ‘Sketch-Based Features (Pocket)’ and ‘Transformation Features’ function in the CATIA Mechanical Design workbench.

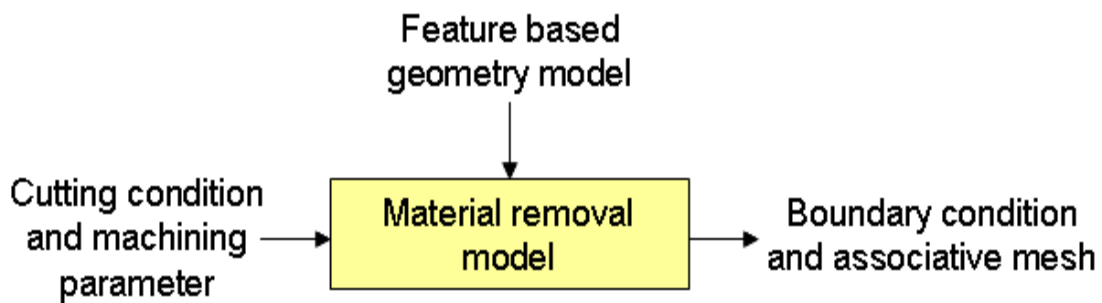


Figure 4.7: Material removal model.

To model the material removal process, first, the created master component from the Feature base geometry model is called. Using the CATIA sketcher workbench, a sketch of cutter geometry starting with the circle profile is created on top of the master component plane. To define the starting location of the cutter with respect to the cutter radius and radial depth of cut, contextual horizontal (*Constraint 1*) and vertical constraints (*Constraint 2*) are added as shown in Figure 4.8. Once the cutter starting location is defined, by using the ‘Sketch-Based Features (Pocket)’ the materials in the master component which is coincidence with the cutter shape are deleted. A constraint

is added to define the volume to be removed with respect to the axial depth of cut (*Constraint 3*). The first material removal model is saved as a new *mrr(i+1).CATPart* file, where $i = 0$ to m . m denotes the cutter feed step with respect to the machining length.

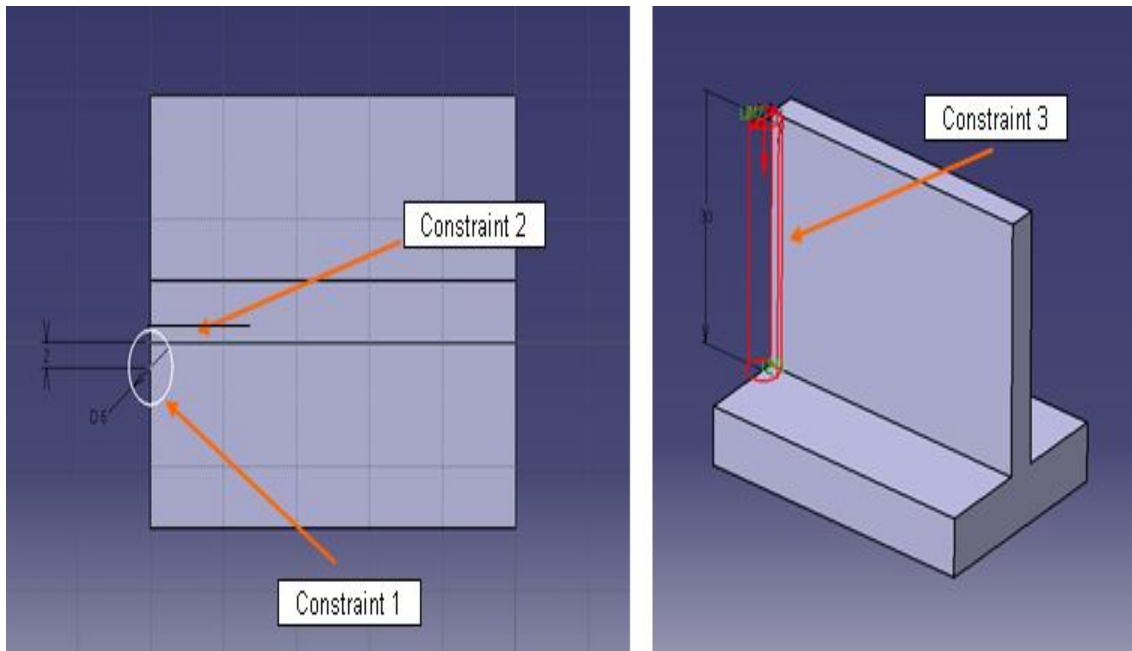


Figure 4.8: Contextual horizontal and vertical constraints for tool diameter, radial and axial depth of cut for the starting cutter location for T-Shape Component.

Then, for the subsequent step, the cutter location are move to the next feed step position. By using the ‘Transformation Features’ function, the cutter profile created in the first step is copy and transform to the next cutter feed step location for element deletion. The new material removal model is saved as a new *mrr(i+1).CATPart* file. A constraint is added to define the distance of the cutter location between each feed step and total number of feed step with respect to the machining length as shown in Figure 4.9.

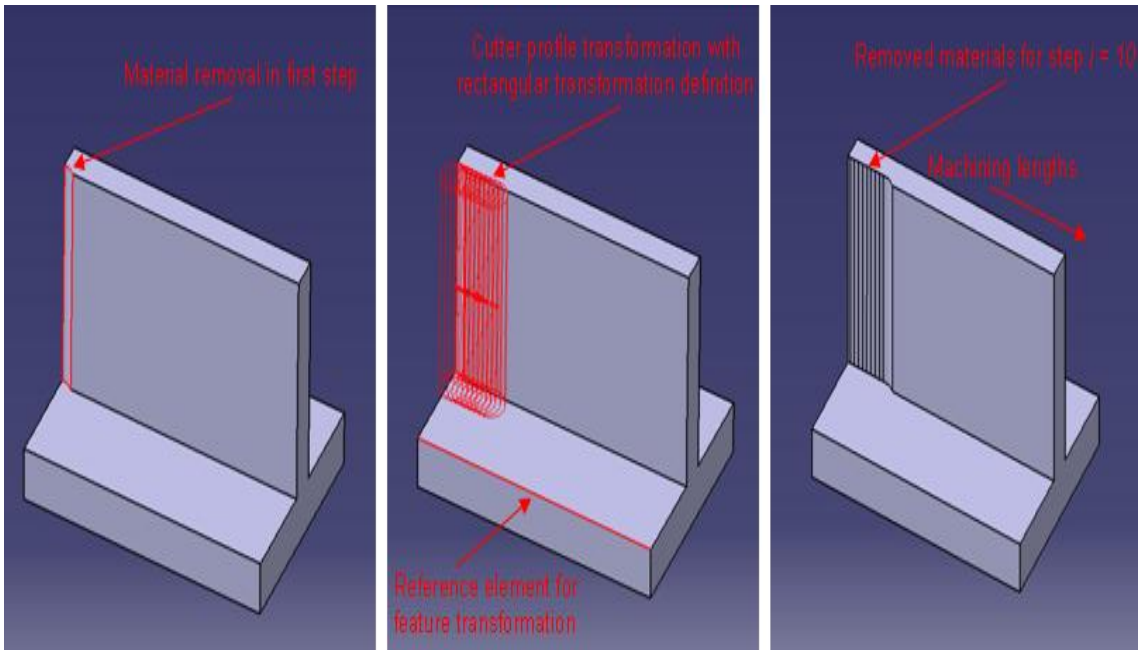


Figure 4.9: Cutter profile transformation for modelling the material removal process for T-Shape Component.

Again, an interactive graphical user interface is developed for the user to input the machining parameter for the material removal model such as tool diameter, axial depth of cut, radial depth of cut and the machining length. An interactive graphical user interface for material removal parameter is shown in Figure 4.10.

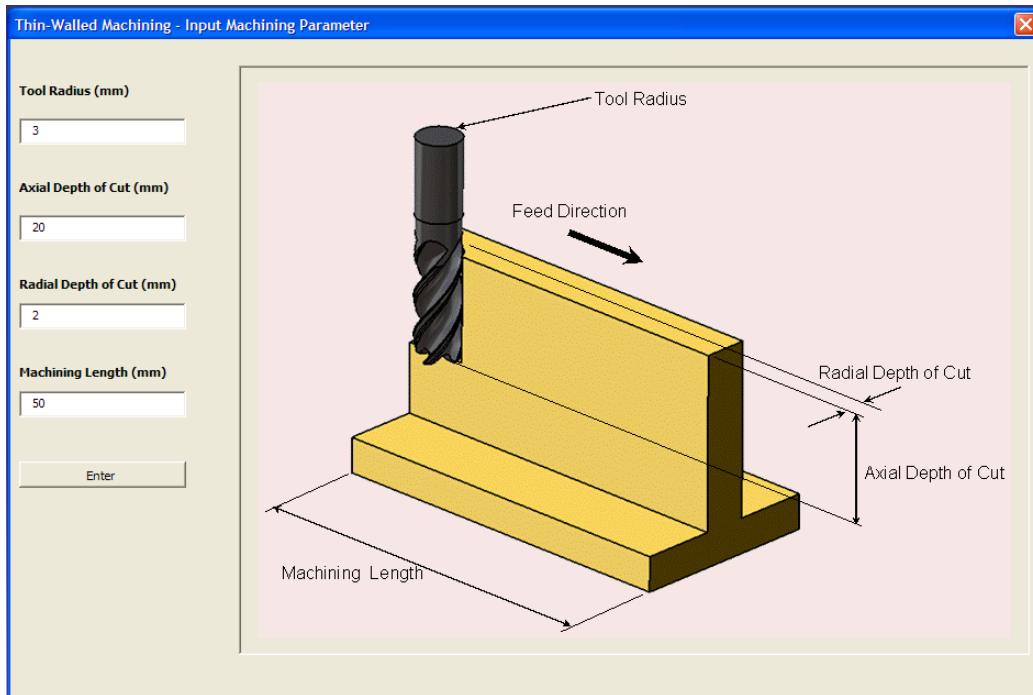


Figure 4.10: Interactive graphical user interface for material removal model parameter for T-Shape Component.

4.3.4 Deflection Analysis Model

The purpose of the deflection analysis model is to calculate the part deflection produced during the machining process. The magnitude of part deflection is predicted using finite element analysis in CATIA Generative Structural Analysis workbench. Analysis information such as nodes, elements, material properties, boundary conditions and the predicted cutting force from the machining load model will be as an input for the FE analysis to perform static analysis for part deflection prediction as shown in Figure 4.11.

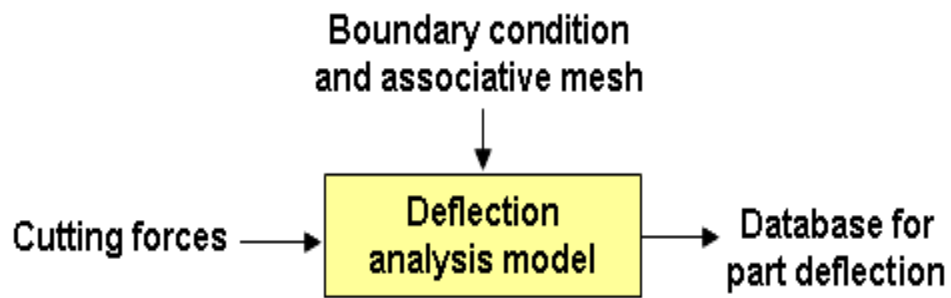


Figure 4.11: Deflection analysis model.

The predicted cutting forces from the machining loads model are applied and placed on the relevant nodes in the transient surface at pre-defined cutting position of the component as shown in Figure 4.12. The part deflection can be predicted at any selected cutting position according to the user's requirement by calling the created pre-defined material removal parts ($mrr(i+1).CATPart$) from the material removal model.

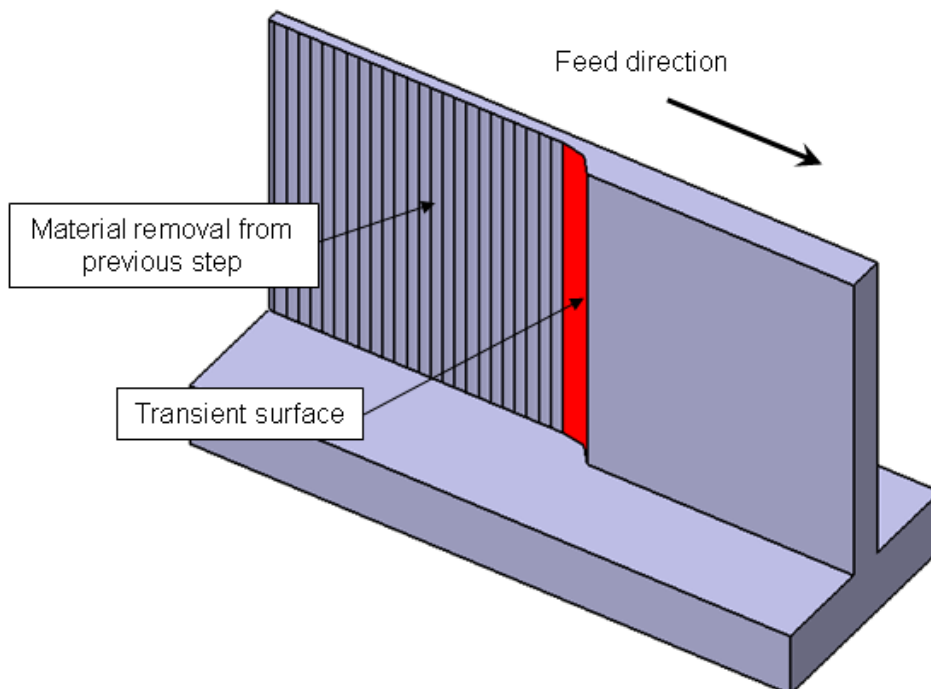


Figure 4.12: Transient surface at pre-defined cutting position.

The FEA results which contain the displacement values are stored in a knowledge-based template and saved in a native *ASCII file* format as shown in Figure 4.13. The next input data ($mrr(i+1).CATPart$) from material removal model of the next cutter feed position is call for the subsequent analysis. Finally, after repeating this procedure at different selected cutting position along the feed direction, the complete surface wall deflections of the component are obtained. The output from the deflection analysis model is used to generate the training data set to perform the statistical analysis.

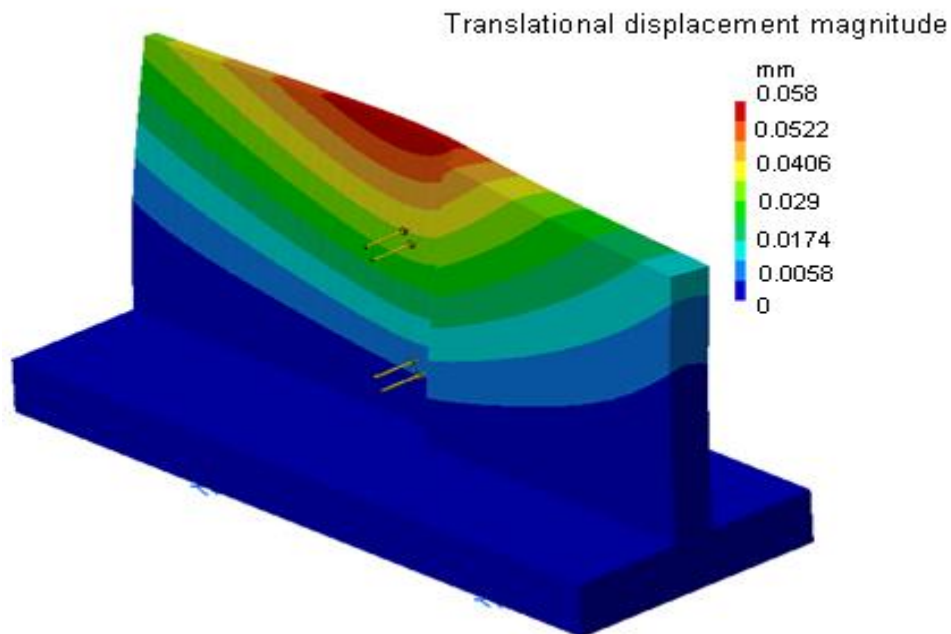


Figure 4.13: Sample window shows the deflection analysis for T-Shape component geometries.

4.3.5 Multiple Regression Analysis Model

The reason for regression model is that the analysis so far is specific to a few points. In shop floor environment, these points can be any value within a range. To

allow prediction of deflection at the unknown points, a regression model is used for shop floor processing. Multiple regression technique is used to perform the statistical analysis to determine the correlation between a criterion variable; wall deflection and a combination of a predictor variables namely speed, feed rate, radial depth of cut, wall thickness, wall height and wall length. Regression analysis is used to understand which among the independent variables are related to the dependent variable, and to explore the forms of these relationships [173]. The training data set for the regression analysis were generated from the FEA results with reference to component attribute and machining parameter using the previous describe methodology as shown in Figure 4.14.

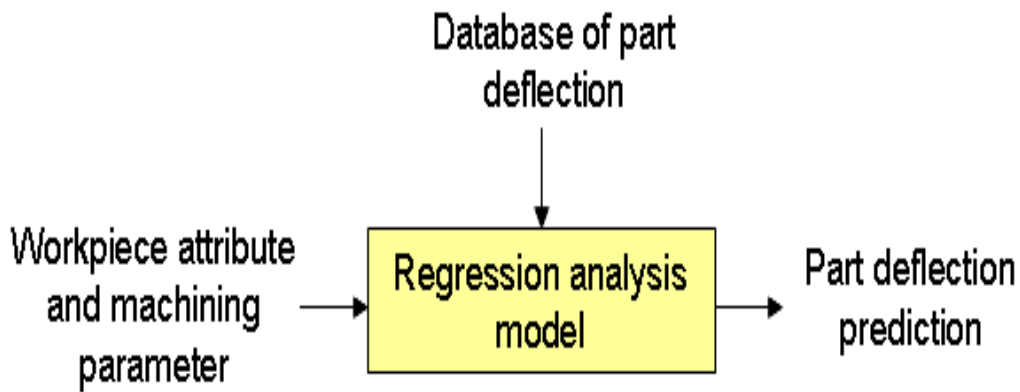


Figure 4.14: Multiple regression model.

The multiple regression model can be expressed as:

$$y_{D1, D2, D3, D4, D5} = \beta_0 + \beta_S S + \beta_F F + \beta_C C + \beta_T T + \beta_H H + \beta_L L$$

where y = displacement (μm) at $D1, D2, D3, D4$ and $D5$

$$(D1=0L, D1=1/4L, D2=1/2L, D3=3/4L, D5=L)$$

S = Speed (rpm)

F = Feed rate (mmpt)

C = Radial depth of cut (mm)

T = Workpiece thickness (mm)

H = Workpiece height (mm)

L = Workpiece length (mm)

The general null hypotheses was described as the effects of speed, feed rate, radial depth of cut, workpiece thickness, workpiece height and workpiece length on displacement do not significantly differ from zero. The null hypotheses and alternative hypotheses can be written as:

$$H_o = \beta_S = \beta_F = \beta_C = \beta_T = \beta_H = \beta_L = 0$$

H_a = at least one of the β does not equal to zero

The multiple regression model is verified by confirming the statistical significance of the estimated parameters and the goodness of fit of the model. R-squared, analyses of the pattern of residuals and hypothesis testing were used to verify the goodness of fit of the model. While, F-test of the overall fit are use to verified the statistical significance of the estimated parameters. MINITAB software was used for performing the multiple regression and statistical analysis.

4.4 Break Down Of Monolithic Component into Standard Features

To develop an efficient hybrid model for practical industry relevance, it is necessary to analyse the different thin-wall aerospace structural components. Generally, the aerospace monolithic component composed of multiple pockets that contain thin-wall structures in order to reduce their weight, while maintaining their stiffness. These components include the skin, the spar and the rib. To efficiently analysing these structural components, they are broken into a series of unit elements with different features. A generalized unit-element of component features in the aerospace monolithic component is depicted in Figure 4.15.

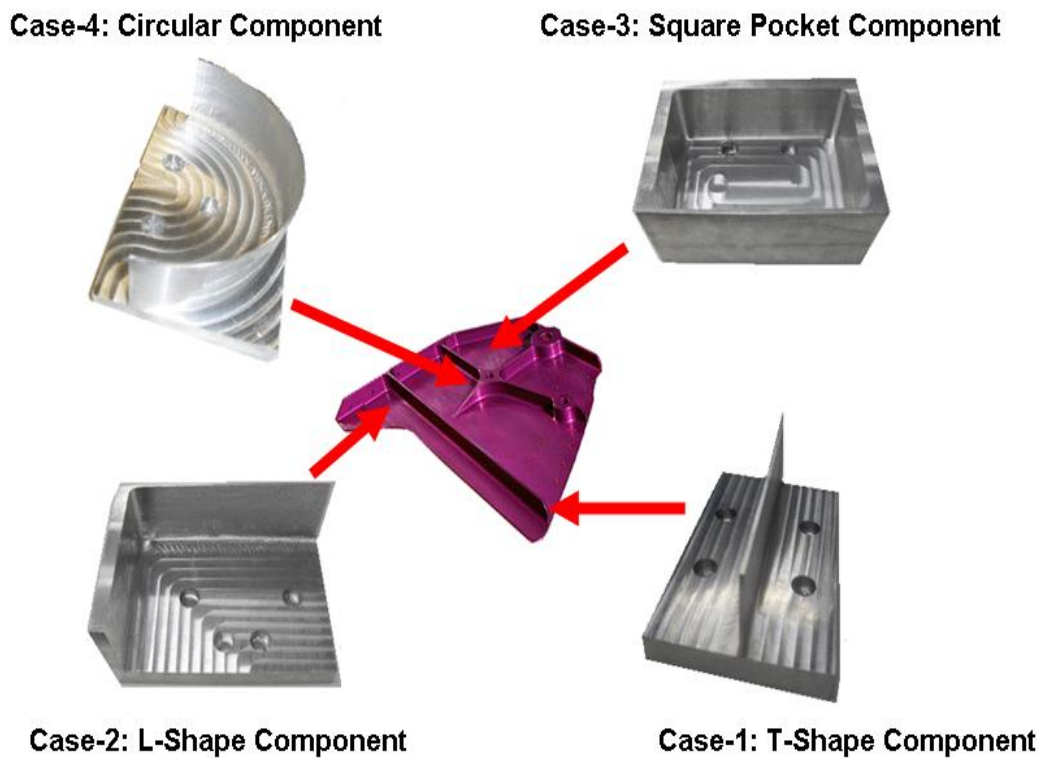


Figure 4.15: A generalized unit-element of component features in the aerospace monolithic component.

Similarly using the methodology as in Section 4.3.1 to 4.3.5 for the T-Shape component, the deflection prediction for L-Shape component, Square pocket component and Circular shape component were developed in the hybrid model. Figure 4.16 to Figure 4.18 shows the developed GUI for the different type of thin-wall components in the hybrid model.

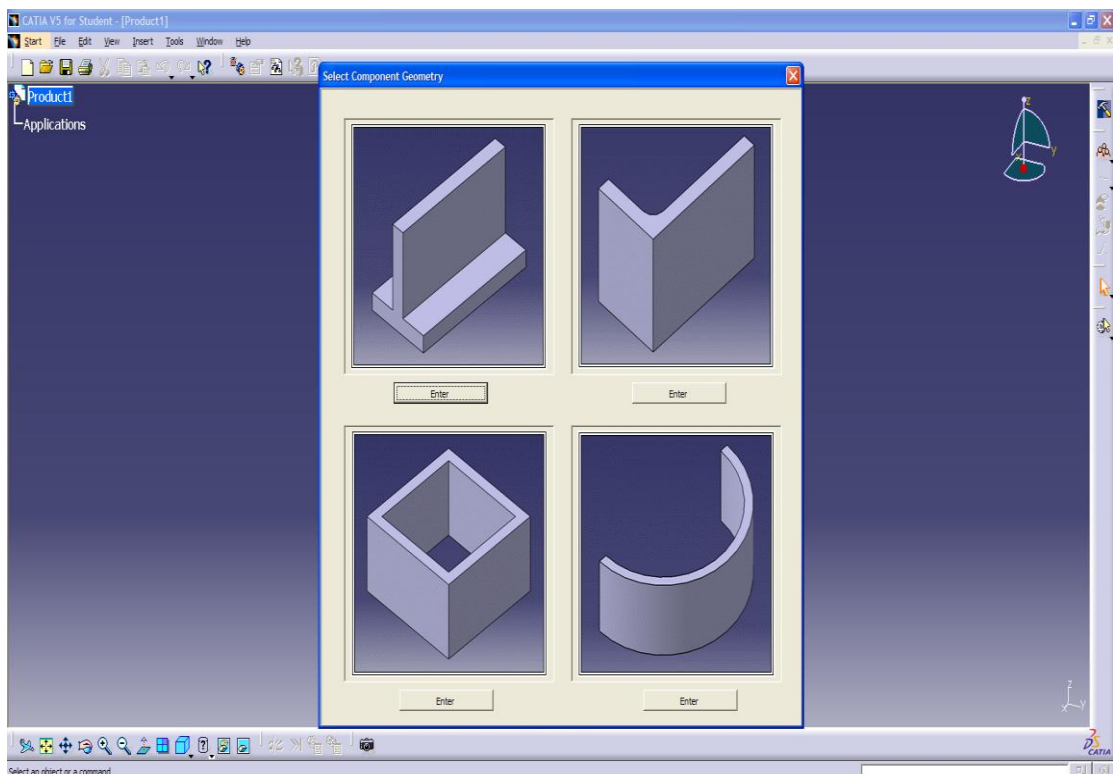


Figure 4.16: Sample window shows the developed GUI in CATIA for analysis input graphic information for different type of thin-wall components.

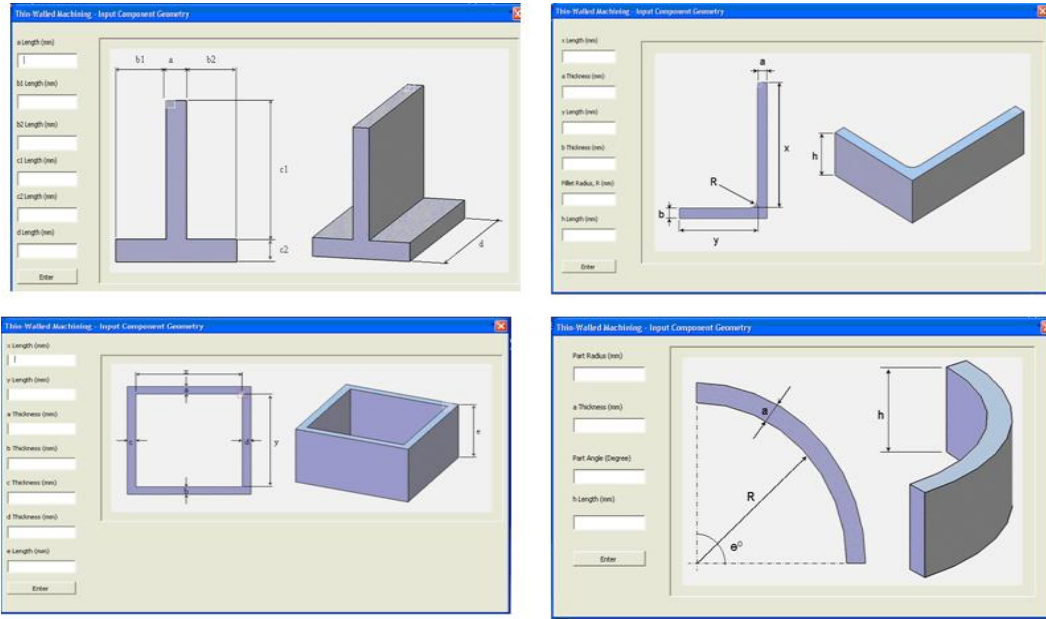


Figure 4.17: Sample window shows the GUI input alphanumeric information of part creation for different type of thin-wall components as in Section 4.3.2.

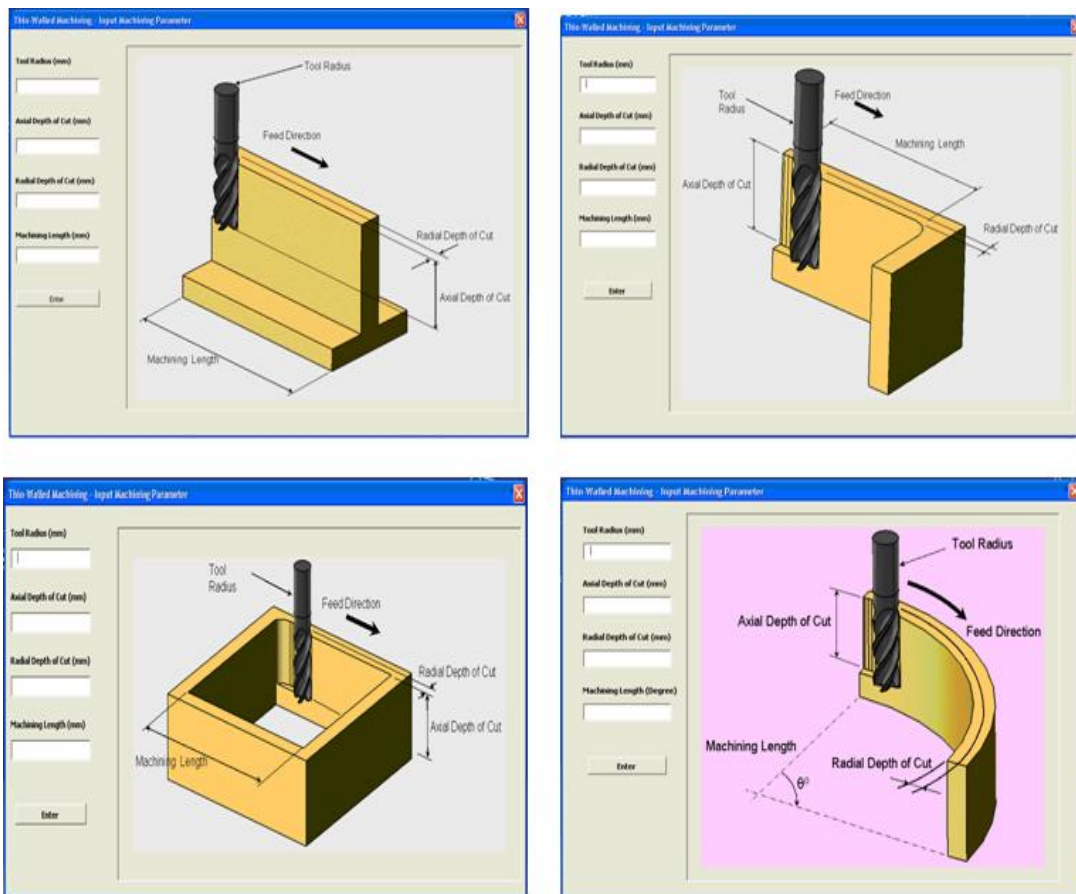


Figure 4.18: Sample window shows the GUI input alphanumeric information of material removal process for different type of thin-wall components as in Section 4.3.3.

4.5 Cutter Compensation Strategy

Once the prediction of wall deflection equations at different location along the wall length is established, the cutter location data need to be adjusted for cutter compensation method. The purpose of cutter compensation method is to eliminate the impact of the surface error on machining the thin wall feature. To perform the cutter compensation, the new cutter locations are created by offsetting the predicted deflection to the opposite direction with the same magnitudes. Based on this new cutter compensation data, the new NC codes are generated and replace the initial cutter location data to perform the machining compensation method. A detail explanation on cutter compensation method will be described later in Chapter 8.

4.6 Summary

The new hybrid methodology is an integrated FEA, statistical sampling and regression methodology that is designed to eliminate the excessive computational requirements in traditional FEA only analysis. The hybrid methodology consists of five models, each of which is designed on the most appropriate software platform including MATLAB, CATIA, MINITAB and VISUAL BASIC. The parameters in the system are validated by experiment data that form the basis of statistical hypothesis. Four basic thin-wall geometries feature that contain in typical aerospace monolithic component are developed at present and the system is flexible to take more complicated shape if

necessary. Once the hybrid model is developed, the regression model can produce suggested cutter compensation values in less than 10 seconds.

CHAPTER 5

CUTTING FORCE PREDICTION FOR HELICAL ENDMILL TOOL

5.1 Introduction

The prediction of cutting forces during machining is one of the key component models in the hybrid model for deflection prediction on machining thin-walled workpiece as it determines the magnitude of the wall deflection and dependent with the machining parameters. On the other hand, predictions of cutting forces in milling process are often needed for establishment of automation or optimisation in the cutting process. For a past few decades, there has been extensive research conducted in developing force models for the milling process. The development of force model can be classified in two approaches namely the mechanistic force model and the mechanics force model.

From literatures it revealed that the mechanistic force model gives an accurate milling force prediction compare to mechanics force model. Hence, mechanistic force model as shown in [174, 175, 176, 177, 179 and 180] was used for the cutting forces prediction in the hybrid model. The objective of this chapter is to validate the predicted cutting force generated during the machining process using a helical endmill cutter. This chapter will first explain the mechanistic force model approach and the engagement limits for the helical tool endmill. Then, experimental procedure for the determination of cutting force coefficients using the measured mean cutting force value will be explain. Lastly, the predicted cutting force are validate with the sets of experimental test.

5.2 Mechanistic Modelling of Milling Forces

In continuous cutting, the forces can be analytically modelled with a simple continuous expression as the tool is constantly immersed in the work material. However, in the case of interrupted cutting, a discontinuous expression is involved which complicates and limits the options for analytical analysis [178]. The orientation and magnitude of cutting forces constantly vary with time due to the rotation and travel of cutting tool at the same instant. In addition, the tool geometry and cutting parameters, such as feed rate and radial immersion affect the orientation and magnitude of the cutting forces.

In mechanistic force model approach, the cutting forces are related to average chip thickness by cutting force coefficient calibrated experimentally for a particular workpiece material tool pair [179]. Then, the cutting forces produced by the same cutter with different machining parameters can be predicted analytically by using the calibrated force coefficient.

By considering that the cutting forces are relative to the cutting area, the varying cutting forces can be analytically modelled using the corresponding cutting areas. Fundamentally, the cutting forces are a function of the chip geometry because the relative motion causes a chip geometry that varies with time. Hence, obtaining the instantaneous chip area throughout the tool rotation is important to estimate the cutting forces magnitude. As a first approximation, the forces during cutting are proportional to the instantaneous cutting area. Consider the milling force diagram in Figure 5.0 which

shown the elemental tangential, dF_t , and dF_r cutting forces acting on flute (j_{th}) of an end mill corresponding to an infinitesimal element thickness can be expressed as;

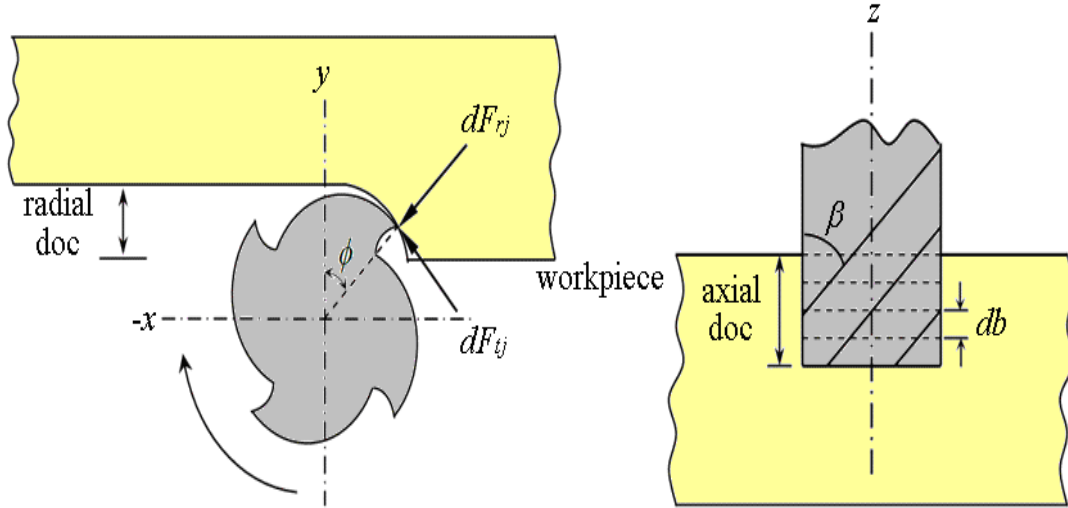


Figure 5.1: Differential milling forces applied on an end mill.

$$dF_{tj}(\phi, z) = [K_{te} + K_{tc}h_j(\phi, z)]dz \quad (5.0a)$$

$$dF_{rj}(\phi, z) = [K_{re} + K_{rc}h_j(\phi, z)]dz \quad (5.0b)$$

where;

dF_{tj} is differential force in the tangential direction

dF_{rj} is differential force in the radial direction

K_{tc} and K_{rc} are the specific cutting force coefficients for tangential and radial direction

K_{te} and K_{re} are specific edge cutting force coefficients for tangential and radial direction

ϕ is the tool's immersion angle start from positive y-axis.

At a certain location on the cutting edge, the chip thickness h_j , can be estimated as:

$$h_j(\phi, z) = f_i \sin \phi(z) \quad (5.1)$$

where

f_i is the feed per tooth and

$\phi(z)$ is the entry and exit angle for flute j at certain position in the axial direction, z .

Since in this study using a multiple flute helical endmill tool, due to the engagement of flutes at different axial tool locations, the force generated during the machining operation vary periodically along the tool axis. When multiple teeth are in contact with the work material during the cutting process, the cutting forces on each tooth are sum to obtain the total cutting forces generate by the too. The total possible number of teeth that is contact with the work material during the cutting process depends upon the depth of cut, the tool geometry, and the radial immersion [180]. In other words, there may not be any contact of cutter-workpiece at some points which resulting in zero intensity. Due to the helix effect on the cutting tool, the force intensities are shifted along the axial direction when the cutter rotates. In addition, the start or exit of the cutting edge is different along the tool vertical axis due to the helix angle inclination. Figure 5.2 shows the effect of helical endmill geometry which causes the delay to the cutting edge.

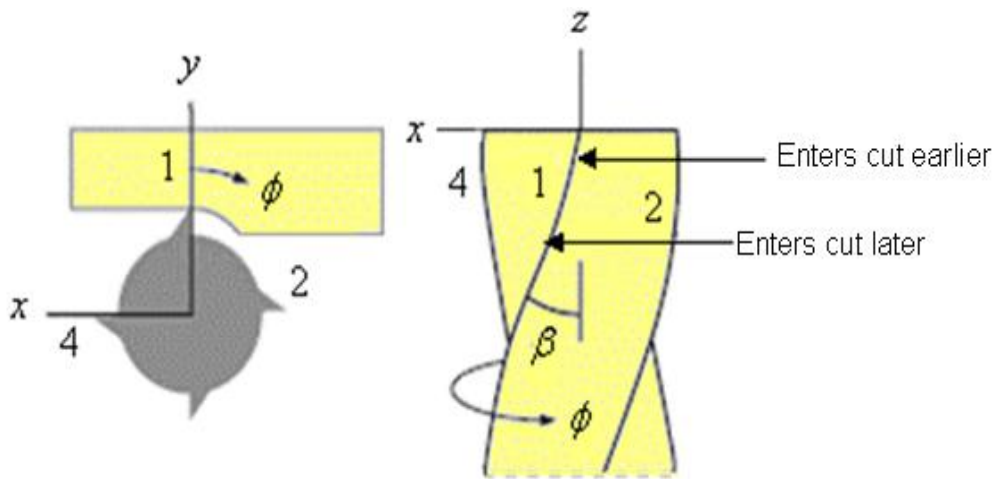


Figure 5.2: Delay cause by the helical end mill geometry on the cutting edge.

The unwrapped form of cylindrical end mill part surface in relation with engagement limits is shown in Figure 5.3. The cutting zone in the part surface is bounded by two vertical lines ϕ_{st} and ϕ_{ex} , and two horizontal lines $z = 0$ and $z = b$, where b is the axial depth of cut.

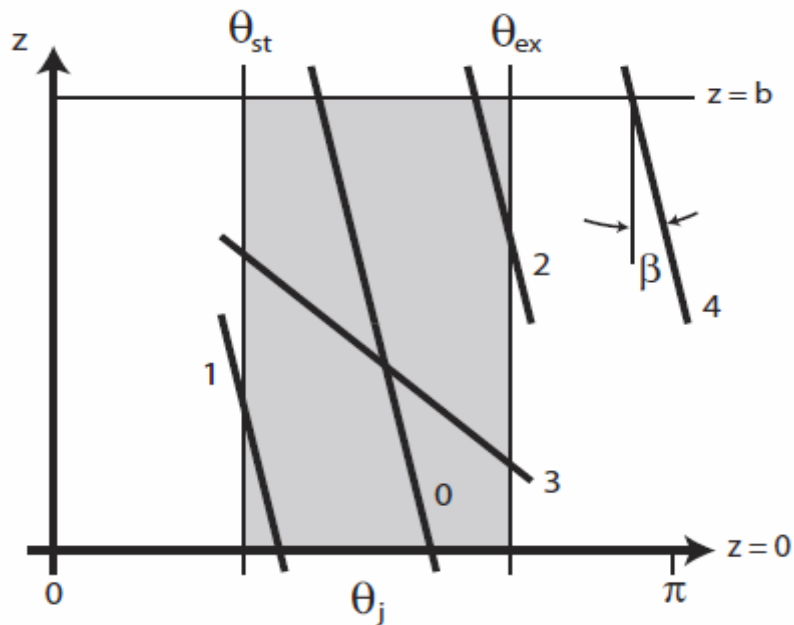


Figure 5.3: Helical endmill cutting zone contact cases [179].

In down milling ϕ_{ex} is always π and ϕ_{st} is always 0 in up milling condition. Based on Figure 5.3, the cutting tool enters into and exits out to the work material in four different possible intersections, in which; the depth of cut varies from case to case based on the tool rotation angle. The engagement limits are bounded between $z = 0$ and $z = b$ in the vertical axis. The engagement limits for the intersection for the different cases, shown in Figure 5.3, are as follows:

$$\text{If } \frac{2 \tan \beta b}{D} \leq \phi_{ex} - \phi_{st}$$

$$\text{For case 1, } \phi_{st} \leq \phi \leq \frac{2b \tan \beta}{D}, z_{jl} = 0 \text{ and } z_{ju} = \frac{D\phi}{2 \tan \beta}$$

$$\text{For case 0, } \frac{2b \tan \beta}{D} \leq \phi \leq \phi_{ex} - \phi_{st}, z_{jl} = 0 \text{ and } z_{ju} = b$$

$$\text{For case 2, } \phi_{ex} - \phi_{st} \leq \phi \leq \phi_{ex} - \phi_{st} + \frac{2b \tan \beta}{D}, z_{jl} = \frac{D\phi - 2(\phi_{ex} - \phi_{st})}{2 \tan \beta} \text{ and } z_{ju} = b$$

$$\text{For case 4, } \phi_{ex} - \phi_{st} + \frac{2b \tan \beta}{D} < \phi, \text{ the tooth is not engaged.}$$

$$\text{If } \frac{2 \tan \beta b}{D} > \phi_{ex} - \phi_{st}$$

$$\text{For case 1, } \phi_{st} \leq \phi \leq \phi_{ex} - \phi_{st}, z_{jl} = 0 \text{ and } z_{ju} = \frac{D\phi}{2 \tan \beta}$$

$$\text{For case 3, } \phi_{ex} - \phi_{st} \leq \phi \leq \frac{2b \tan \beta}{D}, z_{jl} = \frac{D\phi - 2(\phi_{ex} - \phi_{st})}{2 \tan \beta} \text{ and } z_{ju} = b$$

$$\text{For case 2, } \phi_{ex} - \phi_{st} \leq \phi \leq \phi_{ex} - \phi_{st} + \frac{2b \tan \beta}{D}, z_{jl} = \frac{D\phi - 2(\phi_{ex} - \phi_{st})}{2 \tan \beta} \text{ and } z_{ju} = b$$

$$\text{For case 4, } \phi_{ex} - \phi_{st} + \frac{2b \tan \beta}{D} < \phi, \text{ the tooth is not engaged.}$$

Once the engagement limit is determined, the tangential and radial forces given by Equation 5.0a and 5.0b are transformed to the feed, x and normal, y direction. The total milling forces produced on each tooth are integrated and summed within the engagement limit using Equation 5.2a and 5.2b to obtain the total instantaneous forces magnitude.

$$F_{xj}(\phi) = \frac{R}{\tan \beta} \left\{ K_{te} \sin \phi(z) - K_{re} \cos \phi(z) + \frac{f_t}{4} [K_{rc} (2\phi(z) - \sin 2\phi(z)) - K_{tc} \cos 2\phi(z)] \right\}_{z_{jl}}^{z_{ju}} \quad (5.2a)$$

$$F_{yj}(\phi) = -\frac{R}{\tan \beta} \left\{ -K_{re} \sin \phi(z) - K_{te} \cos \phi(z) + \frac{f_t}{4} [K_{tc} (2\phi(z) - \sin 2\phi(z)) + K_{rc} \cos 2\phi(z)] \right\}_{z_{jl}}^{z_{ju}} \quad (5.2b)$$

where

$z_{jl}(\phi)$ is the lower axial engagement limits of the in cut portion of the flute j

$z_{ju}(\phi)$ is the upper axial engagement limits of the in cut portion of the flute j .

5.3 Determination of Cutting Force Coefficients

The cutting force coefficients are determine using the experimental mean cutting force by fitting points in the data as a function of chip loads. The mean milling force is determine by considering the nonzero switching function and summation of force for all teeth and can be written as [180]:

$$\bar{F}_x = \left[\frac{N_i b f_i}{8\pi} (-K_{tc} \cos(2\phi) + K_{rc}(2\phi - \sin 2\phi)) + \frac{N_i b}{2\pi} (K_{te} \sin(\phi) - K_{re} \cos(\phi)) \right]_{\phi_{st}}^{\phi_{ex}} \quad (5.3)$$

$$\bar{F}_y = \left[\frac{N_i b f_i}{8\pi} (K_{tc}(2\phi - \sin(2\phi)) + K_{rc}(\cos(2\phi))) - \frac{N_i b}{2\pi} (K_{te} \cos(\phi) - K_{re} \sin(\phi)) \right]_{\phi_{st}}^{\phi_{ex}} \quad (5.4)$$

For slotting with 100% radial immersion, $\phi_{st} = 0$ and $\phi_{ex} = 180$ deg, hence Equations 5.3 and 5.4 can be simplify to;

$$\bar{F}_x = \frac{N_i b K_{rc}}{4} f_i + \frac{N_i b K_{re}}{\pi} \quad (5.5)$$

$$\bar{F}_y = \frac{N_i b K_{tc}}{4} f_i + \frac{N_i b K_{te}}{\pi} \quad (5.6)$$

Equations 5.5 and 5.6 show the mean force expressions for x and y direction, which represents the function of chip loads and cutting force coefficients. By fitting points in the data as a function of chip loads and mean force value, the cutting force coefficients can be determine using the slope and intercept values and can be written as;

$$K_{rc} = \frac{4a_{1x}}{N_i b} \quad ; \quad K_{re} = \frac{\pi \cdot a_{0x}}{N_i b} \quad (5.7)$$

$$K_{tc} = \frac{4a_{1y}}{N_i b} \quad ; \quad K_{te} = \frac{\pi \cdot a_{0y}}{N_i b} \quad (5.8)$$

The obtained cutting force coefficients from Equations 5.7 and 5.8 were use in Equations 5.2a and 5.2b to calculate the total instantaneous forces generate in the milling process.

5.4 Experimental Cutting Force Coefficients

Several slotting tests were performed to obtain the cutting force coefficients for a particular tool-workpiece material combination. The experimental procedure consists of mean cutting force acquisition for a series of slotting tests at varying chip loads. Experimental cutting force data were obtained for a 6 mm diameter, 4-flute carbide endmill with 38 helix angle. A block of Ti-6Al-4V workpiece with a thickness of 20 mm was mounted on a Kistler three-component dynamometer. The chip loads are varying in the range of 0.0125 – 0.125 mm/tooth in 0.0125 mm/tooth steps with a 2 mm axial depth of cut. The mean cutting forces in each x and y directions were measured for each run and plotted as a function of the chip loads per tooth as shown in Figure 5.4. Once the relation between the mean cutting force and chip loads are obtained, the cutting force coefficients can be determined using the slope and intercept values as in Section 5.3.

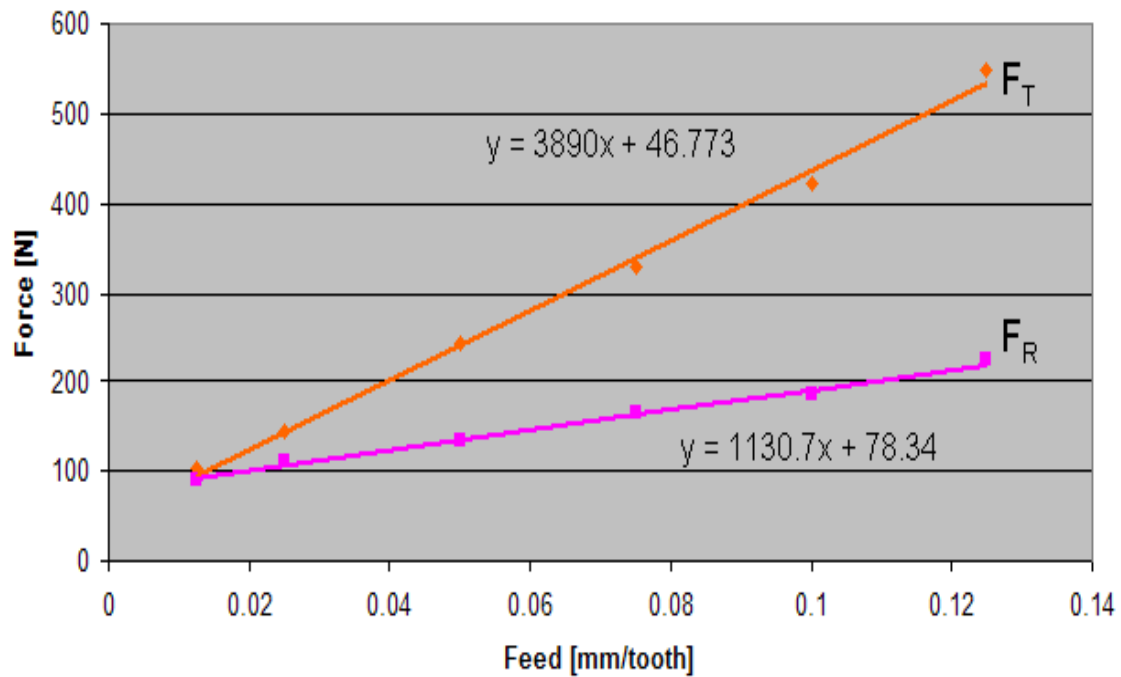


Figure 5.4: Relation between feed per tooth and mean force per revolution for slotting condition.

A statistical test was performed to validate the fitting data. From the statistical test indicates a significant relation between mean force and chip loads with coefficient of determination, r^2 values of 0.9963 and 0.995 for F_t and F_r respectively. Using Equations 5.7 through 5.8 and the slope and intercept values from the fitting data, the cutting force coefficients (K_{rc} , K_{tc} , K_{re} and K_{te}) are determined and are presented in Table 5.1.

Table 5.1: Estimated cutting constants and edge constants for the milling force prediction.

Coefficients	
K_{tc} [N/mm ²]	1945
K_{te} [N/mm]	18.375
K_{rc} [N/mm ²]	565.35
K_{re} [N/mm]	30.776

5.5 Comparison Between Predicted and Experiment Cutting Forces

In order to verify the predicted cutting forces, a similar set of cutting experiment have been carried out. Both up-milling and down-milling conditions with a different set of machining parameter were carried out using a 6 mm diameter carbide endmill. The workpiece material was Ti-6Al-4V titanium alloy with a Young modulus of $1.14 \times 10^{11} \text{ N/m}^2$ and Yield Strength of $8.25 \times 10^8 \text{ N/m}^2$. The cutting force coefficients K_{rc} , K_{tc} , K_{re} and K_{te} were identified from experiments as in the previous section. The predicted cutting forces for feed direction (F_x) and normal direction (F_y) were compared with the measured experimental forces at a sampling rate of 1 ms intervals. Table 5.2 shows the cutting parameter used for both prediction and experimental cutting force.

Table 5.2: Cutting parameter used for both prediction and experimental cutting force.

Run	Speed (rpm)	Feed (mmpt)	ADOC (mm)	RDOC (%)	Start Angle (Degree)	Exit Angle (Degree)
1	3500	0.06	10	25	0	41.41
2	3500	0.06	10	50	0	60
3	3500	0.04	10	75	0	75.52
4	3500	0.06	10	25	138.59	180
5	3500	0.06	10	50	120	180
6	3500	0.04	10	75	104.48	180

Figures 5.5 through 5.7 shows a sample of predicted and experiment cutting forces for up-milling condition for a different set of machining parameters. While, Figures 5.8 through 5.10 shows a sample of predicted and experiment cutting forces for down-milling condition for a different set of machining parameters. From the result, it

can be observed that the cutting force increases with increasing radial immersion especially for the normal direction (F_y) for both up-milling and down-milling condition which agreed with the result obtained from literatures for machining titanium alloys [181, 182 and 183]. In addition, increasing the feed rate increase the cutting forces in feed direction (F_x). For the cutting conditions used in this study, it is generally observed that the predicted forces are in very good agreement with the experimental forces.

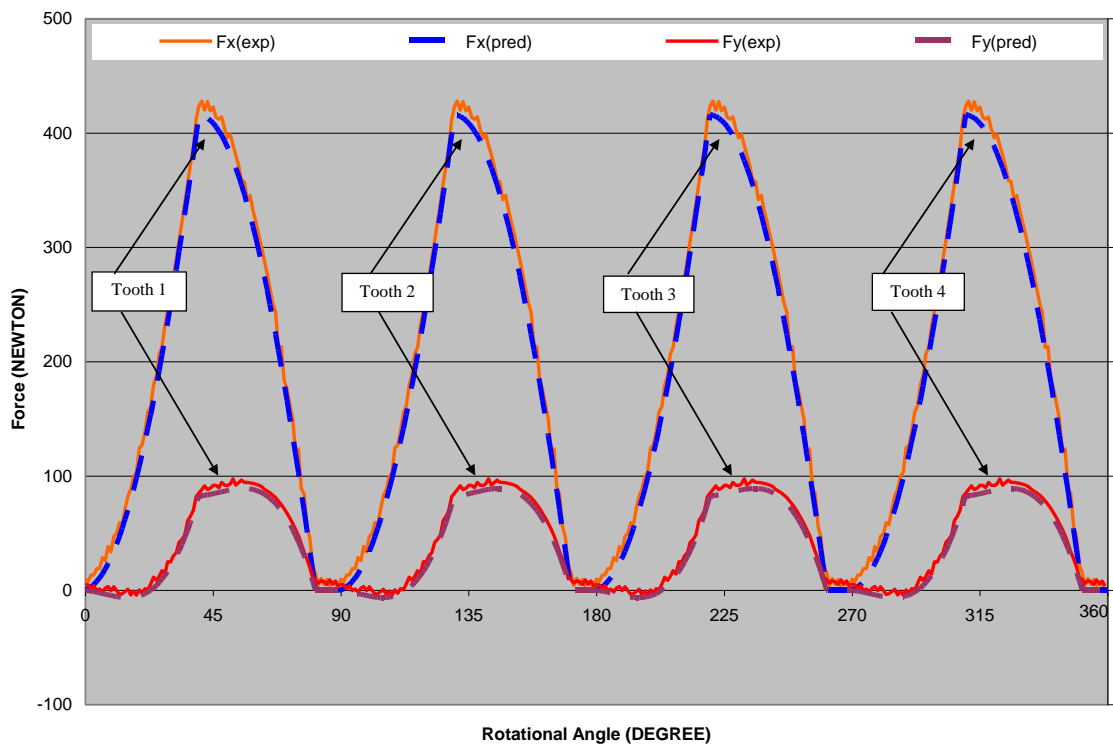


Figure 5.5: Comparison between predicted and experimental cutting forces. (Material: Ti6Al4V, 25% immersion up-milling, $ft = 0.06$ mm/tooth, ADOC = 10 mm, $S = 3500$ rpm; tool: 4 flute carbide end mill, $d = 6$ mm)

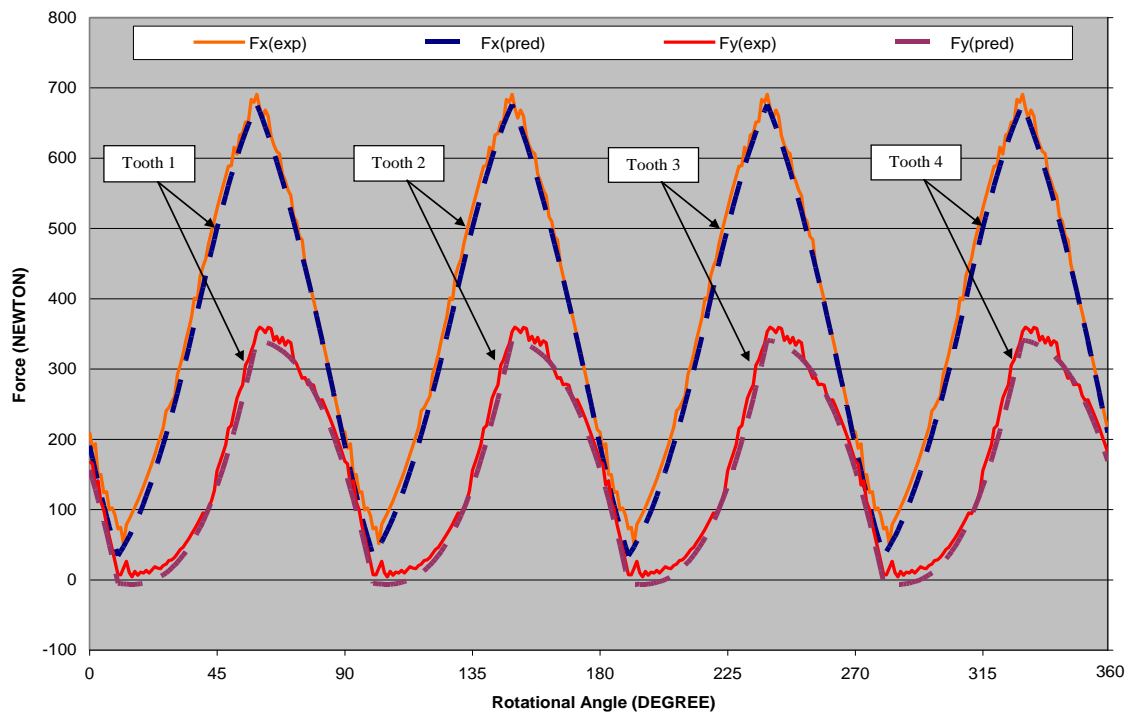


Figure 5.6: Comparison between predicted and experimental cutting forces. (Material: Ti6Al4V, 50% immersion up-milling, $f_t = 0.06$ mm/tooth, ADOC = 10 mm, $S = 3500$ rpm; tool: 4 flute carbide end mill, $d = 6$ mm)

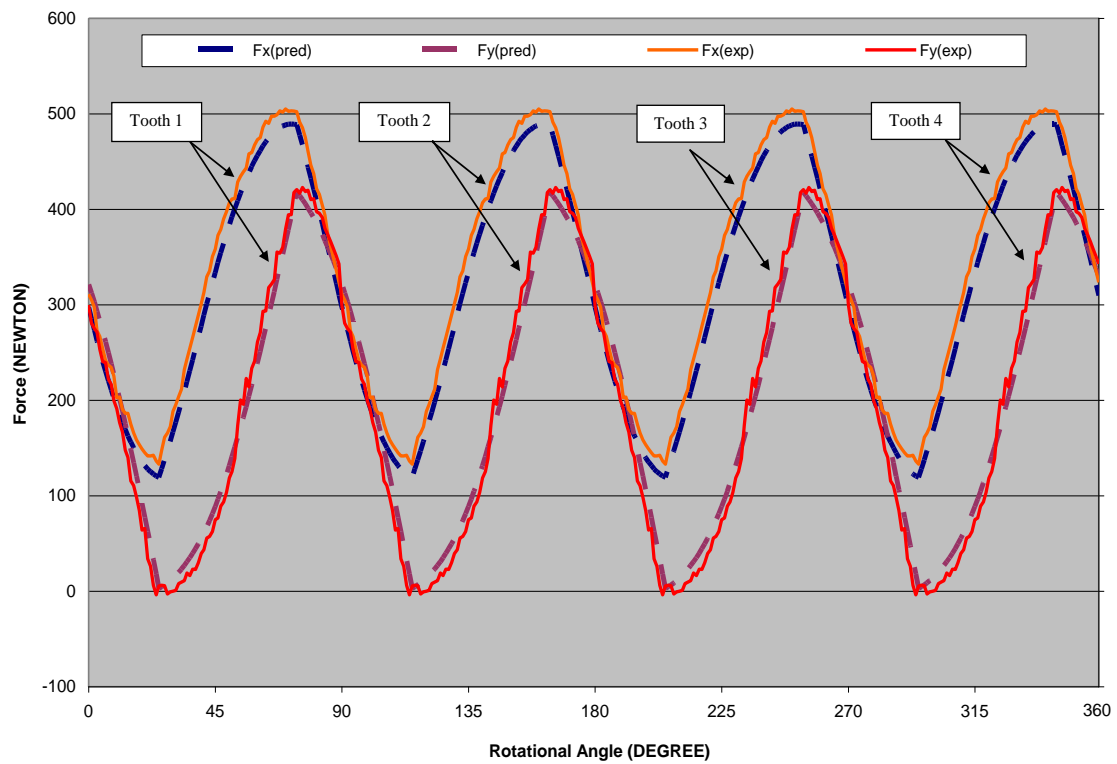


Figure 5.7: Comparison between predicted and experimental cutting forces. (Material: Ti6Al4V, 75% immersion up-milling, $f_t = 0.04$ mm/tooth, ADOC = 10 mm, $S = 3500$ rpm; tool: 4 flute carbide end mill, $d = 6$ mm)

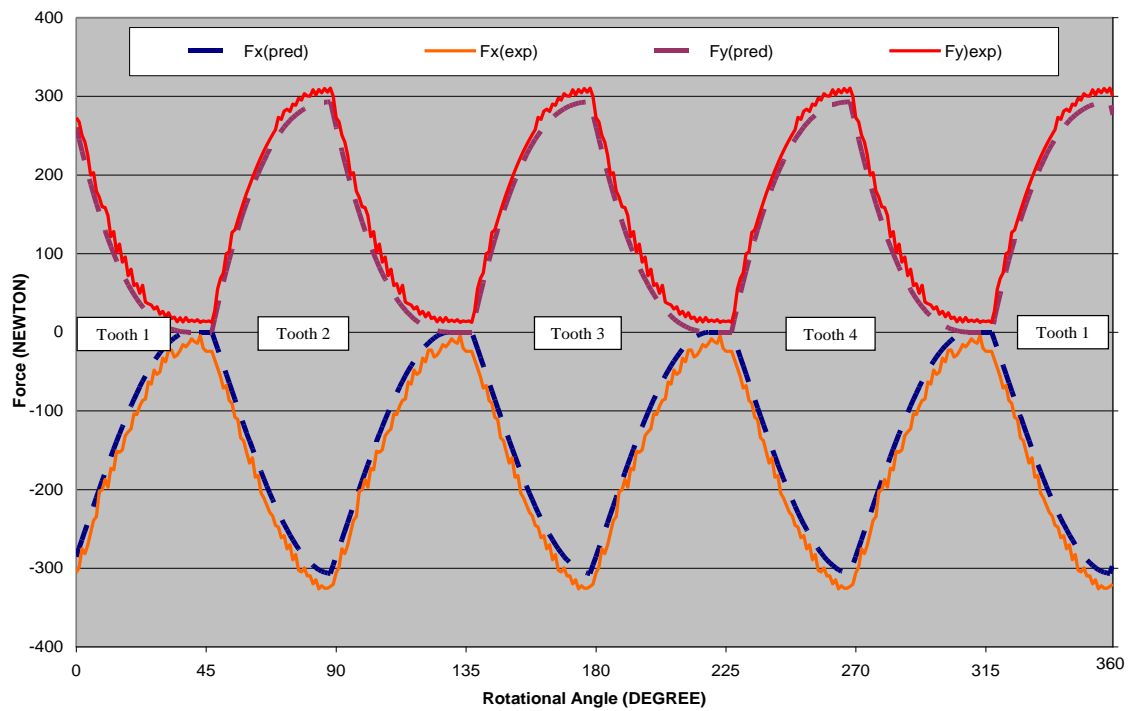


Figure 5.8: Comparison between predicted and experimental cutting forces. (Material: Ti6Al4V, 25% immersion down-milling, $f_t = 0.06$ mm/tooth, ADOC = 10 mm, $S = 3500$ rpm; tool: 4 flute carbide end mill, $d = 6$ mm)

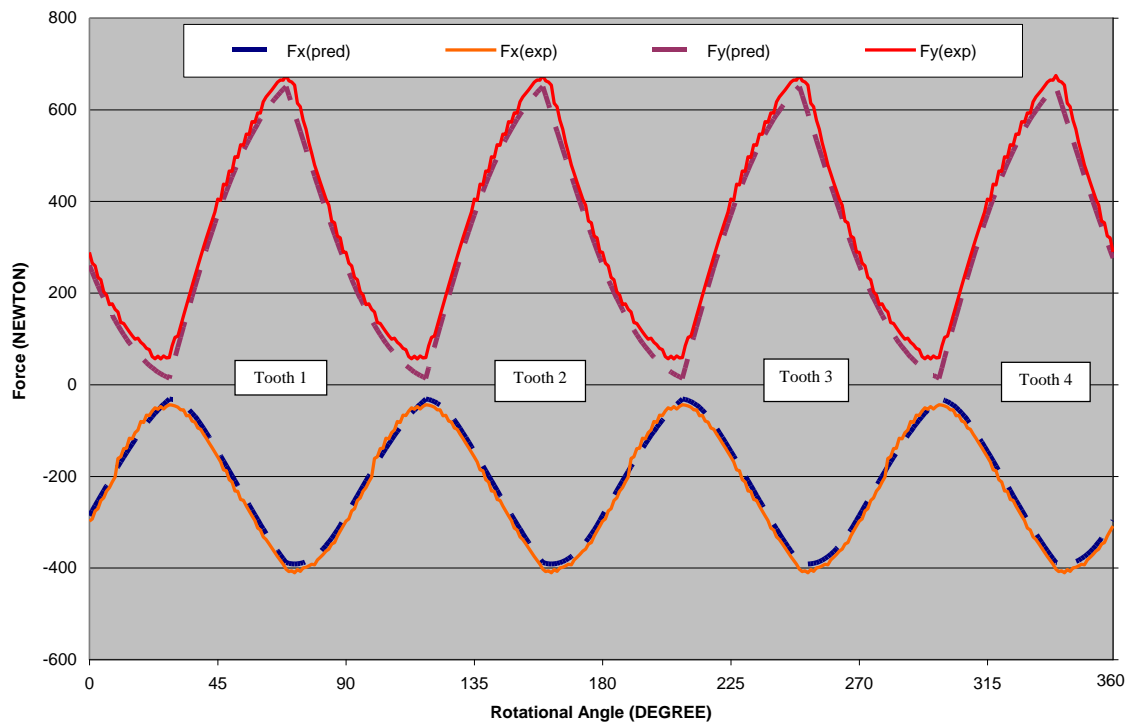


Figure 5.9: Comparison between predicted and experimental cutting forces. (Material: Ti6Al4V, 50% immersion down-milling, $f_t = 0.06$ mm/tooth, ADOC = 10 mm, $S = 3500$ rpm; tool: 4 flute carbide end mill, $d = 6$ mm)

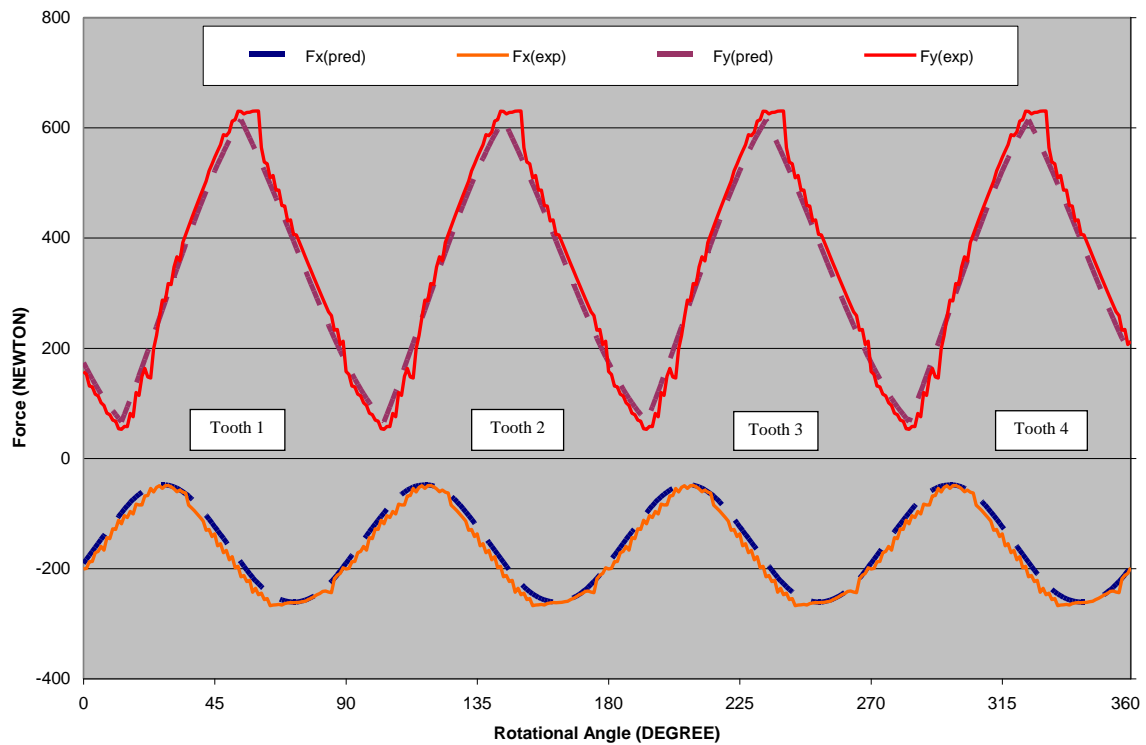


Figure 5.10: Comparison between predicted and experimental cutting forces. (Material: Ti6Al4V, 75% immersion down-milling, $f_t = 0.04$ mm/tooth, ADOC = 10 mm, $S = 3500$ rpm; tool: 4 flute carbide end mill, $d = 6$ mm)

5.6 Summary

The mechanistic cutting force model and experimental procedure to determine the cutting force coefficients via linear regression were presented. The cutting force coefficients were determined using the measure mean cutting force at varying chip loads for a particular tool-workpiece material combination. Using the cutting force coefficients obtained, the analytical cutting force are validate with the sets of experimental test. The predicted forces generated by using the force model showed good agreement with the experimentally measured forces. The prediction of cutting forces during machining is one of the key component models in the hybrid model for

deflection prediction on machining thin-wall workpiece as it determine the magnitude of the wall deflection and dependent with the machining parameters. The calculated cutting force will be as an input for the deflection analysis model as in Section 4.3.4.

CHAPTER 6

Modelling Part Deflection for Thin-Wall Machining

6.1 Introduction

Deformation or part deflection is more likely to occur in the machining of thin-wall part due to weaker stiffness of thin wall [184]. Investigations on the effect of structural deflections on the cutting process are necessitated to ensure the dimensional accuracy of the machine part. In engineering analysis, bodies of complex geometry subjected to multiple boundary conditions and loading are often encountered. Under such complex conditions it is difficult to derive a theoretical solution for the continuum. Experimentation is usually carried out to obtain the solution for the continuum which usually time consuming and expensive [185]. To overcome the disadvantage, Finite Element method (FEM) is used for modelling the analysis which discretize a complex continuum into a finite number of regions. The solution is obtained at the discrete nodes, which approximates the solution for the continuum at those points in space and time instead of trying to get the solution for the entire continuum, which has infinite number of points.

This chapter validates the predicted wall deflection for the deflection analysis model as described in Section 4.3.4. This chapter will first explain briefly the finite element formulation for deflection analysis. Then, the procedure to perform the finite element analysis for wall deflection will be explained. Lastly, the predicted wall deflection for each component case as in Section 4.4 are validate with the sets of experimental test.

6.2 Finite Element Formulation for Deflection Analysis

The finite element analysis was developed to take into account the change in component stiffness due to material removal. A finite element formulation for deflection analysis can be found in numerous books [186, 187, 188, 189, 190, 191 and 192]. Only a brief explanation on finite element formulation for deflection analysis is presented. Fundamentally, the equilibrium equation of a solid element structure is solved for the displacement configuration using the force-displacement relationship, as;

$$\{F\} = [K] \{d\} \quad (6.0)$$

where,

$\{F\}$ is the vector of nodal forces for the structure,

$[K]$ is the assembled stiffness matrix,

$\{d\}$ is the vector of nodal displacement.

The stiffness matrix, $[K]$ and the force vector, $\{Q\}$ of the 3D structure are expressed as [3];

$$[K] = \int_V [B]^T \{\sigma\} dV = \int_V [B]^T [E][B] dV \quad (6.1)$$

$$\{Q\} = \int_V [N]^T F dV + \sum_i \{P_i\} \quad (6.2)$$

where,

[B] strain-displacement matrix,

{ σ } stress vector,

[N] matrix of shape functions,

{F} body forces,

{P} concentrated forces on the nodes,

[E] elasticity matrix.

The elasticity matrix, [E] consists of modulus of elasticity, E and the Poisson's ratio, ν and can be expressed by;

$$[E] = \frac{E}{(1+\nu)(1-2\nu)} \begin{bmatrix} (1-\nu) & \nu & \nu & 0 & 0 & 0 \\ \nu & (1-\nu) & \nu & 0 & 0 & 0 \\ \nu & \nu & (1-\nu) & 0 & 0 & 0 \\ 0 & 0 & 0 & \frac{1-2\nu}{2} & 0 & 0 \\ 0 & 0 & 0 & 0 & \frac{1-2\nu}{2} & 0 \\ 0 & 0 & 0 & 0 & 0 & \frac{1-2\nu}{2} \end{bmatrix} \quad (6.3)$$

The strain-displacement matrix [B] relates the strains, { ϵ } to the displacement of the structure, {d} as;

$$\{\epsilon\} = [B]\{d\} \quad (6.4)$$

where;

$$\{\varepsilon\} = \begin{Bmatrix} \varepsilon_x \\ \varepsilon_y \\ \varepsilon_z \\ \gamma_{xy} \\ \gamma_{yz} \\ \gamma_{zx} \end{Bmatrix}; \quad [\mathbf{B}] = \begin{bmatrix} \frac{\partial}{\partial x} & 0 & 0 \\ 0 & \frac{\partial}{\partial y} & 0 \\ 0 & 0 & \frac{\partial}{\partial z} \\ \frac{\partial}{\partial y} & \frac{\partial}{\partial x} & 0 \\ 0 & \frac{\partial}{\partial z} & \frac{\partial}{\partial y} \\ \frac{\partial}{\partial z} & 0 & \frac{\partial}{\partial x} \end{bmatrix}; \quad [\mathbf{d}] = \begin{bmatrix} u \\ v \\ w \end{bmatrix} \quad (6.5)$$

where u, v and w are the displacement in x, y and z directions. Once the shape functions and the displacement boundary conditions for the model are defined, the nodal displacement for the structural component can be solved.

6.3 FEM Solution Procedure

CATIA ELFINI finite element solver was used to compute the static case solution of individual element. A MACRO is developed to perform the tasks automatically in CATIA Generative Structural Analysis workbench. The procedure to perform the deflection analysis following a step by step process as follow:

1. *Call mrr(i+1).CATPart file*: The pre-defined material removal part file from the material removal model are call. The pre-defined material removal part contains the component geometry data, material properties, location of the cutter along

the feed direction and the cutting conditions data. Once the data is loaded, the part is send to CATIA Generative Structural Analysis workbench for the finite element analysis.

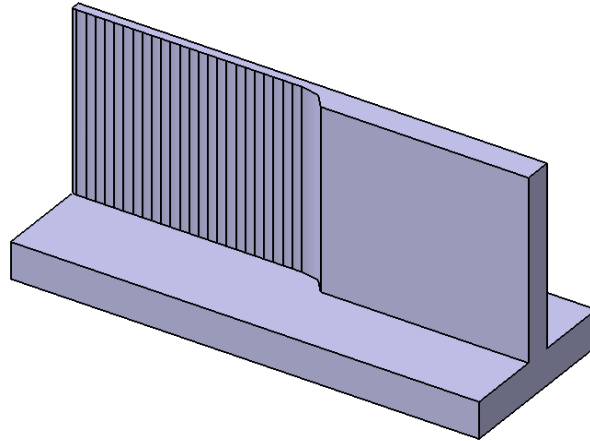


Figure 6.1: The pre-defined material removal part file from the material removal model.

2. *Discretize the part:* The component is divided into discrete number of elements which contains the coordinates of the nodes and the node numbers for elements. A uniform mesh size OCTREE 3D isoparametric-parabolic tetrahedron mesh is generated which associate with the component.

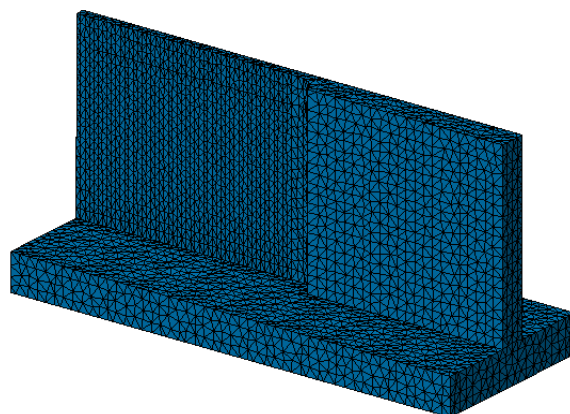


Figure 6.2: OCTREE 3D isoparametric-parabolic tetrahedron mesh associate with the component.

3. *Assign boundary condition:* Once the meshing of the component is completed, a boundary condition is assign to the component. For this case, the bottom surface of the component is fixed in all direction similarly as clamping the component on the machine table.

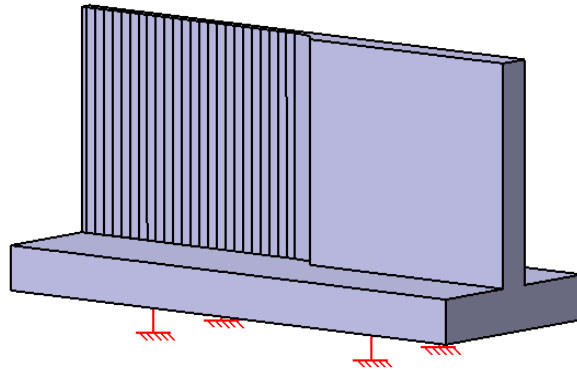


Figure 6.3: Boundary condition assign to the bottom surface of the component.

4. *Assign load vectors:* The calculated cutting forces from the machining loads model are call and places on the relevant nodes in the transient surface of the component as in Section 4.3.4.

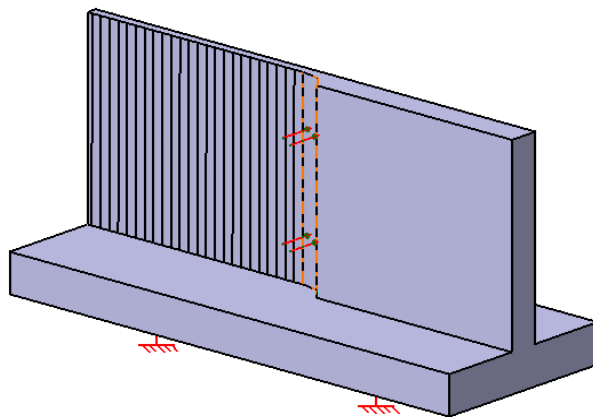


Figure 6.4: Calculated cutting forces from the machining loads model are call and places on the relevant nodes in the transient surface of the component.

5. *Perform the static analysis:* By assembling and solving the finite element equations for each element, the displacements of the wall component at a pre-defined cutter feed step are obtained. The FEA results which contain the displacement values are stored in a knowledge-based template and saved in a native *ASCII file* format.

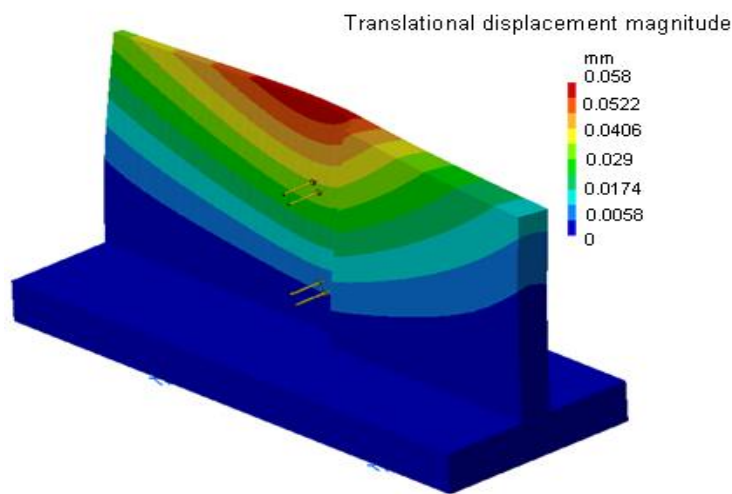


Figure 6.5: Sample window shows the FEA results of the displacement values.

6.4 Part Deflection Validation

In order to verify the predicted part deflection, a similar set of cutting experiment have been carried out. A number of simulations and experiments have been carried out to demonstrate the capabilities of the model. The wall deflection is measured using five Lion Precision ECL 130 inductive displacement sensors. The sensors are mounted at five different equal locations ($S1=0$, $S2=1/4L$, $S3=1/2L$, $S4=3/4L$ and $S5=L$) along the back of the wall. The signals from the displacement sensors are acquire

at a sampling rate of 1 *ms* intervals using National Instrument DAQ card and been analyse using LabVIEW 8.5.1. A 6 mm diameter 4-flute carbide endmill with 38 helix angle carbide endmill was used to machine the thin-wall feature. To eliminate the effect of localize thermal expansion on the machined surface, a small radial of cut were used for all runs. The workpiece material was Ti-6Al-4V titanium alloy with a Young modulus of $1.14 \times 10^{11} \text{ N/m}^2$, Yield Strength of $8.25 \times 10^8 \text{ N/m}^2$ and Poisson ratio of 0.34. The part deflections for all four different component features as in Section 4.4 were validate using a different machining parameter and component attribute. To obtain a precise thin-wall feature without surface errors before the experimental run, all the components are machined using a step method which alternately milling each side of the wall with depth of cut increment [193]. The cutting parameter and component attribute are obtained from the industrial partner Production Parts Pty. Ltd. Australia, for finishing cycle on machining titanium alloy monolithic component. Figure 6.6 shows the experimental setup for result validation.

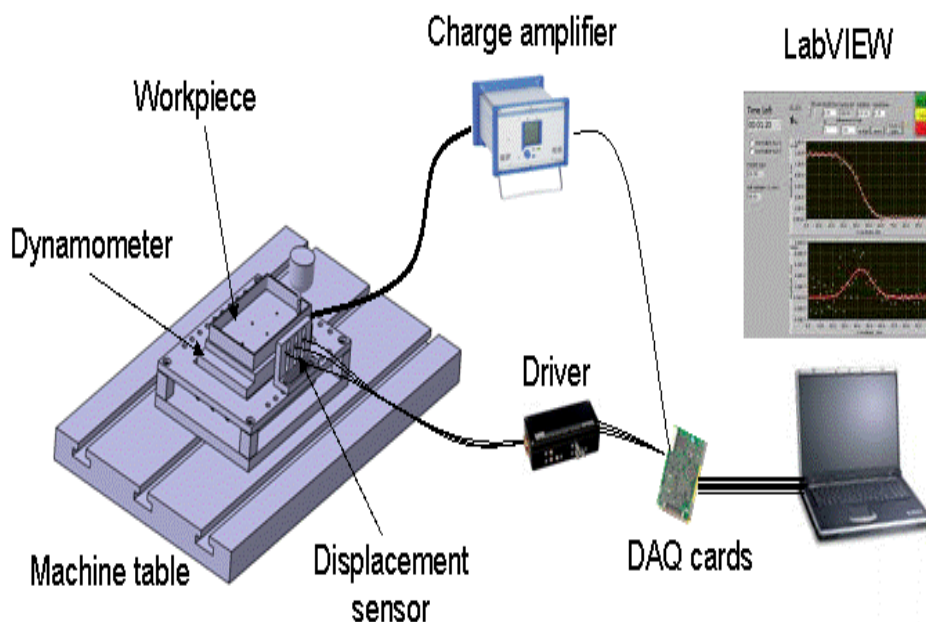


Figure 6.6: Experimental set-up for model validation.

6.4.1 Case 1: T-Shape Component

Table 6.1 shows the cutting parameter and component attribute for the T-Shape Component. A number of simulations and experiments set of cutting parameter and component attribute were performed to analyse the effects of the processing parameter and component attribute to the magnitude of wall deflection. The sensors are mounted at five different equal locations ($S1=0$, $S2=1/4L$, $S3=1/2L$, $S4=3/4L$ and $S5=L$) along the back of the wall. The response of the wall deflection between simulation and experiment were observed and compared for every 5 mm feed step increments.

Figure 6.7 shows the example of displacement values for the five sensors between simulation and experiment for the T-Shape component. From the results obtained from simulation and experiment it can be observed that the deflection magnitudes for the T-Shape component for all the runs are maximums at the two ends. In which, the end of the machining step experienced the maximum deflection compare at the start of the machining step due to the decreasing stiffness of the wall as a result of material removal and the unsupported features at both ends. To a large extent, the more flexible the wall the higher the deflection magnitudes generated. The minimum deflection magnitude for the T-Shape component occurred at the middle of the component length. It can be seen that the machining parameter and component attributes are the key factors in determining the magnitude of deflection as evidenced in the simulation and experimental results.

Table 6.1: Cutting parameter and component attribute use in simulation and experiment for the T-Shape Component.

Machining parameter and component attribute	
a (mm)	2.5 - 4.5
b1 (mm)	10.0
b2 (mm)	10.0
c1 (mm)	10.0 – 20.0
c2 (mm)	5.0
x (mm)	80 - 150
Speed (rpm)	2700 - 4500
Feed Rate (mm/tooth)	0.03 - 0.08
Radial DOC (mm)	0.2 - 3.0
Tool Diameter (mm)	6 (4-flutes)

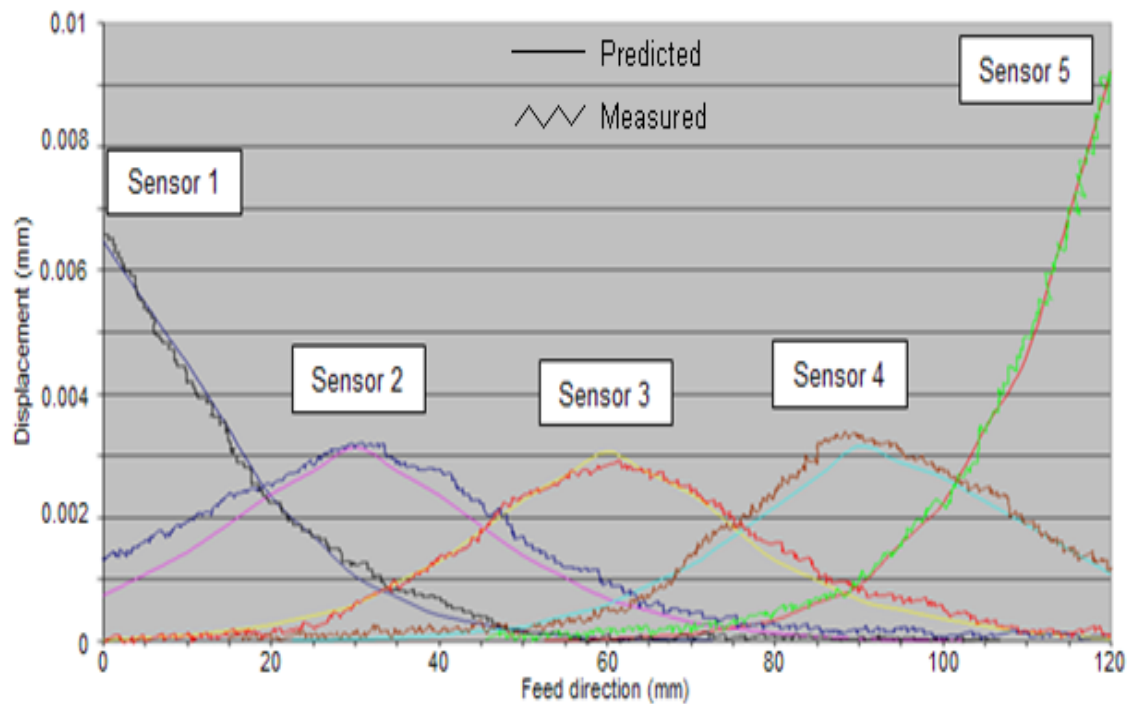


Figure 6.7: A sample window of displacement values for the five sensors between simulation and experiment for the T-Shape component. Machining parameter: $S = 3500$ rpm, $ft = 0.05$ mm/tooth, $rdoc = 0.4$ mm. Component attribute: $a = 2.5$ mm, $c1 = 20$ mm and $x = 120$ mm.

The machining parameter contributes to the magnitudes of the force generated in the machining process while the component attributes reflect the stiffness and rigidity of the wall. Both the displacement magnitude obtained by simulation and experiment are closely match. From the cut plane analysis of the wall, it shows that the upper wall experienced the maximum deflection and is smallest at the bottom of the wall as shown in Figure 6.8.

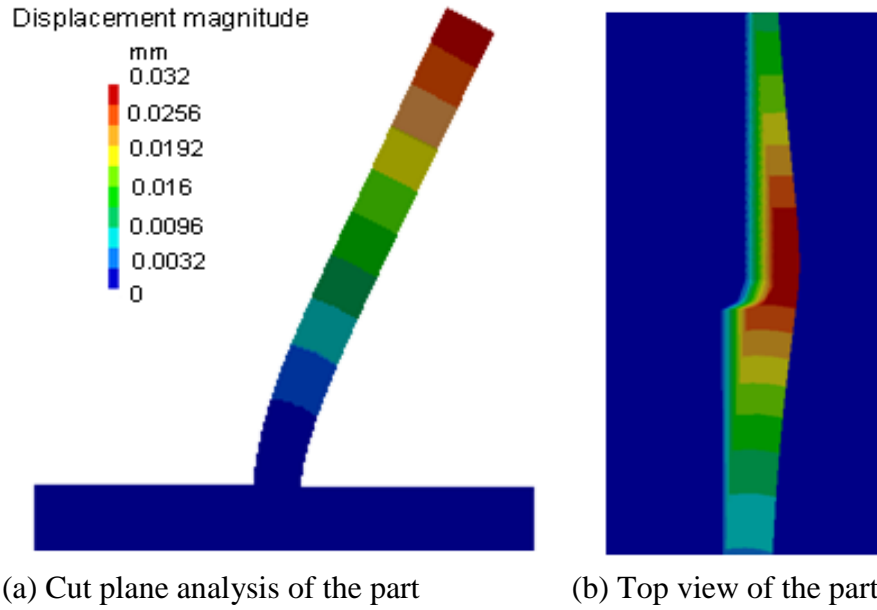


Figure 6.8: Deflection analysis result for T-Shape component at the middle of cutter feed location.

6.4.2 Case 2: L-Shape Component

Table 6.2 shows the cutting parameter and component attribute for the L-Shape Component. A number of simulations and experiments set of cutting parameter and component attribute were performed to analyse the effects of the processing parameter and component attribute to the magnitude of wall deflection. Only one side of the wall dimension (a, x and h) in which machining takes place were varied and the rest (b and y) were kept constant. The sensors are mounted at five different equal locations ($S1=0$, $S2=1/4x$, $S3=1/2x$, $S4=3/4x$ and $S5=x$) along the back of the wall in which the response of the wall deflection between simulation and experiment were observed and compared for every 5 mm feed step increments.

Table 6.2: Cutting parameter and component attribute use in simulation and experiment for the L-Shape Component.

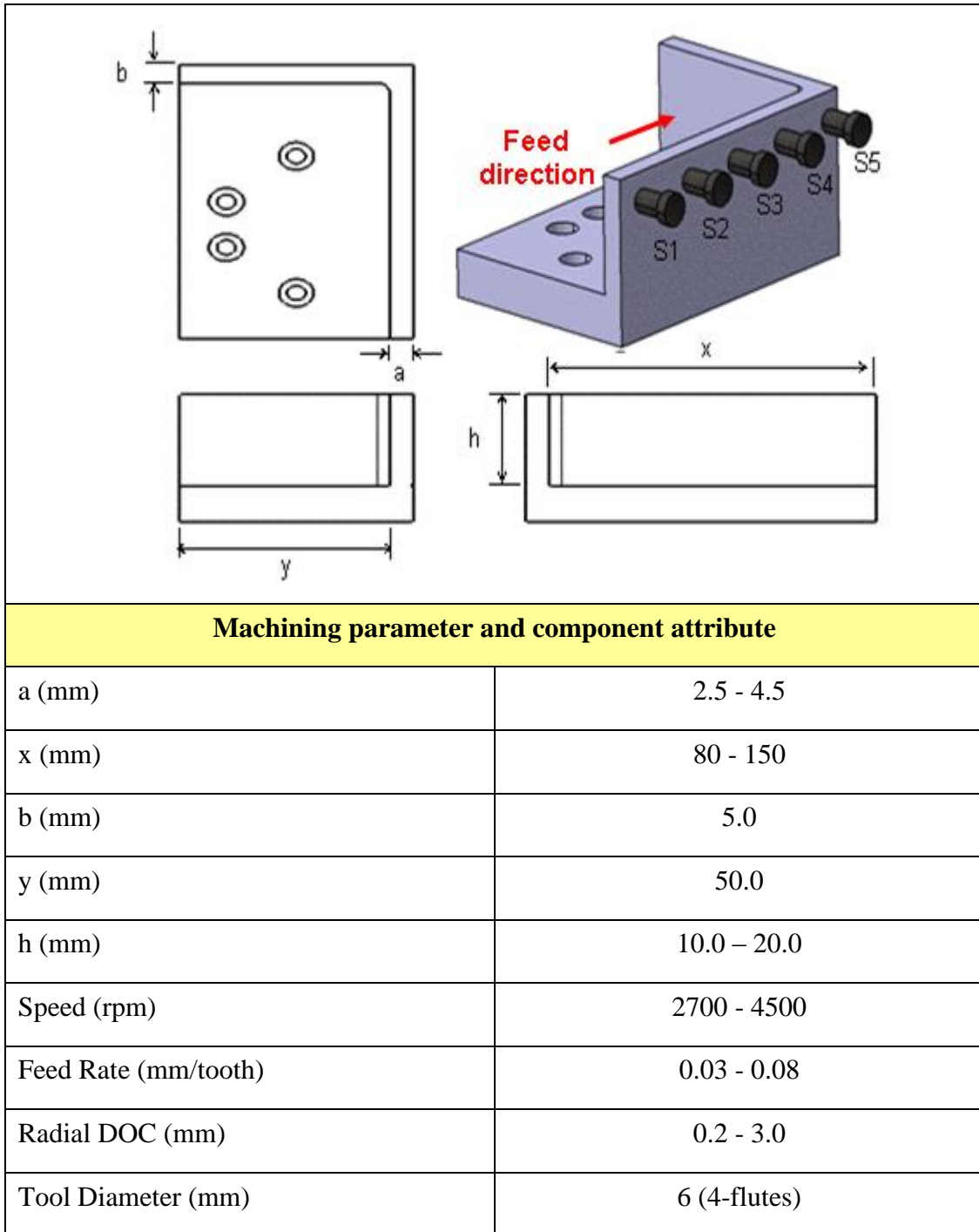


Figure 6.9 shows the example of displacement values for the five sensors between simulation and experiment for the L-Shape component. From the results

obtained from simulation and experiment it can be observed that the deflection magnitudes for all the runs are maximums at the start of machining step and decrease towards the end as a result of supported features at one side. From the simulation and experimental results for the T-Shape component, it shows that the component attributes and machining parameter are the important factors in determining the magnitude of wall deflection.

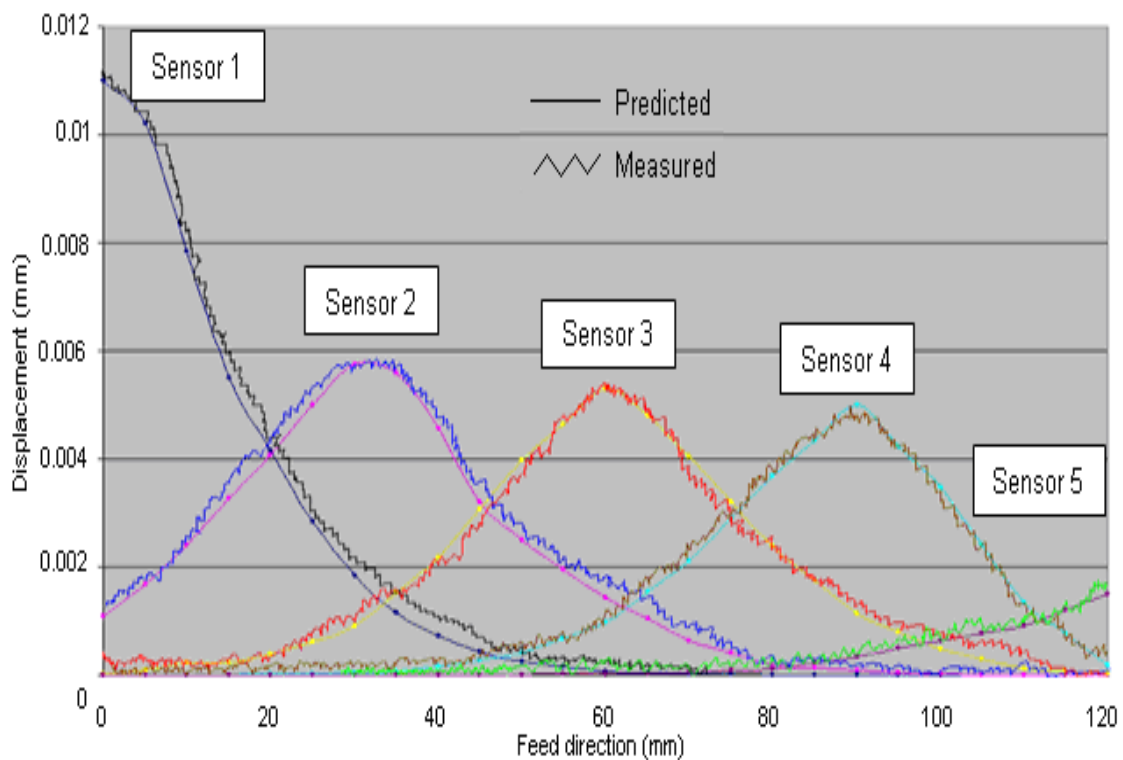


Figure 6.9: A sample window of displacement values for the five sensors between simulation and experiment for the L-Shape component. Machining parameter: $S = 3500$ rpm, $ft = 0.05$ mm/tooth, $rdoc = 0.4$ mm. Component attribute: $a = 2.5$ mm, $c1 = 20$ mm and $x = 120$ mm.

The machining parameter contributes to the magnitudes of the force generated in the machining process while the component attributes reflect the stiffness and rigidity of the wall. Both the displacement magnitude obtained by simulation and experiment are

closely match. From the cut plane analysis of the wall, it shows that the upper wall experienced the maximum deflection and is smallest at the bottom of the wall as shown in Figure 6.10.

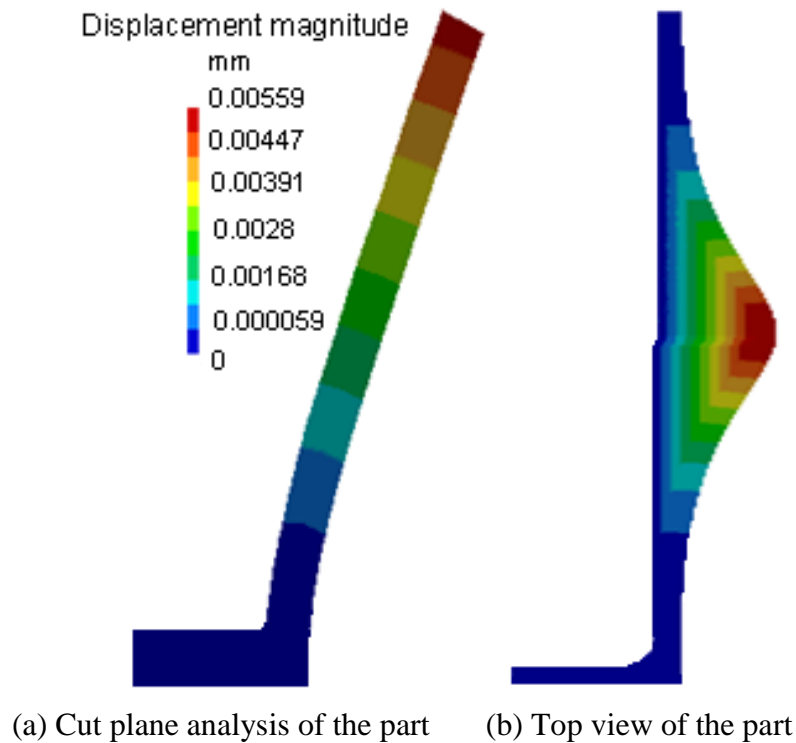


Figure 6.10: Deflection analysis result for L-Shape component at the middle of cutter feed location.

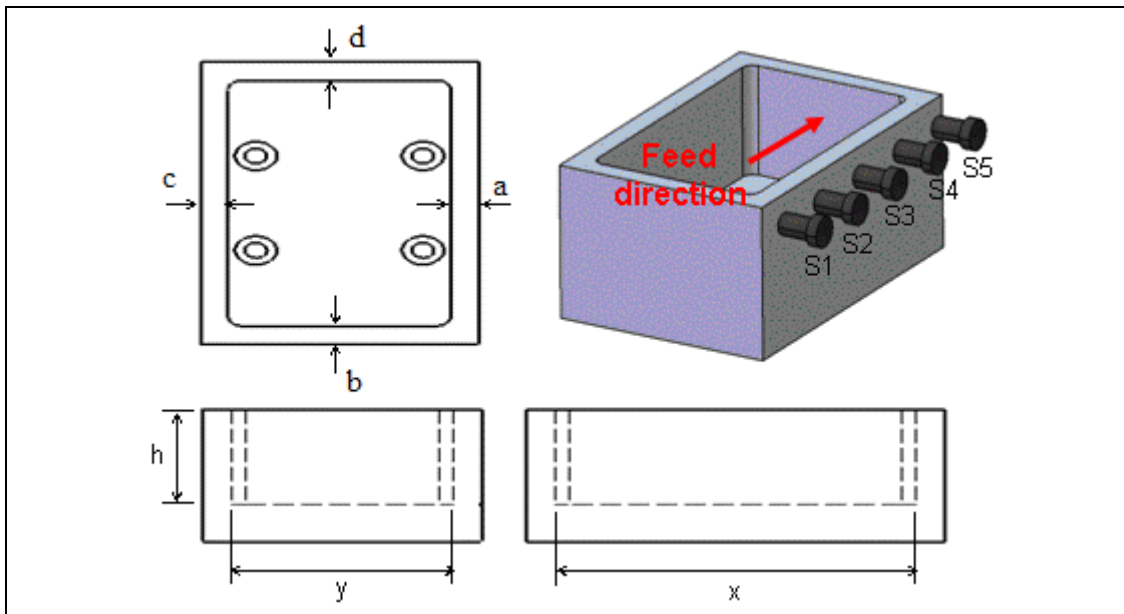
6.4.3 Case 3: Rectangular Pocket Component

Table 6.3 shows the cutting parameter and component attribute for the rectangular pocket component. A number of simulations and experiments set of cutting parameter and component attribute were performed to analyse the effects of the processing parameter and component attribute to the magnitude of wall deflection. Only one side of the wall dimension (b, x and h) in which machining take place were varied

and the rest (a, c, d and y) were kept constant. The sensors are mounted at five different equal locations ($S1=0$, $S2=1/4x$, $S3=1/2x$, $S4=3/4x$ and $S5=x$) along the back of the wall. The response of the wall deflection between simulation and experiment was observed and compared for every 5 mm feed step increments.

Figure 6.11 shows the example of displacement values for the five sensors between simulation and experiment for the rectangular pocket component. From the results obtained from simulation and experiment it can be observed that the deflection magnitudes for all the runs for the rectangular pocket component are maximums at the centre of wall length as a result of supported features at both side. Due to the decreasing stiffness of the wall as a result of material removal, there is an increasing value of deflection magnitudes between two regions (start and end) in the feed direction. From the simulation and experimental results for the rectangular pocket component, it shows that the component attributes and machining parameter are the important factors in determining the magnitude of wall deflection.

Table 6.3: Cutting parameter and component attribute use in simulation and experiment for the rectangular pocket component.



Machining parameter and component attribute	
a (mm)	2.5 - 4.5
b (mm)	5.0
c (mm)	5.0
d (mm)	5.0
x (mm)	80 - 150
y (mm)	50.0
h (mm)	10.0 – 20.0
Speed (rpm)	2700 - 4500
Feed Rate (mm/tooth)	0.03 - 0.08
Radial DOC (mm)	0.2 - 3.0
Tool Diameter (mm)	6 (4-flutes)

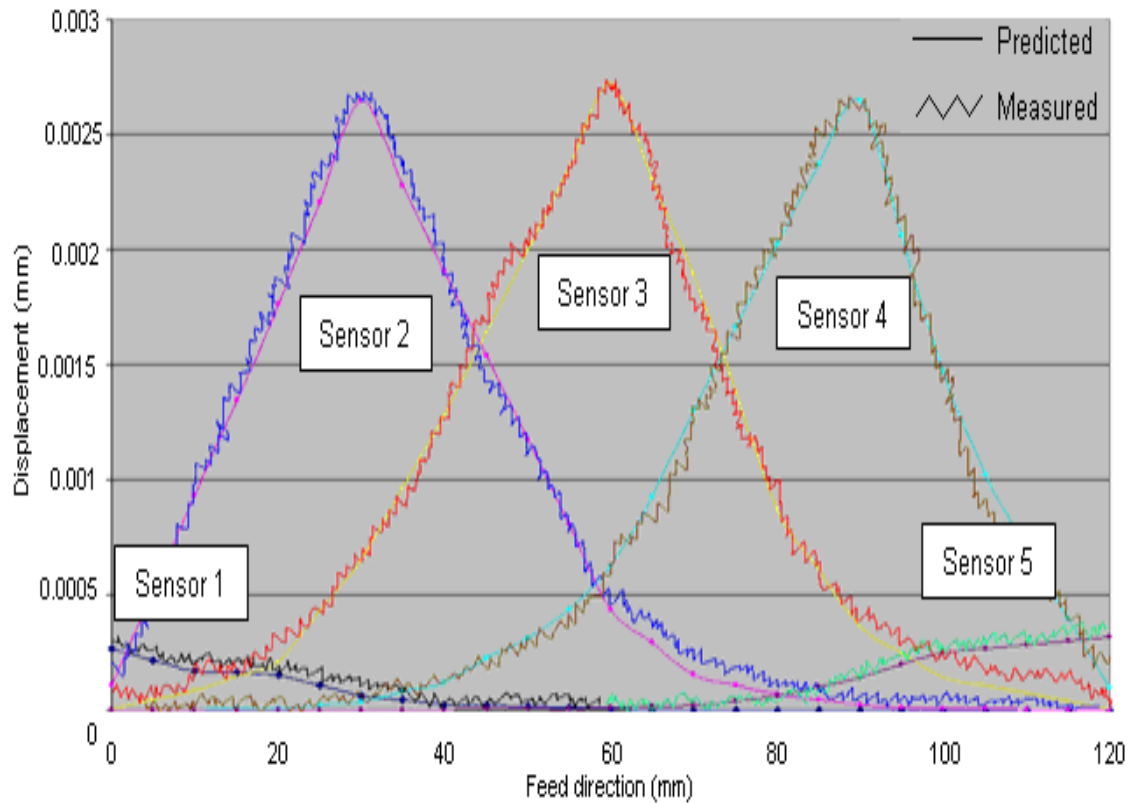
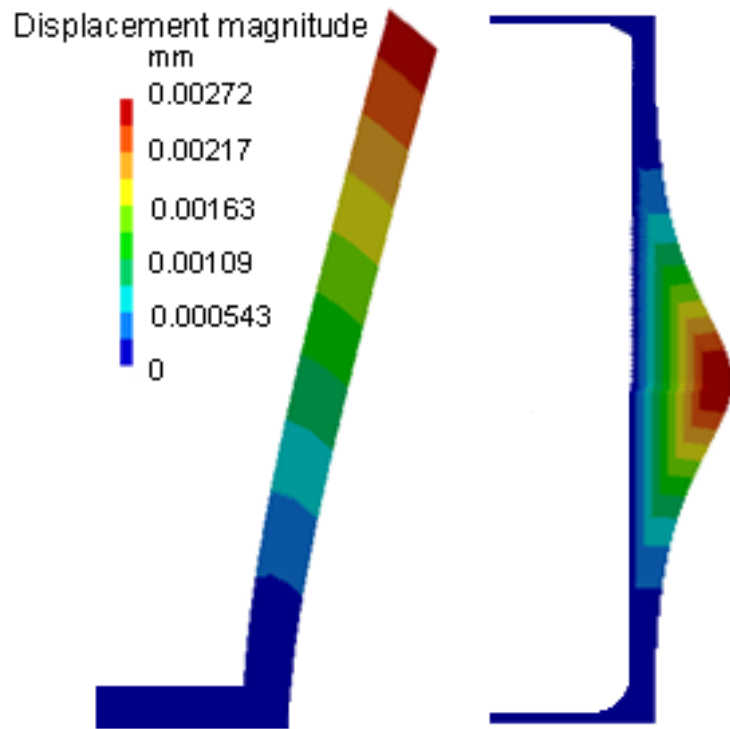


Figure 6.11: A sample window of displacement values for the five sensors between simulation and experiment for the rectangular pocket component. Machining parameter: $S = 3500$ rpm, $ft = 0.05$ mm/tooth, $rdoc = 0.4$ mm. Component attribute: $a = 2.5$ mm, $cI = 20$ mm and $x = 120$ mm.

The machining parameter contributes to the magnitudes of the force generated in the machining process while the component attributes reflect the stiffness and rigidity of the wall. Both the displacement magnitude obtained by simulation and experiment are closely match. From the cut plane analysis of the wall, it shows that the upper wall experienced the maximum deflection and is smallest at the bottom of the wall as shown in Figure 6.12.



(a) Cut plane analysis of the part (b) Top view of the part

Figure 6.12: Deflection analysis result for the rectangular pocket component at the middle of cutter feed location.

6.4.4 Case 4: Circular Component

Table 6.4 shows the cutting parameter and component attribute for the circular component. A number of simulations and experiments set of cutting parameter and component attribute were performed to analyse the effects of the processing parameter and component attribute to the magnitude of wall deflection. The sensors are mounted at five different equal locations ($S1=0$, $S2=1/4\theta$, $S3=1/2\theta$, $S4=3/4\theta$ and $S5=\theta$) along the back of the wall. The response of the wall deflection between simulation and experiment were observed and compared for every 5 mm feed step increments.

Table 6.4: Cutting parameter and component attribute use in simulation and experiment for the circular component.

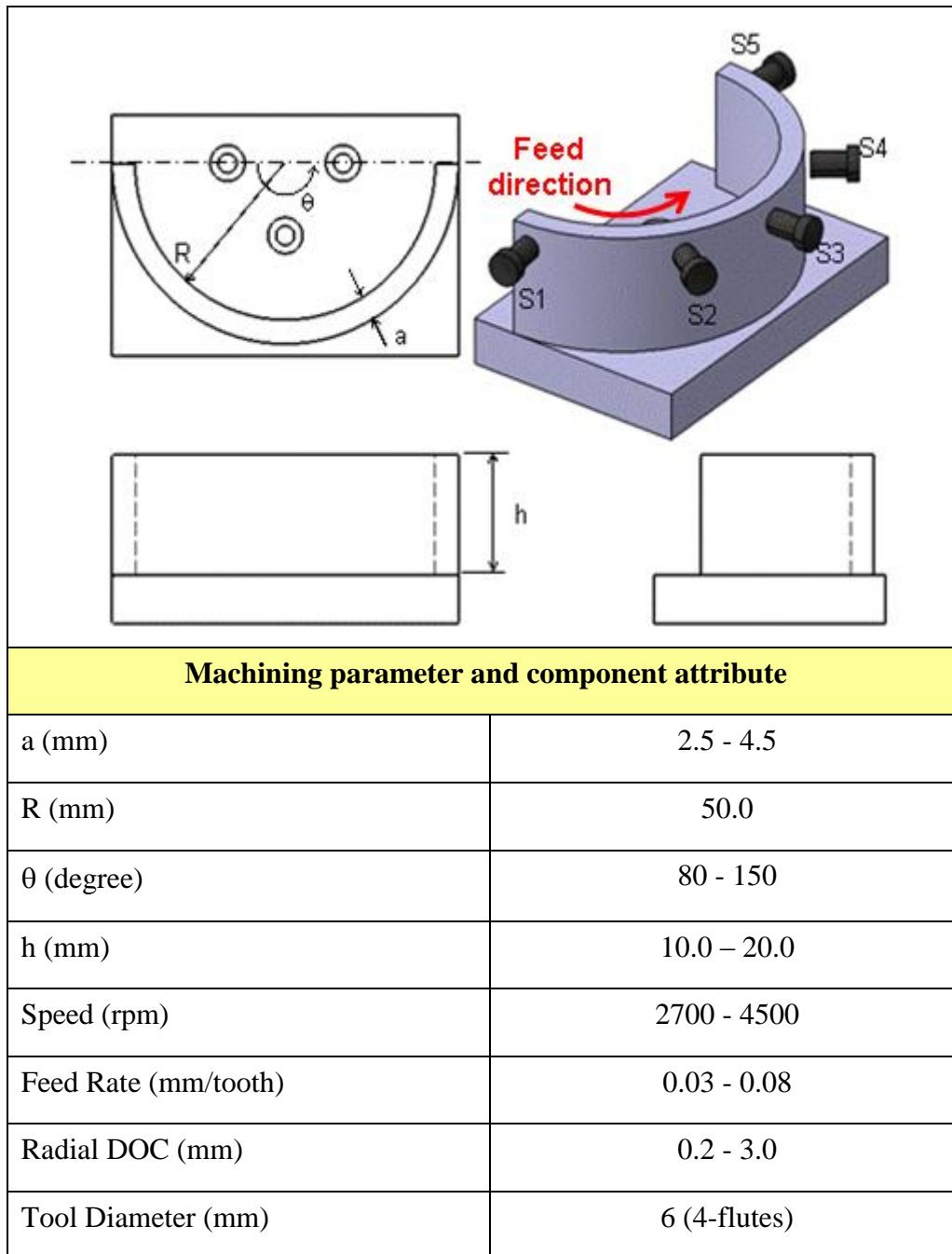


Figure 6.13 shows the example of displacement values for the five sensors between simulation and experiment for the circular component. From the results obtained from simulation and experiment it can be observed that the deflection

magnitudes for the circular component for all the runs are maximums at the two ends. In which, the end of the machining step experienced the maximum deflection compare at the start of the machining step due to the decreasing stiffness of the wall as a result of material removal and the unsupported features at both ends. To a large extent, the more flexible the wall is, the higher the deflection magnitude generates. The minimum deflection magnitude for the circular component occurred at the middle of the component length. It can be seen that the machining parameter and component attributes are the key factors in determining the magnitude of deflection as evidence in the simulation and experimental results.

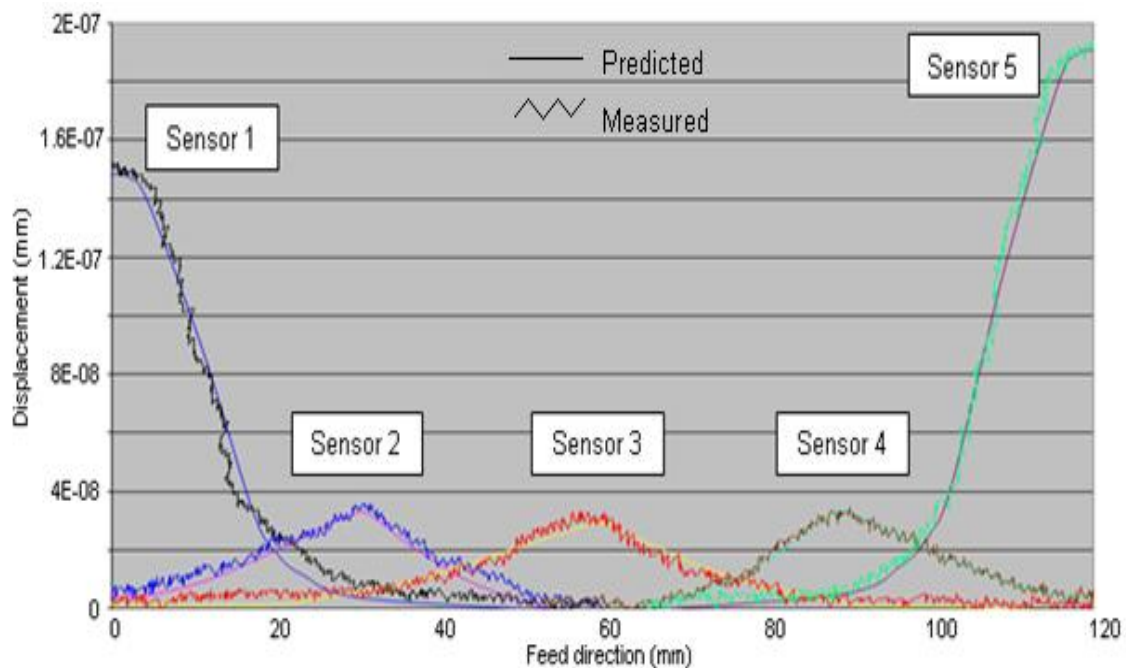


Figure 6.13: A sample window of displacement values for the five sensors between simulation and experiment for the circular component. Machining parameter: $S = 3500$ rpm, $ft = 0.05$ mm/tooth, $rdoc = 0.4$ mm. Component attribute: $a = 2.5$ mm, $cl = 20$ mm and $\theta = 120$ degree.

The machining parameter contributes to the magnitudes of the force generated in the machining process while the component attributes reflect the stiffness and rigidity of

the wall. Both the displacement magnitude obtained by simulation and experiment are closely match. From the cut plane analysis of the wall, it shows that the upper wall experienced the maximum deflection and is smallest at the bottom of the wall as shown in Figure 6.14.

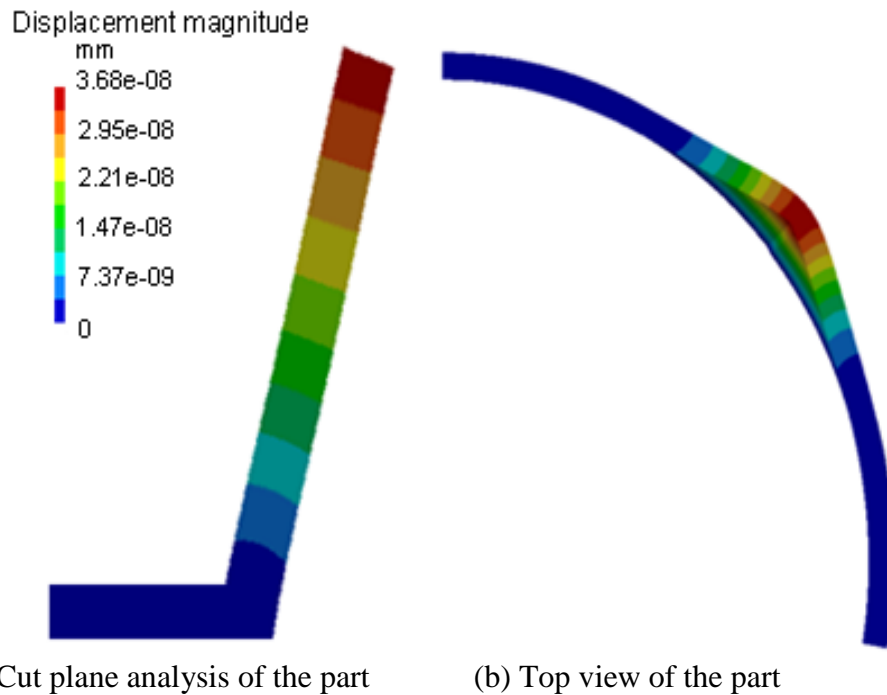


Figure 6.14: Deflection analysis result for the circular component at the middle of cutter feed location.

6.5 Summary

The finite element formulation and procedure to perform the finite element analysis for predicting the wall deflection were explained. The finite element analysis was developed to take into account the change in structure stiffness due to material removal. The deflection analysis model as described in Section 4.3.4 was validated with

the sets of experimental test for a different type of component feature. It can be seen that, the machining parameter and component attributes are the key factors in determining the magnitude of wall deflection as evidence in the simulation and experimental results. In addition, the magnitudes of wall deflection were also related to the different component features as it reflects the structure stiffness boundary condition which proves that the analysis of different component features as in Section 4.4 is necessary. The displacement magnitude obtained by simulation and experiment are closely matched and in good agreement which proves the validity of the model.

CHAPTER 7

**MULTIPLE REGRESSION
ANALYSIS MODEL**

7.1 Introduction

In the previous section, indicated that the machining parameter and component attributes are the key factors in determining the magnitude of wall deflection. In which, the machining parameter contributes to the magnitudes of the force generated in the machining process while the component attributes reflect the stiffness and rigidity of the wall. To examine the correlation between the machining parameter and component attributes to the magnitude of wall deflection a statistical multiple regression analysis is perform [194]. Using the correlation between the criterion variable; part deflection and a combination of a predictor variables namely speed, feed rate, radial depth of cut, wall thickness, wall height and wall length, a mathematical model for the deflection prediction is develop. The training data set for the statistical multiple regression analysis were generated from the FEA results with reference to component attribute and machining parameter using the previous describe methodology as in Section 4.3.1 to 4.3.5.

The objective of this chapter is to validate the statistical multiple regression analysis model for the deflection prediction. This chapter will first explain the step in building the prediction model via the statistical multiple regression analysis. Then, the develop multiple regression analysis model is verified by confirming the statistical significance of the estimated parameters and the goodness of fit of the model using analysis of variance (ANOVA), coefficient of determination (R^2) and hypothesis testing.

7.2 Multiple Regression Analysis Model Building

Multiple regression analysis is important statistical tools that investigates and explore the relationships between independent variables to the dependent variable [195 and 196]. Multiple regression analysis involves a statistical procedure for estimating and making inferences parameters through data fitting [197 and 198]. In general, a multiple regression model relates y to a function of x can be written as;

$$y_i = \beta_1 x_{i1} + \beta_2 x_{i2} + \dots + \beta_p x_{ip} + \varepsilon_i, \quad i = 1, \dots, n \quad (7.0)$$

where y_i = dependent variable

x = independent variables

β = unknown coefficient

i = index of particular independent variable observation

p = number of independent variables

ε_i = error term

From equation 7.0 the multiple regression model representing the wall deflection (D) can be expressed as a function of machining parameters; speed (S), feed rate (F), radial depth of cut (C) and component attributes; wall thickness (T), wall height (H) and wall length (L) (for circular component (θ°)) and can be written as;

$$y_{D1, D2, D3, D4, D5} = \beta_0 + \beta_S S + \beta_F F + \beta_C C + \beta_T T + \beta_H H + \beta_L L \quad (7.1)$$

where; y = deflection (μm) at $D1, D2, D3, D4$ and $D5$

$$(D1=0L, D1=1/4L, D2=1/2L, D3=3/4L, D5=L)$$

S = Speed (rpm)

F = Feed rate ($mmpt$)

C = Radial depth of cut (mm)

T = Workpiece thickness (mm)

H = Workpiece height (mm)

L = Workpiece length (mm) and (θ°)

The wall deflection (D) variable can be predict by solving the unknown coefficients of $\beta_0, \beta_S, \beta_F, \beta_C, \beta_T, \beta_H$ and β_L . These coefficients are to be estimate by using the least squares parameter from the normal equations. From equation 7.0 the residual can be written as [199 and 200];

$$e_i = y_i - \hat{\beta}_1 x_{i1} - \dots - \hat{\beta}_p x_{ip} \quad (7.2)$$

The normal equations are

$$\sum_{i=1}^n \sum_{k=1}^p x_{ij} x_{ik} \hat{\beta}_k = \sum_{i=1}^n x_{ij} y_i \quad j = 1, \dots, p \quad (7.3)$$

In matrix notation, the normal equations are written as

$$(\mathbf{X}^T \mathbf{Y}) \hat{\beta} = \mathbf{X}^T \mathbf{Y} \quad (7.4)$$

where $x_{ij} = ij$ element of \mathbf{X} ,

$y_i = i$ element of the column vector \mathbf{Y}

$\hat{\beta}_j = j$ element of $\hat{\beta}$.

Thus \mathbf{X} is $n \times p$, \mathbf{Y} is $n \times 1$, and $\hat{\beta}$ is $p \times 1$ and the solution is

$$\hat{\beta} = (\mathbf{X}^T \mathbf{X})^{-1} \mathbf{X}^T \mathbf{Y} \quad (7.5)$$

The developed multiple regression model is verified by evaluating relationship between the response variable and the independent controllable variables and the goodness of fit of the model using analysis of variance (ANOVA), coefficient of determination (R^2) and hypothesis testing [201]. The general null hypotheses for the model can be describe as the effects of speed, feed rate, radial depth of cut, workpiece thickness, workpiece height and workpiece length on deflection do not significantly differ from zero. The null hypotheses and alternative hypotheses can be written as:

$$H_0 = \beta_S = \beta_F = \beta_C = \beta_T = \beta_H = \beta_L = 0 \quad (7.6a)$$

$$H_a = \text{at least one of the } \beta \text{ does not equal to zero} \quad (7.6b)$$

The coefficient of determination (R^2) of the model is given by;

$$R^2 = 1 - \frac{SS_{ERR}}{SS_{TOT}} \quad (7.7)$$

where SS_{ERR} = Sum of square of residuals

SS_{TOT} = Total sum of square

7.3 Determination of Multiple Regression Analysis Model for Deflection Prediction

The training data set for the statistical multiple regression analysis were generated from the FEA results with reference to component attribute and machining parameter. Design of experiment L_{27} orthogonal array was used as experimental layout plan. The selection of an appropriate orthogonal array is based on the total number degrees of freedom. The degrees of freedom are defined as the number of constraints between process parameters that decide the minimum number of requirement for the test [202 and 203]. Based on six factors and three levels test within each factor, total of 27 runs were conducted for performing the multiple regression analysis. Table 7.1 and 7.2 shows the parameter and experimental layout for the prediction of wall deflection. MINITAB software was used for performing the multiple regression and statistical analysis.

Table 7.1: Machining parameter and component attribute experimental layout for the prediction of wall deflection.

	Factors	Level 1	Level 2	Level 3
<i>S</i>	Speed, <i>rpm</i>	3500	4000	4500
<i>F</i>	Feed, <i>mmpt</i>	0.03	0.05	0.07
<i>C</i>	Radial DOC, <i>mm</i>	0.2	0.4	0.6
<i>T</i>	Workpiece Thickness, <i>mm</i>	2.0	2.5	3.0
<i>L</i>	Workpiece Length, <i>mm and</i> θ^*	80	100	120
<i>H</i>	Speed, <i>rpm</i>	3500	4000	4500

*for circular component

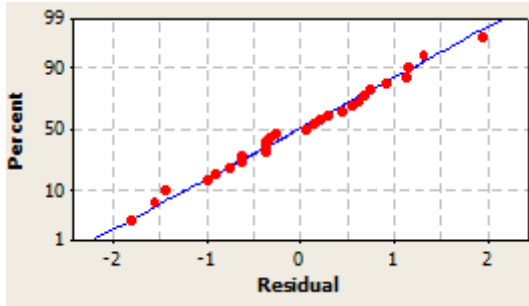
Table 7.2: L_{27} orthogonal array experimental layout plan.

Trials	<i>S</i>	<i>F</i>	<i>C</i>	<i>T</i>	<i>L</i>	<i>H</i>
1	L1	L1	L1	L1	L1	L1
2	L1	L1	L1	L1	L2	L2
3	L1	L1	L1	L1	L3	L3
4	L1	L2	L2	L2	L1	L1
5	L1	L2	L2	L2	L2	L2
6	L1	L2	L2	L2	L3	L3
7	L1	L3	L3	L3	L1	L1
8	L1	L3	L3	L3	L2	L2
9	L1	L3	L3	L3	L3	L3
10	L2	L1	L2	L3	L1	L2
11	L2	L1	L2	L3	L2	L3
12	L2	L1	L2	L3	L3	L1
13	L2	L2	L3	L1	L1	L2
14	L2	L2	L3	L1	L2	L3
15	L2	L2	L3	L1	L3	L1
16	L2	L3	L1	L2	L1	L2
17	L2	L3	L1	L2	L2	L3
18	L2	L3	L1	L2	L3	L1
19	L3	L1	L3	L2	L1	L3
20	L3	L1	L3	L2	L2	L1
21	L3	L1	L3	L2	L3	L2
22	L3	L2	L1	L3	L1	L3
23	L3	L2	L1	L3	L2	L1
24	L3	L2	L1	L3	L3	L2
25	L3	L3	L2	L1	L1	L3
26	L3	L3	L2	L1	L2	L1
27	L3	L3	L2	L1	L3	L2

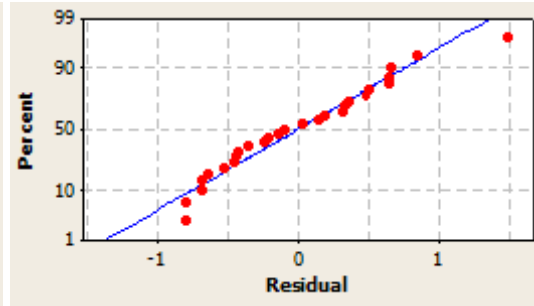
7.3.1 Case 1: T-Shape Component

From equation 7.0 to 7.5, the coefficients of all predictor variables are established to form a mathematical model in relation with the magnitude of wall deflection. Assumptions of normality and independence of residuals were first checked using a normal probability and residual plot. The normal probability plot of the residuals for deflection at $D1$, $D2$, $D3$, $D4$ and $D5$ shows the data for each case are spread roughly along the straight line which indicates that the normal distribution of residuals was satisfied. On the other hand, the residual plot shows that the residuals are randomly dispersed in both positive and negative along the run which indicates a linear regression model is appropriate for the data as shown in Figure 7.1.

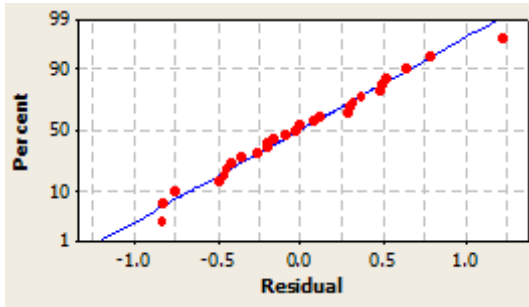
From the ANOVA analysis, the F statistic values of the regression for $D1$, $D2$, $D3$, $D4$ and $D5$ were 88.51, 118.68, 100.86, 45.26 and 75.42 respectively. The high F statistic values denoted that there is a significance value in the models to reject the null hypothesis (H_0) in which every predictor variable's coefficient was equal to zero. In addition, the high F statistic values from the ANOVA confirm the acceptance of alternative hypothesis (H_a), in which at least one of the coefficients was not equal to zero. Hence, from the ANOVA analysis it can be conclude that the machining parameter and component attributes were the significant process variables that affect the magnitude of wall deflection for the T-shape component. Table 7.3 shows the ANOVA analysis for the T-shape component.



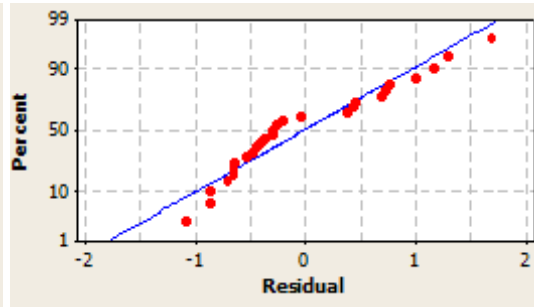
(a) Normal probability plot for D1



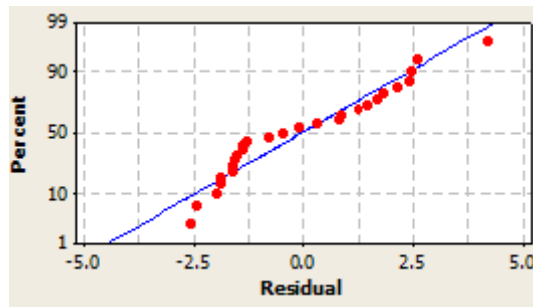
(b) Normal probability plot for D2



(c) Normal probability plot for D3



(d) Normal probability plot for D4



(e) Normal probability plot for D5

Figure 7.1: Normal probability and residual plot for T-shape component.

Table 7.3: ANOVA analysis for the T-shape component.

	DF	SS	MS	F	P
<i>D1</i>					
Regression	6	597.870	99.645	88.51	0.000
Residual Error	20	22.517	1.126		
Total	26	620.386			
<i>D2</i>					
Regression	6	312.302	52.050	118.68	0.000
Residual Error	20	8.772	0.439		
Total	26	321.073			
<i>D3</i>					
Regression	6	206.831	34.472	100.86	0.000
Residual Error	20	6.836	0.342		
Total	26	213.667			
<i>D4</i>					
Regression	6	200.587	33.431	45.26	0.000
Residual Error	20	14.773	0.739		
Total	26	215.359			
<i>D5</i>					
Regression	6	2074.49	345.75	75.42	0.000
Residual Error	20	91.69	4.58		
Total	26	2166.18			

The R^2 obtained from the regression analysis for deflection at *D1*, *D2*, *D3*, *D4* and *D5* were 96.4%, 97.3%, 96.8%, 93.1% and 95.8% respectively, which indicated high correlation coefficient between the dependent variable and the predicted value. The predicted and the predictor variables (*S*, *F*, *C*, *T*, *H* and *L*) are closely linked, as indicated by the R^2 values. The constants and coefficients of all predictor variables for the T-shape component models are listed in Table 7.4. Based on these coefficients, the multiple regression models for *D1*, *D2*, *D3*, *D4* and *D5* can be written as, respectively:

$$D1 = - 8.68 + 0.000719 S + 95.3 F + 24.6 C - 5.34 T - 0.0278 L + 0.820 H \quad (7.8a)$$

$$D2 = - 2.40 + 0.000280 S + 45.9 F + 17.8 C - 4.46 T - 0.0270 L + 0.593 H \quad (7.8b)$$

$$D3 = - 3.68 + 0.000297 S + 47.8 F + 14.9 C - 3.25 T - 0.0196 L + 0.462 H \quad (7.8c)$$

$$D4 = - 4.80 + 0.000981 S + 42.6 F + 11.8 C - 2.63 T - 0.0123 L + 0.366 H \quad (7.8d)$$

$$D5 = - 18.6 + 0.00450 S + 127 F + 41.4 C - 8.54 T - 0.0279 L + 0.817 H \quad (7.8e)$$

Table 7.4: The model coefficients for T-shape component.

	<i>D1</i>	<i>D2</i>	<i>D3</i>	<i>D4</i>	<i>D5</i>
<i>Constant</i>	-8.68	-2.40	-3.68	-4.8	-18.6
<i>S</i>	0.000719	0.000280	0.000297	0.000981	0.00450
<i>F</i>	95.3	45.9	47.8	42.6	127
<i>C</i>	24.6	17.8	14.9	11.8	41.4
<i>T</i>	-5.34	-4.46	-3.25	-2.63	-8.54
<i>L</i>	-0.0278	-0.0270	-0.0196	-0.0123	-0.0279
<i>H</i>	0.820	0.593	0.462	0.366	0.817

7.3.2 Case 2: L-Shape Component

For the case of L-shape component, the normal probability plot of the residuals for deflection at *D1*, *D2*, *D3*, *D4* and *D5* shows the data for each case are spread roughly along the straight line which indicates that the normal distribution of residuals was satisfied. The residual plot shows that the residuals are randomly dispersed in both positive and negative along the run which indicates a linear regression model is appropriate for the data as shown in Figure 7.2.

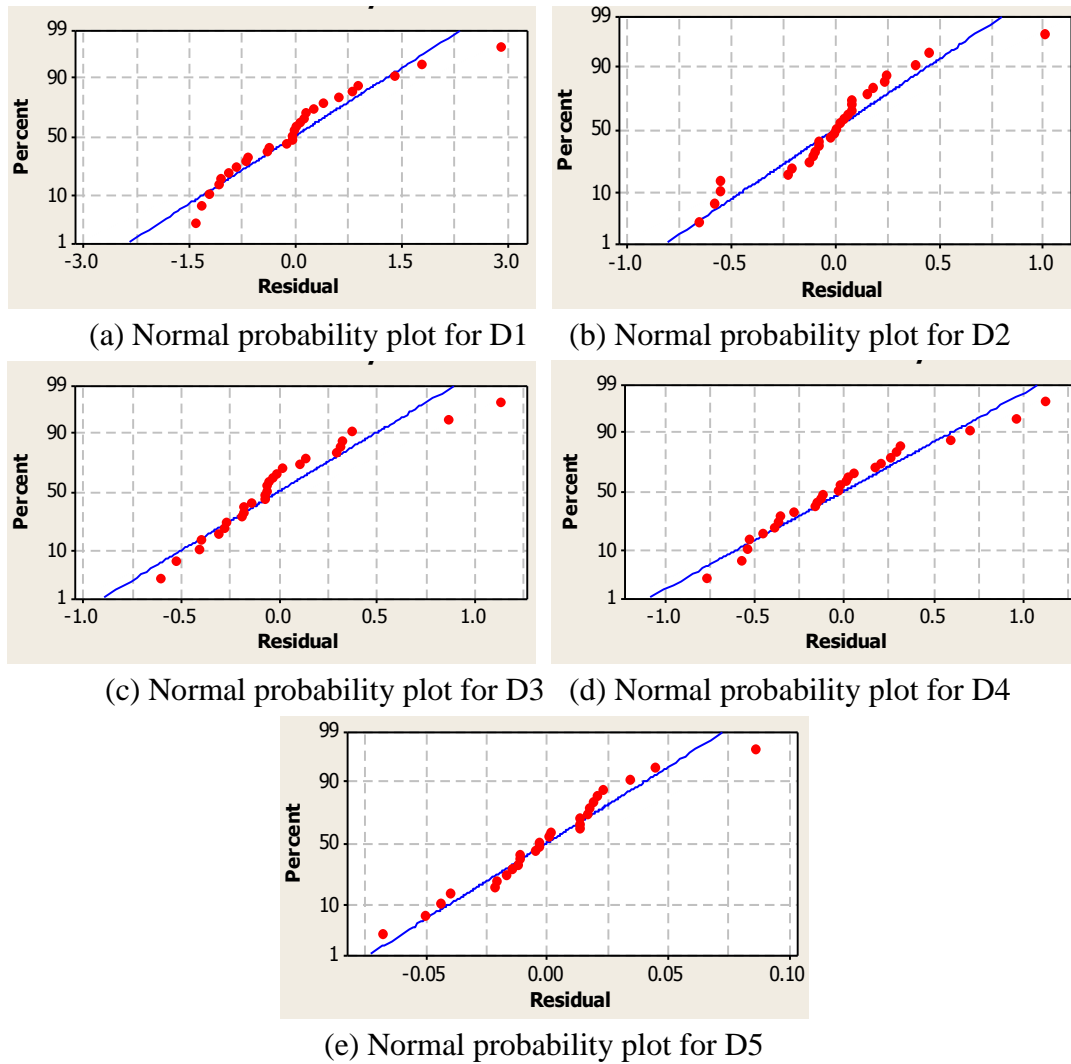


Figure 7.2: Normal probability and residual plot for L-shape component.

From the ANOVA analysis, the F statistic values of the regression for $D1$, $D2$, $D3$, $D4$ and $D5$ were 71.21, 158.8, 114.53, 67.92 and 131.48 respectively. The high F statistic values denoted that there is a significant value in the models to reject the null hypothesis (H_0) in which every predictor variable's coefficient was equal to zero. In addition, the high F statistic values from the ANOVA confirm the acceptance of alternative hypothesis (H_a), in which at least one of the coefficients was not equal to zero. Hence, from the ANOVA analysis it can be conclude that the machining

parameter and component attributes were the significant process variables that affect the magnitude of wall deflection for the L-shape component. Table 7.5 shows the ANOVA analysis for the L-shape component.

Table 7.5: ANOVA analysis for the L-Shape component.

	DF	SS	MS	F	P
<i>D1</i>					
Regression	6	561.343	93.557	71.21	0.000
Residual Error	20	26.275	1.314		
Total	26	587.618			
<i>D2</i>					
Regression	6	147.830	24.638	158.88	0.000
Residual Error	20	3.101	0.155		
Total	26	150.932			
<i>D3</i>					
Regression	6	132.431	22.072	114.53	0.000
Residual Error	20	3.854	0.193		
Total	26	136.285			
<i>D4</i>					
Regression	6	115.638	19.273	67.92	0.000
Residual Error	20	5.675	0.284		
Total	26	121.313			
<i>D5</i>					
Regression	6	0.99696	0.16616	131.48	0.000
Residual Error	20	0.02528	0.00126		
Total	26	1.02223			

The R^2 obtained from the regression analysis for deflection at *D1*, *D2*, *D3*, *D4* and *D5* were 95.5%, 97.9%, 97.2%, 95.3% and 97.5% respectively, which indicated high correlation coefficient between the dependent variable and the predicted value. The predicted and the predictor variables (*S*, *F*, *C*, *T*, *H* and *L*) are closely linked, as

indicated by the R^2 values. The constants and coefficients of all predictor variables for the L-shape component models are listed in Table 7.6. Based on these coefficients, the multiple regression models for $D1$, $D2$, $D3$, $D4$ and $D5$ can be written as, respectively:

$$D1 = - 9.23 + 0.00257 S + 127 F + 13.3 C - 4.54 T - 0.0445 L + 0.603 H \quad (7.9a)$$

$$D2 = - 5.66 + 0.00141 S + 84.3 F + 7.08 C - 2.47 T - 0.0312 L + 0.398 H \quad (7.9b)$$

$$D3 = - 4.94 + 0.00105 S + 71.6 F + 8.05 C - 2.47 T - 0.0262 L + 0.357 H \quad (7.9c)$$

$$D4 = - 1.97 + 0.000777 S + 58.7 F + 7.13 C - 2.46 T - 0.0239 L + 0.247 H \quad (7.9d)$$

$$D5 = - 0.334 - 0.000057 S + 5.28 F + 0.956 C - 0.085 T + 0.00078 L + 0.0221 H \quad (7.9e)$$

Table 7.6: The model coefficients for L-shape component.

	<i>D1</i>	<i>D2</i>	<i>D3</i>	<i>D4</i>	<i>D5</i>
<i>Constant</i>	-9.23	-5.66	-4.94	-1.97	-0.334
<i>S</i>	0.00257	0.00141	0.00105	0.000777	-0.000057
<i>F</i>	127	84.3	71.6	58.7	5.28
<i>C</i>	13.3	7.08	8.05	7.13	0.956
<i>T</i>	-4.54	-2.47	-2.47	-2.46	-0.085
<i>L</i>	-0.0445	-0.0312	-0.0262	-0.0239	0.00078
<i>H</i>	0.603	0.398	0.357	0.247	0.0221

7.3.3 Case 3: Rectangular Pocket Component

For the case of rectangular pocket component, the normal probability plot of the residuals for deflection at $D1$, $D2$, $D3$, $D4$ and $D5$ shows the data for each case are spread roughly along the straight line which indicates that the normal distribution of residuals was satisfied. The residual plot shows that the residuals are randomly

dispersed in both positive and negative along the run which indicates a linear regression model is appropriate for the data as shown in Figure 7.3.

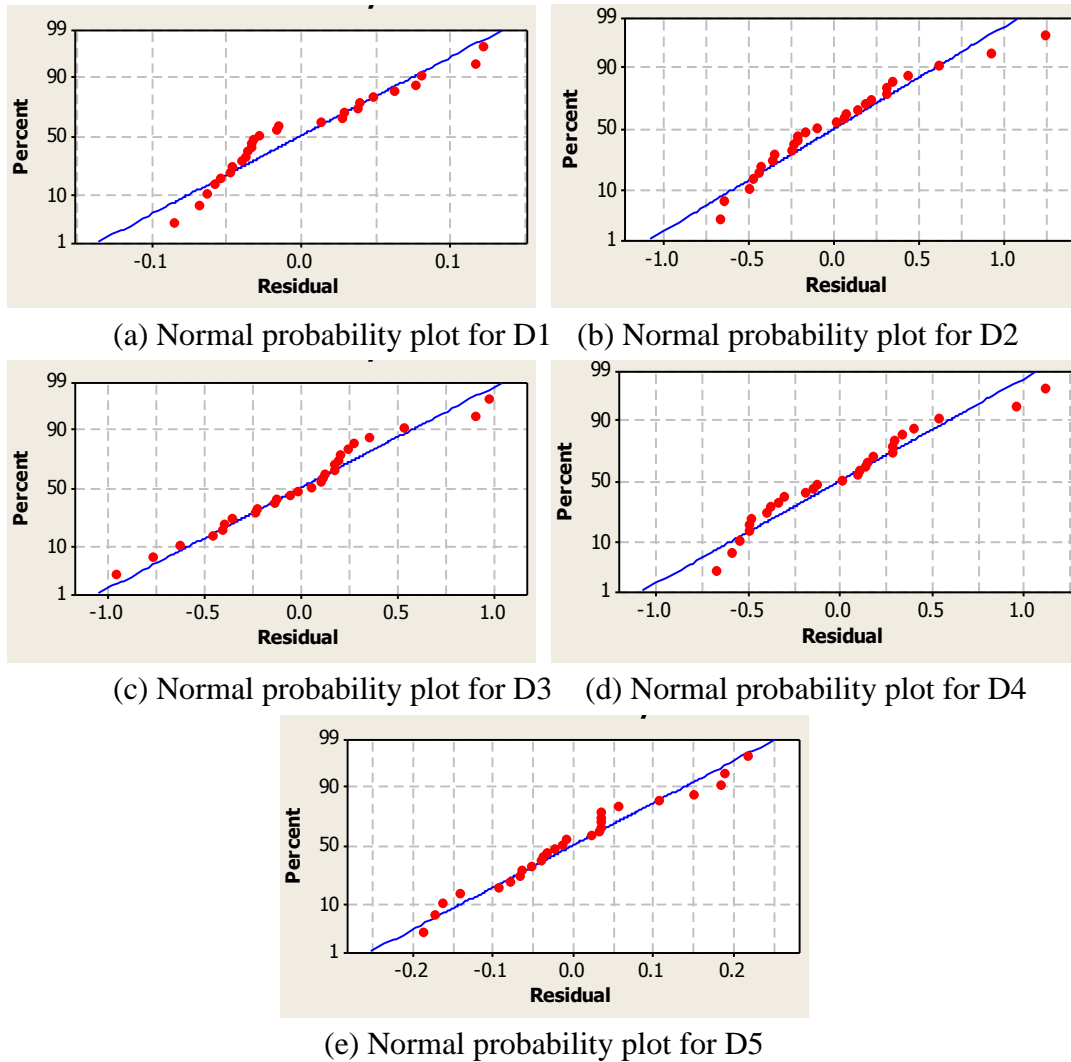


Figure 7.3: Normal probability and residual plot for rectangular pocket component.

From the ANOVA analysis, the F statistic values of the regression for $D1$, $D2$, $D3$, $D4$ and $D5$ were 159.05, 242.35, 287.16, 257.35 and 68.30 respectively. The high F statistic values denoted that there is a significance value in the models to reject the null hypothesis (H_0) in which every predictor variable's coefficient was equal to zero. In

addition, the high F statistic values from the ANOVA confirm the acceptance of alternative hypothesis (H_a), in which at least one of the coefficients was not equal to zero. Hence, from the ANOVA analysis it can be conclude that the machining parameter and component attributes were the significant process variables that affect the magnitude of wall deflection for the rectangular pocket component. Table 7.7 shows the ANOVA analysis for the rectangular pocket component.

Table 7.7: ANOVA analysis for the rectangular pocket component.

	DF	SS	MS	F	P
<i>D1</i>					
Regression	6	4.17424	0.69571	159.05	0.000
Residual Error	20	0.08748	0.00437		
Total	26	4.26173			
<i>D2</i>					
Regression	6	408.702	68.117	242.35	0.000
Residual Error	20	5.621	0.281		
Total	26	414.323			
<i>D3</i>					
Regression	6	451.212	75.202	287.16	0.000
Residual Error	20	5.238	0.262		
Total	26	456.449			
<i>D4</i>					
Regression	6	424.371	70.728	257.35	0.000
Residual Error	20	5.497	0.275		
Total	26	429.867			
<i>D5</i>					
Regression	6	6.2019	1.0336	68.30	0.000
Residual Error	20	0.3027	0.0151		
Total	26	6.5045			

The R^2 obtained from the regression analysis for deflection at $D1$, $D2$, $D3$, $D4$ and $D5$ were 97.9%, 98.6%, 98.9%, 98.7% and 95.3% respectively, which indicated high correlation coefficient between the dependent variable and the predicted value. The predicted and the predictor variables (S , F , C , T , H and L) are closely linked, as indicated by the R^2 values. The constants and coefficients of all predictor variables for the rectangular pocket component models are listed in Table 7.8. Based on these coefficients, the multiple regression models for $D1$, $D2$, $D3$, $D4$ and $D5$ can be written as, respectively:

$$D1 = - 1.27 + 0.000369 S + 3.82 F + 1.92 C - 0.400 T + 0.000342 L + 0.0137 H \quad (7.10a)$$

$$D2 = - 13.2 + 0.00420 S + 33.1 F + 17.6 C - 4.54 T + 0.0128 L + 0.108 H \quad (7.10b)$$

$$D3 = - 14.3 + 0.00462 S + 32.9 F + 18.2 C - 4.75 T + 0.0108 L + 0.122 H \quad (7.10c)$$

$$D4 = - 13.7 + 0.00439 S + 27.8 F + 18.0 C - 4.50 T + 0.00988 L + 0.119 H \quad (7.10d)$$

$$D5 = - 1.60 + 0.000484 S + 5.50 F + 2.17 C - 0.554 T + 0.00103 L + 0.0188 H \quad (7.10e)$$

Table 7.8: The model coefficients for rectangular pocket component.

	<i>D1</i>	<i>D2</i>	<i>D3</i>	<i>D4</i>	<i>D5</i>
<i>Constant</i>	-1.27	-13.2	-14.3	-13.7	-1.60
<i>S</i>	0.000369	0.00420	0.00462	0.00439	0.000484
<i>F</i>	3.82	33.1	32.9	27.8	5.50
<i>C</i>	1.92	17.6	18.2	18.0	2.17
<i>T</i>	-0.400	-4.54	-4.75	-4.50	-0.554
<i>L</i>	0.000342	0.0128	0.0108	0.00988	0.00103
<i>H</i>	0.0137	0.108	0.122	0.119	0.0188

7.3.4 Case 4: Circular Component

For the case of circular component, the normal probability plot of the residuals for deflection at $D1$, $D2$, $D3$, $D4$ and $D5$ shows the data for each case are spread roughly along the straight line which indicates that the normal distribution of residuals was satisfied. The residual plot shows that the residuals are randomly dispersed in both positive and negative along the run which indicates a linear regression model is appropriate for the data as shown in Figure 7.4.

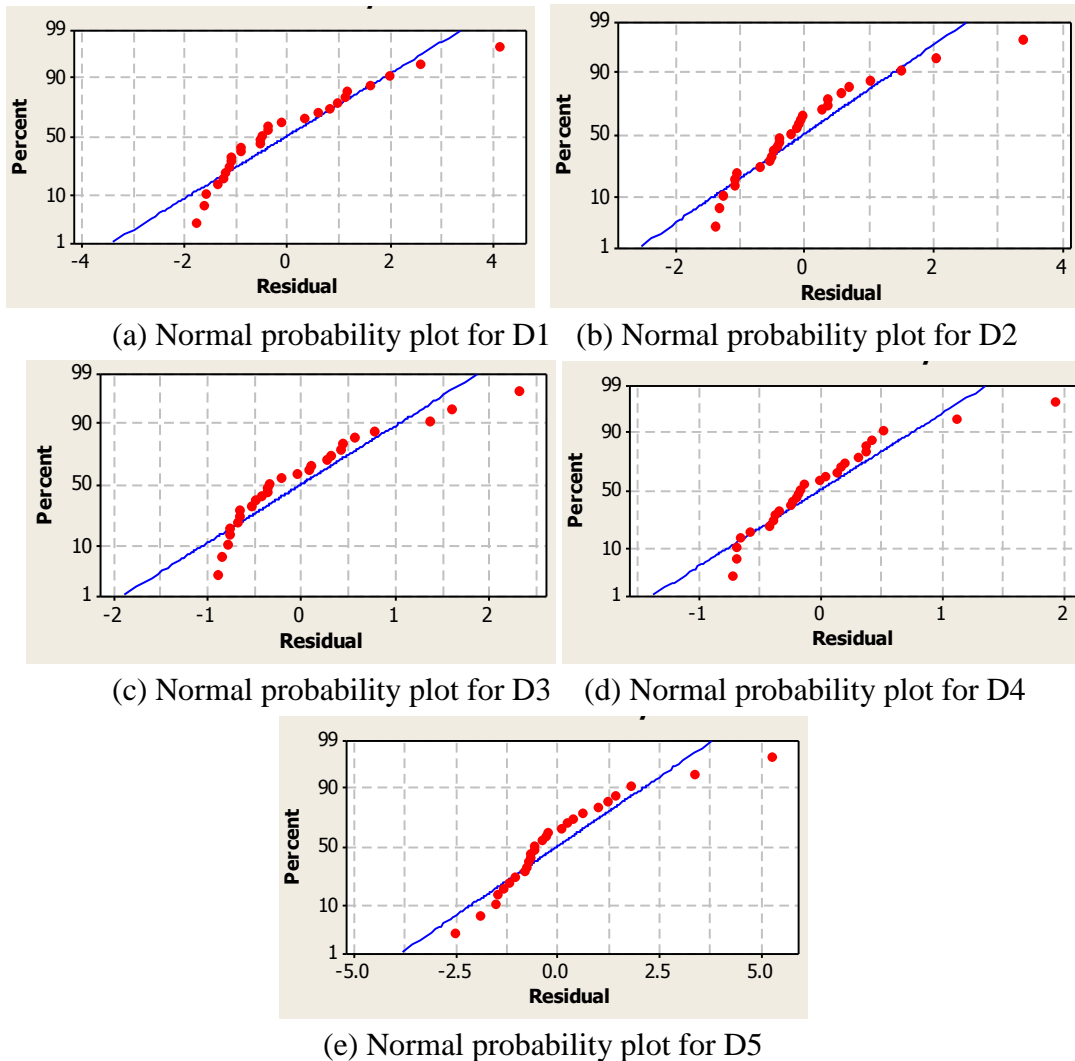


Figure 7.4: Normal probability and residual plot for circular component.

From the ANOVA analysis, the F statistic values of the regression for $D1$, $D2$, $D3$, $D4$ and $D5$ were 54.60, 56.73, 66.78, 82.98 and 85.98 respectively. The high F statistic values denoted that there is a significance value in the models to reject the null hypothesis (H_0) in which every predictor variable's coefficient was equal to zero. In addition, the high F statistic values from the ANOVA confirm the acceptance of alternative hypothesis (H_a), in which at least one of the coefficients was not equal to zero. Hence, from the ANOVA analysis it can be conclude that the machining parameter and component attributes were the significant process variables that affect the magnitude of wall deflection for the circular component. Table 7.9 shows the ANOVA analysis for the circular component.

Table 7.9: ANOVA analysis for the circular component.

	DF	SS	MS	F	P
<i>D1</i>					
Regression	6	572.409	95.401	34.58	0.000
Residual Error	20	55.178	2.759		
Total	26	627.587			
<i>D2</i>					
Regression	6	290.519	48.420	31.69	0.000
Residual Error	20	30.555	1.528		
Total	26	321.073			
<i>D3</i>					
Regression	6	196.609	32.768	38.42	0.000
Residual Error	20	17.058	0.853		
Total	26	213.667			
<i>D4</i>					
Regression	6	206.414	34.402	76.91	0.000
Residual Error	20	8.946	0.447		
Total	26	215.359			
<i>D5</i>					
Regression	6	2095.85	349.31	99.95	0.000
Residual Error	20	69.89	3.49		
Total	26	2165.75			

The R^2 obtained from the regression analysis for deflection at $D1$, $D2$, $D3$, $D4$ and $D5$ were 91.26%, 90.5%, 92.0%, 95.8% and 96.8% respectively, which indicated high correlation coefficient between the dependent variable and the predicted value. The predicted and the predictor variables (S , F , C , T , H and L) are closely linked, as indicated by the R^2 values. The constants and coefficients of all predictor variables for the circular component models are listed in Table 7.10. Based on these coefficients, the multiple regression models for $D1$, $D2$, $D3$, $D4$ and $D5$ can be written as, respectively:

$$D1 = 0.24 + 0.000227 S + 76.6 F + 21.9 C - 5.75 T - 0.0401 L + 0.668 H \quad (7.11a)$$

$$D2 = 4.65 - 0.000103 S + 31.2 F + 15.6 C - 4.78 T - 0.0365 L + 0.469 H \quad (7.11b)$$

$$D3 = 1.86 - 0.000025 S + 36.1 F + 13.2 C - 3.53 T - 0.0276 L + 0.376 H \quad (7.11c)$$

$$D4 = 3.72 + 0.000136 S + 37.3 F + 13.4 C - 3.68 T - 0.0334 L + 0.380 H \quad (7.11d)$$

$$D5 = - 2.10 + 0.00248 S + 114 F + 45.1 C - 11.1 T - 0.0783 L + 0.907 H \quad (7.11e)$$

Table 7.10: The model coefficients for circular component.

	<i>D1</i>	<i>D2</i>	<i>D3</i>	<i>D4</i>	<i>D5</i>
<i>Constant</i>	0.24	4.65	1.86	3.72	-2.10
<i>S</i>	0.000227	0.000103	0.000025	0.000136	0.00248
<i>F</i>	76.6	31.2	36.1	37.3	114.0
<i>C</i>	21.9	15.6	13.2	13.4	45.1
<i>T</i>	-5.75	-4.78	-3.53	-3.68	-11.1
<i>L</i>	-0.0401	-0.0365	-0.0276	-0.0334	-0.0783
<i>H</i>	0.668	0.469	0.376	0.380	0.907

7.4 Summary

The multiple regression analysis model building for predicting the wall deflection were explained. The multiple regression analysis models for each component case were developed to take into account the effect of machining parameter and component attributes to the magnitude of wall deflection. The multiple regression analysis model were verified by confirming the statistical significance of the estimated parameters and the goodness of fit of the model using analysis of variance (ANOVA), coefficient of determination (R^2) and hypothesis testing. The results obtained from the verification test shows a good capability of the model in predicting the magnitude of wall deflection from the predictor variables (S , F , C , T , H and L).

CHAPTER 8

TOOL PATH COMPENSATION BASED ON WALL DEFLECTION

8.1 Introduction

In general, there are two types of method to reduce the occurrence of surface error in machining process, namely errors avoidance and errors compensation. The error avoidance method involves altering of machining parameters by trial and error physical work in order to control the error to minimum [204]. However, this method tends to lower the efficiency of machining performance as it require longer machining times and lower material removal rates. In errors compensation method, the errors are predicted and compensated instead. Hence, errors compensation method is less costly and can be practically used for industries to reduce the errors in machining process.

The objective of this chapter is to validate the cutter compensation method to reduce the surface error produced during machining the thin-wall feature. The cutter compensation method is based on the adjustment of cutter path with respect to the magnitude of predicted wall deflection. This chapter will first explain the methodology and step involve for the cutter compensation method. Then, the develop cutter compensation method is verified with the set of experimental test for different case of component.

8.2 Mirror Cutter Compensation Method

The cutter compensation method is based on the adjustment of cutter path by integrating with the magnitude of wall deflection. The cutter compensation is achieved

by shifting the nominal cutter path to the opposite direction of the machining surface by an estimated amount of offset based on predicted wall deflection as in Chapter 7. The effects of wall deflection from the initial cutter path generate by the CAM system for machining thin-wall component is shown in Figure 8.1(a). While, Figure 8.1 (b) shows the effects of wall deflection with cutter path compensation.

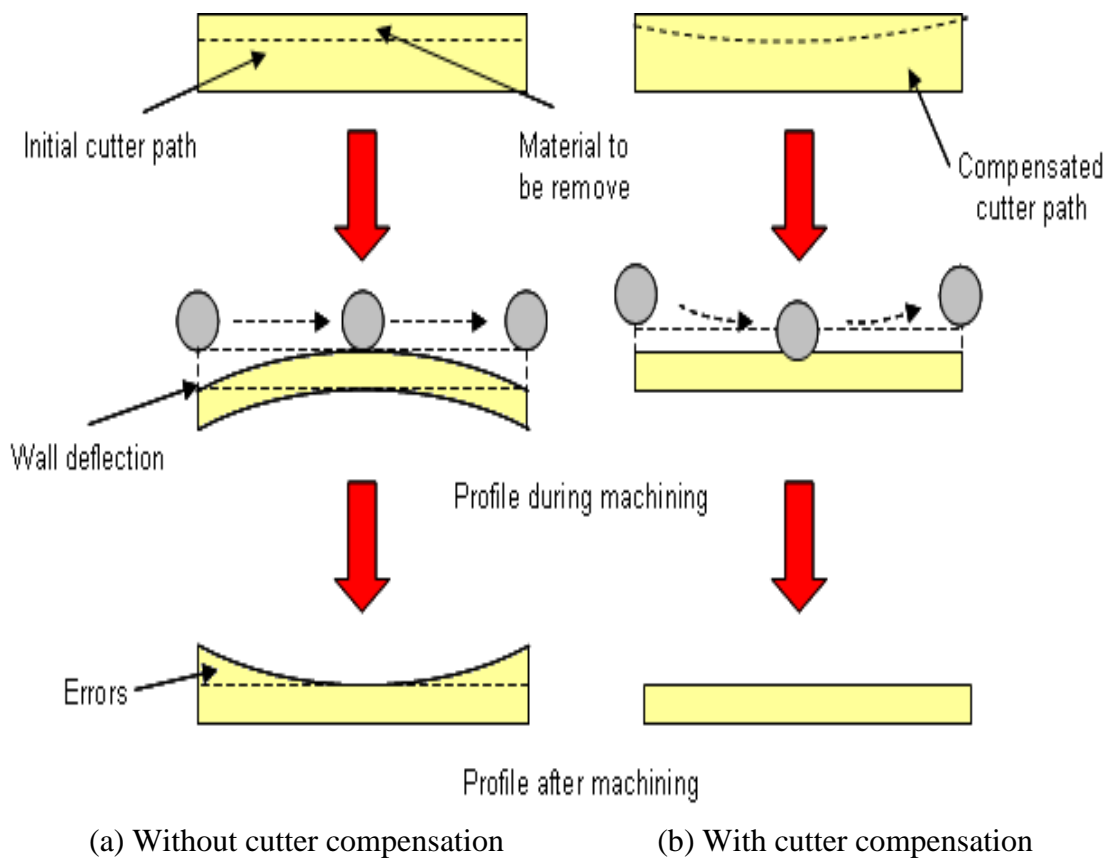


Figure 8.1: Effects of machining surface on cutter path.

A mirror compensation method was used to obtain the compensated trajectory of cutter location [205]. The purpose of mirror cutter compensation method is to reduce the impact of the machining error on the thin-wall feature [206]. As shown in Figure 8.2, the initial cutter location point generate from CAM is denoted as $C_{initial}$ and the

predicted deflection magnitude as δ_{pred} . Hence, the compensated trajectory of cutter location C_{comp} can be defined as;

$$C_{comp} = C_{initial} + \delta_{pred} \quad (8.0)$$

Based on the compensated trajectory of cutter location C_{comp} , a new command line defining the cutter compensation location is generated as an NC code instruction and replace the initial cutter location data to perform the machining compensation method as shown in Figure 8.2. In Chapter 6 indicates that the wall deflection is time-varying with the cutter position. Hence, for accuracy of the tool path modification for compensation, the six predicted deflection points were connected by creating an arc between the six predicted points in EdgeCAM design module.

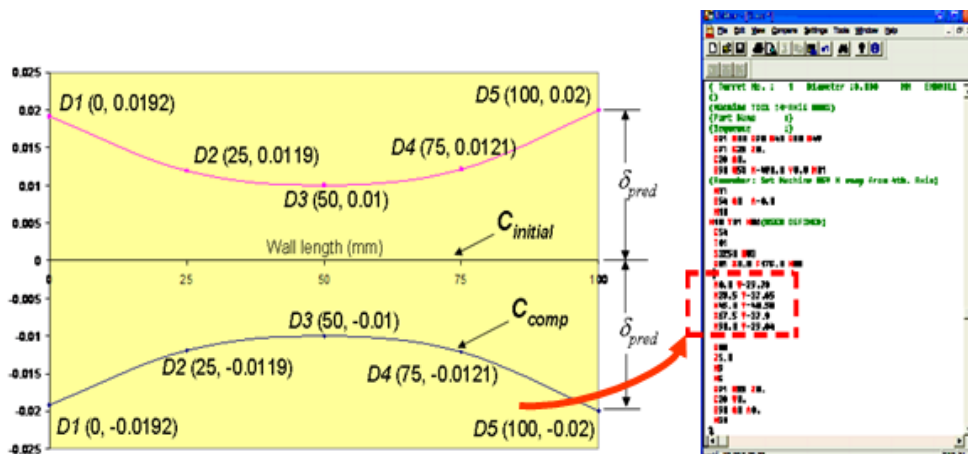


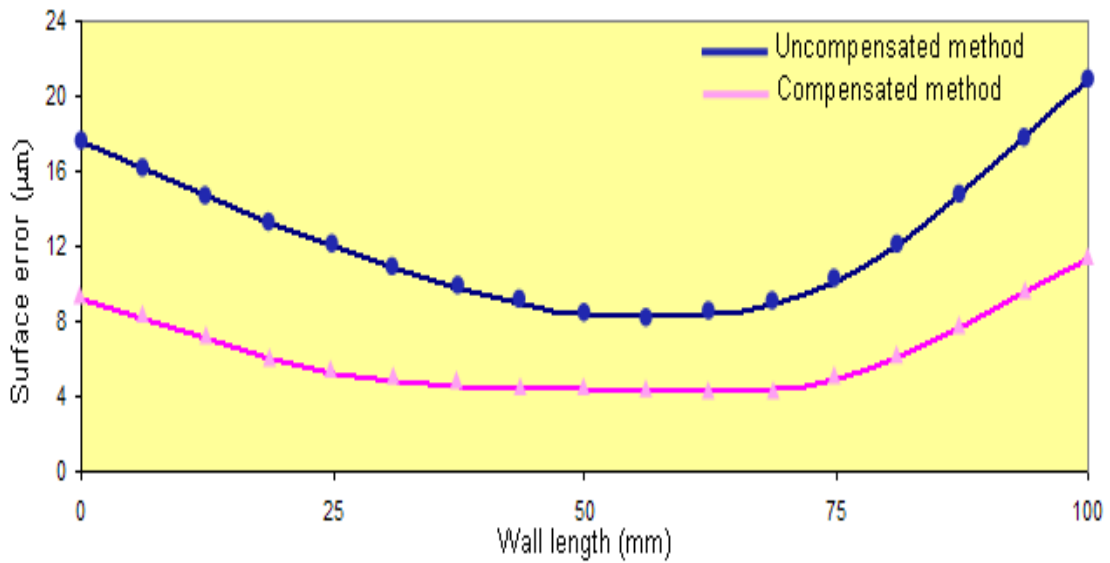
Figure 8.2: Cutter compensation method.

8.3 Cutter Compensation Validation

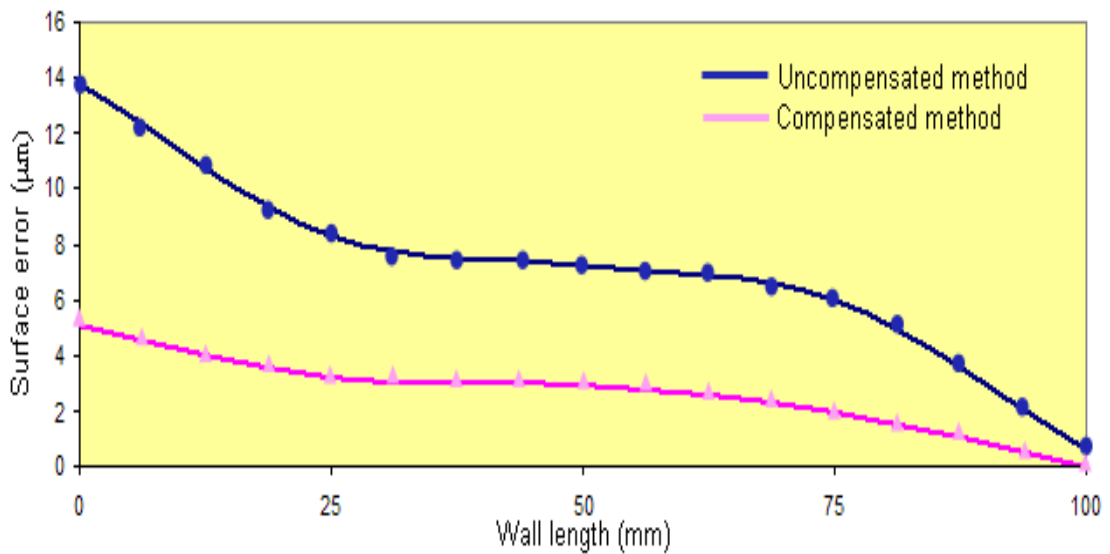
A number of experimental test have been carried out to demonstrate the capabilities of the cutter compensation model. Surface errors are measure along the

machine surface at uniform intervals using Renishaw On-Machine Wireless Intuitive Measurement probe. Surface error profile for the compensated and uncompensated model were measured at same locations and compared. A 6 mm diameter 4-flute carbide endmill with 38 helix angle carbide endmill was used to machine the thin-wall feature. The workpiece material was Ti-6Al-4V titanium alloy with a Young modulus of $1.14 \times 10^{11} \text{ N/m}^2$, Yield Strength of $8.25 \times 10^8 \text{ N/m}^2$ and Poisson ratio of 0.34. EdgeCAM software was used to generate the compensated and uncompensated cutter path for finishing cycle in machining the thin-wall feature.

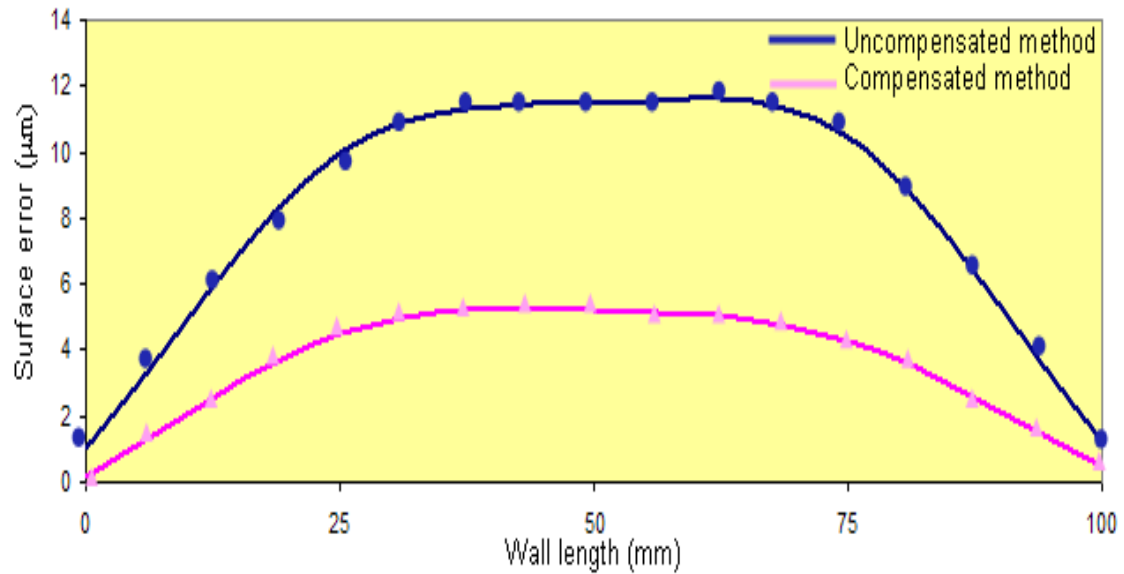
Figure 8.3 (a) to (d) shows the example of surface error variation between compensated and uncompensated model for every component case. For the case of uncompensated method, the surface error produce are closely match with the shape of predicted wall deflection. This confirms the validity of the proposed wall deflection prediction methodology. From Figure 8.3 shows that, the magnitude of surface error depend on the shape of the component. For the case of T-shape component the surface error are maximums at the two ends. In which, the end of the machining step experienced the maximum deflection compare at the start of the machining step due to the decreasing stiffness of the wall as a result of material removal and the unsupported features at both ends. For the L-shape component, one side of the wall is support which result a maximum surface error at the start of machining step and decrease towards the end of the supported side. The surface error magnitude for the rectangular pocket component is maximums at the centre of wall length due to the supported features at both sides. In addition, there is an increasing value of surface error magnitudes between two regions (start and end) in the feed direction as a result of change in wall thickness.



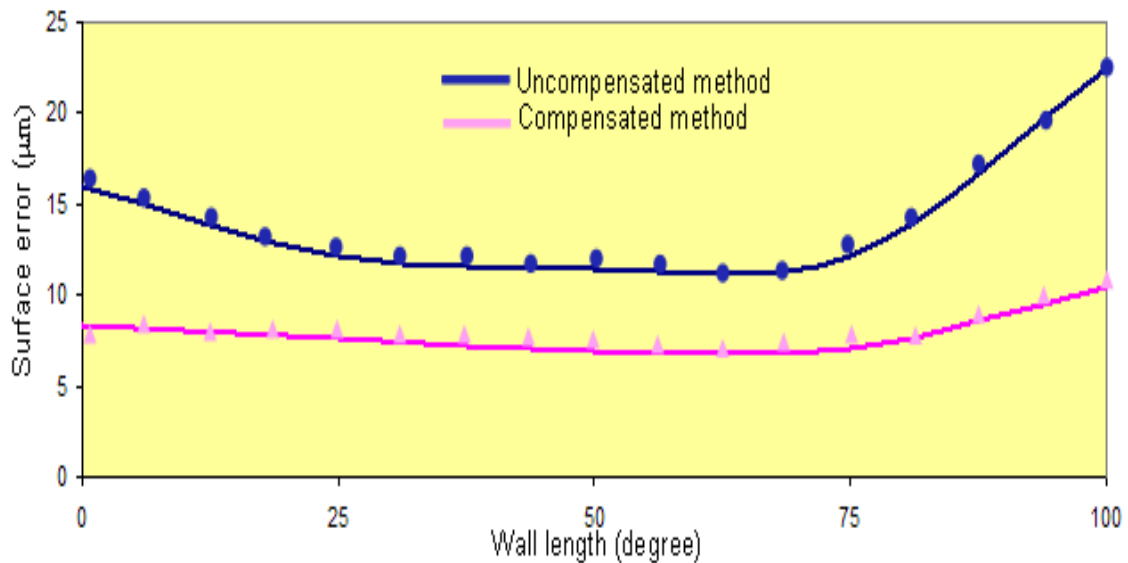
(a) Surface error variation between compensated and uncompensated model for T-shape component. Machining parameter: $S = 4000$ rpm, $ft = 0.05$ mm/tooth, $rdoc = 0.6$ mm. Component attribute: *wall thickness* = 2.0 mm, *wall length* = 100 mm and *wall height* = 20 mm.



(b) Surface error variation between compensated and uncompensated model for L-shape component. Machining parameter: $S = 4000$ rpm, $ft = 0.05$ mm/tooth, $rdoc = 0.6$ mm. Component attribute: *wall thickness* = 2.0 mm, *wall length* = 100 mm and *wall height* = 20 mm.



(c) Surface error variation between compensated and uncompensated model for rectangular pocket component. Machining parameter: $S = 4000$ rpm, $ft = 0.05$ mm/tooth, $rdoc = 0.6$ mm. Component attribute: *wall thickness* = 2.0 mm, *wall length* = 100 mm and *wall height* = 20 mm.



(d) Surface error variation between compensated and uncompensated model for circular component. Machining parameter: $S = 4000$ rpm, $ft = 0.05$ mm/tooth, $rdoc = 0.6$ mm. Component attribute: *wall thickness* = 2.0 mm, *wall length* = 100 degree and *wall height* = 20 mm.

Figure 8.3 (a) to (d): Surface error variation between compensated and uncompensated model for all the component cases.

For the case of machining with cutter compensation method, the results show that after applying the cutter compensation method, the machine surface errors are reduced. By adopting the cutter compensation method, which shifts the cutter location in opposite direction from the machine surface, the machining forces acting normal to the surface decrease hence reducing the magnitude of wall deflection. In addition, the undercut machine surface produced in uncompensated method can be avoided thus improving the component accuracy. It is noted that although adopting the cutter compensation method reduces surface error, it does not totally eliminate the occurrence of machine surface error. This is due to the fact of other occurrence involved in the machining process such as dynamics of the system, machining environment and non continuous interrupted cutting that contribute to the occurrence of machine surface error [207 and 208].

By inserting geometrical parameters of the parts used in the tests described in this chapter, the computational time required to predict the thin wall deflection in each case has been reduced to less than 10 seconds in all cases, after the parameters are entered through the computer program's user interface. This change compares favourably with traditional FEA methods described in Chapter 3.

8.4 Summary

The cutter compensation method based on the adjustment of cutter path with respect to the magnitude of wall deflection has been explained. The cutter compensation call mirror method is achieved by shifting the nominal cutter path to the opposite

direction of the machining surface. Based on the compensated trajectory of cutter location, a new command line defining the cutter compensation location are generate as an NC code instruction and replace the initial cutter location data to perform the machining compensation. A number of experimental run were conducted for each component case to validate the effectiveness of the model. From the experimental results, shows that the machine surface errors were improved by adopting the cutter compensation method hence validate the effectiveness and flexibility of the model in improving the component accuracy for machining thin-wall feature.

CHAPTER 9

CONCLUDING REMARKS

9.1 Research Contribution

This thesis is focused on the prediction of wall deflection during machining thin-wall feature. The following conclusions can be drawn from the performed analysis and the obtained results:

1. A new novel hybrid methodology for the prediction of wall deflection during machining thin-wall feature has been developed.
2. A complete simulation system has been developed for part creation, material removal process, prediction of milling force distribution, static analysis for deflection of the thin-wall feature and mathematical model associated with cutting parameters and component attributes.
3. Cutting forces, static analysis of wall deflection and mathematical model associated with cutting parameters and component attributes are predicted and experimentally validate.
4. The cutting force coefficients, which relate the milling force to the average chip thickness, are expressed using mechanistic curve fitting and calibration techniques for the carbide cutting tool and titanium alloys material.

5. The finite element model has been used to generate a database of machining parameter and component attributes that influence to the magnitude of wall deflection. Using a statistical multiple regression, a mathematical model has been developed from the database, thus allowing the prediction of wall deflection for a wide class of problems from a very simple equation. It was shown that the influence of coefficient model can be a useful aid in the selection of the component geometry and machining parameter.
6. All results have been derived for four different cases of typical aerospace component, but it is shown that these results can be applicable for other component shape and materials. Prediction of the surface errors due to the flexibility of the wall can be easily predicted within minutes.
7. A customize computer program has been developed for the proposed model. The developed computer program is an integrated data exchanges between modules upon users input on the design information and machining parameter for automatically generate the solid model, material removal model and FEM analysis. The developed computer program has improved the analysis time and makes the task easier to perform. In addition, by using a same platform between CAD and FEM analysis those problems associated with the data exchange are eliminated.
8. The cutter compensation method based on the adjustment of cutter path with respect to the magnitude of wall deflection has been developed and tested. The

cutter compensation method is able to reduce the machine surface errors thus improving the component accuracy for machining thin-wall feature. By adopting the cutter compensation method, only one machining pass is required to machine the thin-wall feature compared to the current practice in step method which requires a few machining passes.

9. To date there is no design software available that includes the effect of the wall deflection on machining thin-wall component. The developed models will provide an interactive prediction capability to suit the industrial applications. This will substantially improve the productivity and lower the machining cost. Based on these models, the cutter compensation can be found in less than 10 seconds and the corresponding actions implementing compensation onto the CNC machines can be done in minutes, thus decreasing the design and development time. The software has been tested by Production Parts Pty. Ltd. and proved to be fit for use as a commercial system.

9.2 Recommendations for Future Work

The present study provides a starting point for the analysis on the dynamics of thin-wall structures during machining while taking into account the continuous change of thickness of the wall. The following topics could be pursued for future research work:

1. Develop an expert CAD/CAE/CAM system that can automatically detect the thin-wall feature and adjusting the NC code instruction and replace the initial cutter location data to perform the machining compensation.
2. Extending the predictive model to deal with more complex and arbitrary component shape of thin-wall monolithic component.
3. Extending the predictive model to deal with other non-structural low rigidity aerospace component such as turbine blade and impellers.
4. As this project only focused on effects induced by the machining process, extension of the analysis that consider the initial workpiece stress and product warpage that might result from it would be worth.
5. Extending the cutter compensation strategy for the application of 5-axis machining technique.

Publications

The work presented in this thesis has been published in the following:

International journal

1. R. Izamshah R.A, John P.T Mo, Songlin D., Finite element analysis of machining thin-wall parts, Journal Key Engineering Materials Vol. 458 (2011) pp 283-288.
2. Songlin D., R. Izamshah R.A, John P.T Mo, Y. Zhu, Chatter detection in high speed machining of titanium alloys, Journal Key Engineering Materials Vol. 458 (2011) pp 289-294.
3. Songlin D., R. Izamshah R.A, John P.T Mo, Q. Liu, Online tool life prediction in the machining of titanium alloys, Journal Key Engineering Materials Vol. 458 (2011) pp 355-361.
4. Songlin D., R. Izamshah R.A, John P.T Mo, Y. Zhu, The development of an economic model for the milling of titanium alloys, Journal Key Engineering Materials Vol. 458 (2011) pp 362-367.

5. R. Izamshah R.A, John P.T Mo, Songlin D., Deflection prediction for machining titanium aerospace components, Journal of Mechanical Engineering and Technology Vol. 3 No. 1 (2011) (*accepted for publication*).
6. R. Izamshah R.A, John P.T Mo, Songlin D., Hybrid deflection prediction on machining thin-wall monolithic aerospace component, Journal of Engineering Manufacture (2011) (*accepted for publication*).

Conference proceedings and workshop

1. R. Izamshah R.A, John P.T Mo, Songlin D., Task automation for modelling deflection prediction on machining thin-wall part with Catia V5, 2011 International Conference on Mechanical, Industrial and Manufacturing Engineering, Melbourne, Australia 15-16 January 2011.
2. John P.T Mo, R. Izamshah R.A, Songlin D., Challenges in optimising the machining process of titanium alloys for JSF manufacturing, Proceedings Australian JSF Advanced Technology and Innovation Conference, Department of Defence, Australian Government, Australia 3rd - 4th May 2010.
3. John P.T Mo, R. Izamshah R.A, Songlin D., Challenges in optimising the machining process of titanium alloys, DMTC and DIIC Workshop on Manufacturing Innovation in Titanium Processing, Australia 1st June 2010.

References

- [1] J. Hawlena and M. Mindur, The analysis of changes in exploitation characteristics of the world civil aviation, *Logistics and Transport* No. 2 (9) (2009) 17-22.

- [2] P. Hurk, Het hogesnelheidsverspanen van aluminium (in Dutch), in: *MB Produktietechniek*, Vol. 64 No. 1/2 (1998) 10-15.

- [3] Makino-USA, Thin Wall Machining, <http://www.makino.com/about/article/10-1-2002/Thin_Wall_Machining>, 2010 (accessed 10th April 2010).

- [4] W. Tongyue, H. Ning and L. Liang, Stability of milling of thin-walled workpiece, *International Conference on Mechanic Automation and Control Engineering (MACE)* (2010) 3408-3411.

- [5] L. Arnaud, O. Gonzalo, S. Seguy, H. Jauregi and G. Peigné, Simulation of low rigidity part machining applied to thin-walled structures, *International Journal Adv. Manuf. Technology* 54 (2011) 479–488.

- [6] S. Herranz, F. J. Campa, L. N. López, A. Rivero, A. Lamikiz, E. Ukar, J. A. Sánchez and U. Bravo, The milling of airframe components with low rigidity: A general approach to avoid static and dynamic problems, *Proceedings of the*

Institution of Mechanical Engineers, Part B: Journal of Engineering Manufacture, Vol. 219 No. 11 (2005) 789-801.

- [7] M. A. Elbestawi and R. Sagherian, Dynamics modelling for the prediction of surface errors in the milling of thin-walled sections, Journal of Materials Processing Technology 25 (1991) 215-228.

- [8] M. Popma, Computer aided process planning for high-speed milling of thin-walled parts, PhD. Thesis, University of Twente, Netherlands, (2010).

- [9] D. Lohitha, A finite element method for ring rolling processes, PhD. Thesis, Ohio University, (1998).

- [10] R. W. Fitzgerald, Mechanics of materials, 2nd edition, Addison-Wesley Publishing Company Inc., Massachusetts, USA (1982).

- [11] G. Yang, Elastic and plastic mechanics, People Education Published Inc., PRC, (1980).

- [12] E. Budak and Y. Altintas, Peripheral milling conditions for improved dimensional accuracy, International Journal of Machine Tools and Manufacture 34 (1994) 907-918.

- [13] E. Budak and Y. Altintas, Modeling and avoidance of static form errors in peripheral milling of plates, *International Journal of Machine Tools and Manufacture* 35 (3) (1995) 459–476.
- [14] W.A Kline, R.E. DeVor and I.A. Shareef, The prediction of surface accuracy in end milling, *ASME J. Eng. Ind.* 104 (1982) 272-278.
- [15] R. Sagherian and M.A. Elbestawi, A simulation system for improving machining accuracy in milling, *Computers in Industry* 14 (1990) 293-305.
- [16] J.S Tsai and C.L. Liao, Finite element modelling of static surface errors in the peripheral milling of thin-walled wall, *Journal of Materials Processing Technology* 94 (1999) 235-246.
- [17] Y. Altintas, D. Montgomery and E. Budak, Dynamic peripheral milling of flexible structures, *Journal of Engineering for Industry (Transaction of the ASME)* 114 (1992) 137-145.
- [18] S. Ratchev, W. Huang, S. Liu and A.A Becker, Milling error prediction and compensation in machining of low-rigidity parts, *International Journal of Machine Tools and Manufacture* 44 (2004) 1629-1641.

- [19] S. Ratchev, S. Liu, W. Huang and A.A Becker, A flexible force model for end milling of low-rigidity parts, *International Journal of Machine Tools and Manufacture* Vol. 153-154 (2004) 134-138.
- [20] S. Ratchev, E. Govender, S. Nikov, K. Phuah, and G. Tsiklos, Force and deflection modelling in milling of low-rigidity complex parts, *Journal of Material Processing Technology*, Vol. 143-144 (2003) 796-801.
- [21] S. Ratchev, W. Huang, S. Liu, and A. A. Becker, Modelling and simulation environment for machining of low-rigidity components, *Journal of Materials Processing Technology*, Vol. 153-154 No. 10 (2004) 67-73.
- [22] S. Ratchev, S. Nikov, and I. Moualek, Material removal simulation of peripheral milling of thin wall low-rigidity structures using FEA, *Advances in Engineering Software*, Vol. 35 No. 8-9 (2004) 481-491.
- [23] S. Ratchev, S. Liu, and A. A. Becker, Error compensation strategy in milling flexible thin-wall parts, *Journal of Materials Processing Technology*, Vol. 162-163 (2005) 673-681.
- [24] S. Ratchev, S. Liu, W. Huang and A. A. Becker, An advanced FEA based force induced error compensation strategy in milling, *International Journal of Machine Tools and Manufacture* Vol. 46 No. 5 (2006) 542-551.

- [25] J.W. Sutherland and R.E. DeVor, An improved method for cutting force and surface error prediction in flexible end milling systems, *Journal of Engineering for Industry (Transaction of the ASME)* 108 (1986) 269-279.
- [26] S. Charles, B. Eynard, P. Bartholomew and C. Paleczny, Standardisation of the finite element analysis data exchanges in aeronautics concurrent engineering, *Journal of Computing and Information Science in Engineering*, Vol. 5 No 1 (2005) 63-66.
- [27] S. Spitzzy and A. Rappoportz, Integrated feature-based and geometric CAD data exchange, *ACM Symposium on Solid Modeling and Applications* (2004).
- [28] A. Rappoport, An architecture for universal CAD data exchange. *Solid Modeling*, ACM Press (2003) 266–269.
- [29] J. Li, S. Han, S. Shin, S. Lee, Y. Kang, H. Cho, H. Kim, I. Song, I. Kim, and P. Rathore, CAD data exchange using the macro-parametrics approach: an error report, *International Journal of CAD/CAM* Vol. 10, No. 2 (2011) 1-7.
- [30] F. Bianconi, Bridging the gap between CAD and CAE using STL files, *International Journal of CAD/CAM* Vol. 2 No. 1 (2002) 55-67.

- [31] U. Gabbert and P. Wehner, The product data model as a pool for CAD-FEA Data, *Engineering with Computers* 14, Springer-Verlag London Limited (1998) 115-122.
- [32] T. Burns, *Applied statics and strength of materials*, 2nd Ed., Clifton Park, NY: Delmar/Cengage Learning, (2010).
- [33] J. Liu, *Fixture design for thin-walled parts*, Master's Thesis, University of Manitoba, Winnipeg, Canada, (1993).
- [34] H. Ning, W. Zhigang, J. Chengyu and Z. Bing, Finite element method analysis and control stratagem for machining deformation of thin-walled components, *Journal of Material Processing Technology*, Vol. 139 (2003) 332-336.
- [35] J. Ye, Large deflection analysis of axisymmetric circular plates with variable thickness using the boundary element method, *Appl. Math. Modelling*, Vol. 15 (1991) 325-328.
- [36] M. Hosseini and H. Abbas, Neural network approach for failure analysis of rectangular plates under wedge impact, *Latin American Journal of Solids and Structures* 5 (2008) 171-186.

- [37] V. Adan, R. Sherif, S. Hisashi and M. Hidekazu, Influential factors affecting deformation during plate forming by line heating (Report 1), Transactions of JWRI, Vol. 36 No. 1 (2007) 57-64.
- [38] G. M. Nagel and D. P. Thambiratnam, A numerical study on the impact response and energy absorption of tapered thin-walled tubes, International Journal of Mechanical Sciences, Vol. 46 No. 2 (2004) 201-216.
- [39] M. Wan, W. Zhang, G. Tan and G. Qin, Systematic simulation procedure of peripheral milling process of thin-walled workpiece, Journal of Material Processing Technology, Vol. 197 (2008) 122-131.
- [40] M. Wan, W. Zhang, G. Qin and Z. Wang, Strategies for error prediction and error control in peripheral milling of thin-walled workpiece, International Journal of Machine Tools and Manufacture, Vol.48 (2008) 1366-1374.
- [41] R.E. DeVor, W.A. Kline and W. J. Zdeblick, Mechanistic model for the force system in end milling with application to machining airframe structures, Manufacturing Engineering Transactions and North American Manufacturing Research Conference, 8th; Rolla; Mo (1980) 297-303.
- [42] J. E. Williams, E. F. Smart and D. R. Milner, The metallurgy of machining, part 1: Basic considerations and the cutting of pure metals, Metallurgical, Vol. 104 (1982) 3-10.

- [43] Z. Lin and S. Lo, A study of deformation of the machined workpiece and tool under different low cutting velocities with an elastic cutting tool, *International Journal of Mechanical Science*, Vol. 40 (1998) 663-681.
- [44] Z. Lin and Y. Yang, Three dimensional cutting process analysis with different cutting velocities, *Journal of Material Processing Technology*, Vol. 70 (1997) 22-23.
- [45] Y. Turgut, H. Çinici, I. Şahin and T. Findik, Study of cutting force and surface roughness in milling of Al/Sic metal matrix composites, *Scientific Research and Essays* Vol. 6(10) (2011) 2056-2062.
- [46] M. Thomas and Y. Beauchamp, Statistical investigation of modal parameters of cutting tools in dry turning, *International Journal of Machine Tools and Manufacture*, Vol.43 (2003) 1093-1106.
- [47] A. Maana and B. Bhattacharayya, A study on machinability of Al/SiC-MMC, *Journal of Material Processing Technology*, Vol. 140 (2003) 711-716.
- [48] ASM Handbook, Vol. 16: Machining, ASM International, Metals Park, OH, (1989) 7-18.
- [49] W. H. Lai, Modeling of cutting forces in end milling operations, *Tamkang Journal of Science and Engineering*, Vol. 3, No. 1 (2000) 15-22.

- [50] B. K. Fussell and K. Srinivasan, An investigation of the end milling process under varying machining conditions, *Journal of Engineering for Industry*, Vol. 111 (1989) 27-36.
- [51] T. Obikawa and E. Usui, Computational machining of titanium alloy-finite element modeling and a few results, *Journal of Manufacturing Science and Engineering (Transactions of ASME)* 118 (1996) 208-215.
- [52] M. Armendia, A. Garay, L.M. Iriarte and P.J. Arrazola, Comparison of the machinabilities of Ti6Al4V and TIMETAL® 54M using uncoated WC–Co tools, *Journal of Materials Processing Technology* 210 (2010) 197–203.
- [53] Z.A. Zoya and R. Krishnamurthy, The performance of CBN tools in the machining of titanium alloys, *Journal of Materials Processing Technology* 100 (2000) 80–86.
- [54] E.O. Ezugwu, R.B. Da Silva, J. Bonney and Á.R. Machado, Evaluation of the performance of CBN tools when turning Ti–6Al–4V alloy with high pressure coolant supplies, *International Journal of Machine Tools and Manufacture* Vol. 45, No. 9 (2005) 1009-1014.
- [55] E. Kuljanic, F. Miani, M. Fioretti and L. Beltrame, Milling titanium compressor blades with PCD cutter, *Annals of the CIRP* 47 (1998) 61–64.

- [56] N. Corduan, T. Himbart, G. Poulachon, M. Dessoly, M. Lambertin, J. Vigneau and B. Payoux, Wear mechanisms of new tool materials for Ti-6Al-4V high performance machining, *CIRP Annals Manufacturing Technology* Vol. 52, No. 1 (2003) 73-76.
- [57] T. Hidehiko and M. Ryozi, Study on machinability of pure titanium, *Journal of JSPE* 28-6 (1962) 331-339.
- [58] R. Komanduri and W. R. Reed, Evaluation of carbide grades and a new cutting geometry for machining titanium alloys, *Wear* 92 (1983) 113-123.
- [59] R. Komanduri and B.F. Von Turkovich, New observations on the mechanism of chip formation when machining titanium alloys, *Wear* 69 (1981) 179–188.
- [60] R. Komanduri, Some clarifications on the mechanics of the chip formation when machining titanium alloys, *Wear* 76 (1982) 12–34.
- [61] S. Sun, M. Brandt and M.S. Dargusch, Characteristics of cutting forces and chip formation in machining of titanium alloys, *International Journal of Machine Tools and Manufacture*, Vol. 49, No. 7-8 (2009) 561-568.
- [62] J. Barry, G. Byrne and D. Lennon, Observations on chip formation and acoustic emission in machining Ti–6Al–4V alloy, *International Journal of Machine Tools and Manufacture* 41 (2001) 1055–1070.

- [63] A.E. Bayoumi and J.Q. Xie, Some metallurgical aspects of chip formation in cutting Ti6Al4V alloy, *Materials Science and Engineering* 190 (1995) 173-180.
- [64] J.D.P. Velásquez, B. Bolle, P. Chevrier, G. Geandier and A. Tidu, Metallurgical study on chips obtained by high speed machining of a Ti6Al4V alloy, *Materials Science and Engineering* 452–453A (2007) 469–474.
- [65] A. Gente, H.W. Hoffmeister and C.J. Evans, Chip formation in machining Ti6Al4V at extremely high cutting speeds, *CIRP Annals - Manufacturing Technology* Vol. 50, No. 1 (2001) 49-52.
- [66] A.L. Mantle and D.K. Aspinwall, Tool life and workpiece surface roughness when high speed machining a gamma titanium aluminide, *Proceedings of the Fourth International Conference on Progress of Cutting and Grinding*, International Academic Publishers (1998) 89–94.
- [67] S. Sharif, A.S. Mohruni, M.Y. Noordin and V.C. Vencatesh, Optimization of surface roughness prediction model in end milling titanium alloy (Ti-6Al-4V), *Proceeding of ICOMAST* (2006) 55-59.
- [68] P.A. Dearnley and A.N. Grearson, Evaluation of principal wear mechanisms of cemented carbides and ceramics used for a machining titanium alloy IMI 318, *Materials Science and Technology* 2 (1986) 47–58.

- [69] P.D. Hartung and B.M. Kramer, Tool wear in titanium machining, *Annals of CIRP* 32 (1) (1982) 75–80.
- [70] W. Min and Z. Youzhen, Diffusion wear in milling titanium alloys, *Materials and Science Technology* 4 (1988) 548–553.
- [71] F. Nabhani, Wear mechanism of ultra-hard cutting tool materials, *Journal of Materials Processing Technology* 115 (2001) 402–412.
- [72] A. Jawaid and C.H. Che-Haron, Tool wear in machining of titanium alloy Ti–6Al–4V, *Proceedings of the Advances in Materials and Processing Technologies (AMPT 97)* (1997) 562–568.
- [73] D.A.S. Macdougall and J. Harding, A constitutive relation and failure criterion for Ti6Al4V alloy at impact rates of strain, *Journal of the Mechanics and Physics of Solids* 47 (1999) 1157–1185.
- [74] W.S. Lee and C.F. Lin, High-temperature deformation behaviour of Ti6Al4V alloy evaluated by high strain-rate compression tests, *Journal of Materials Processing Technology* 75 (1998) 127–136.
- [75] Z.G. Wang, M. Rahman, Y.S. Wong and X.P. Li, A hybrid cutting force model for high-speed milling of titanium alloys, *CIRP Annals Manufacturing Technology* Vol. 54, No. 1 (2005) 71–74.

- [76] T. Ozel, Investigation of high speed flat end milling process: prediction of chip formation, cutting forces, tool stresses and temperatures, PhD. Thesis, The Ohio State University (1998).
- [77] T. Ozel and T. Altan, Process simulation using finite element method-prediction of cutting forces, tool stresses and temperatures in high-speed flat end milling, *International Journal of Machine Tools and Manufacture* 40/5 (2000) 713–738.
- [78] W.S. Lee and C.F. Lin, High-temperature deformation behaviour of Ti6Al4V alloy evaluated by high strain-rate compression tests, *Journal of Materials Processing Technology* 75 (1-3) (1998) 127–136.
- [79] P. Follansbee and G.T. Gray, An analysis of the low temperature low- and high-strain rate deformation of Ti–6Al–4V, *Metallurgical Transactions* 20A (1989) 863–874.
- [80] Z.G. Wang, Y.S. Wong and M. Rahman, High-speed milling of titanium alloys using binderless CBN tools, *International Journal of Machine Tools and Manufacture* Vol. 45 (2005) 105-114.
- [81] H. Schulz and T. Moriwaki, High speed machining. *Annals of CIRP* 41/2 (1992) 637–643.

- [82] S. Lei and W. Liu, High-speed machining of titanium alloys using the driven rotary tool, *International Journal of Machine Tools and Manufacture* Vol. 42, No. 6 (2002) 653-661.
- [83] B.M. Kramer, On tool materials for high speed machining, *Journal of Engineering for Industry* 109 (1987) 87–91.
- [84] M. Rahman, Z.G. Wang and Y.S. Wong, A review on high-speed machining of titanium alloys, *JSME International Journal Series C*, Vol. 49 No. 1 Special Issue on Advanced Manufacturing Technology (2006) 11-20.
- [85] G. Sutter, A. Molinari, L. Faure, J.R. Klepaczko and D. Dudzinski, An experimental study of high speed orthogonal cutting. *International Journal of Manufacturing Science and Engineering (Transaction of ASME)* 12 (1998) 169-176.
- [86] Y. Tanaka, H. Tsuwa and M. Kitano, Cutting mechanism in ultra-high speed machining, *ASME paper No. 67* (1967) 14.
- [87] P.J. Arrazola, F. Meslin and S. Marya, Serrated chip prediction in numerical cutting models, *Proceedings of the CIRP Congress 8 WMMO* (2005) 115-122.
- [88] M. Calamaz, D. Coupard and F. Girot, A new material model for 2D numerical simulation of serrated chip formation when machining titanium

alloy Ti-6Al-4V, *International Journal of Machine Tools and Manufacture* 48 (2008) 275–288.

[89] D. Umbrello, Finite element simulation of conventional and high speed machining of Ti6Al4V alloy, *Journal of Materials Processing Technology* 196 (2008) 79–87.

[90] J.S. Strenkowski and J.C. Lin, An analytical finite element model for predicting three-dimensional tool forces and chip flow, *Manufacturing Science and Engineering, ASME, MED*, 4 (1996) 273–280.

[91] T. Özel and T. Altan, Modeling of high speed machining processes for predicted tool forces stresses and temperatures using FEM simulations. In: *Proceedings of the CIRP International Workshop on Modeling of Machining Operations*, Atlanta, GA (1998) 225–234.

[92] T. Obikawa and E. Usui, Computational machining of titanium alloy—finite element modeling and a few results, *Journal of Manufacturing Science and Engineering (Transactions of the ASME)* 118 (1996) 208–215.

[93] M. Baker, J. Rösler and C. Siemers, A finite element model of high speed metal cutting with adiabatic shearing, *Computers and Structures* 80 (5,6) (2002) 495–513.

- [94] P.J. Arrazola, D. Ugarte, J.A. Villar, S. Marya, Finite element modelling: a qualitative tool to study high speed machining, in: Fifth International Conference on High Speed Machining (HSM) (2006) 239–246.
- [95] S.Y. Hong, I. Markus and W. Jeong, New cooling approach and tool life improvement in cryogenic machining of Ti–6Al–4V, International Journal of Machine Tools and Manufacture 41 (2001) 2245–2260.
- [96] F. Klocke, W. König and K. Gerschwiler, Advanced machining of titanium and nickel-base alloys, in: Advanced Manufacturing Systems and Technology, CISM Courses and Lecture No. 372, Springer, Wien, (1996) 7–21.
- [97] A. Ikuta, K. Shinozaki, H. Masuda, Y. Tamame, H. Kuroki and Y. Fukaya, Consideration of the adhesion mechanism of Ti alloys using cemented carbide during the cutting process, Journal of Materials. Processing 127 (2002) 251–255.
- [98] N.J. Churi, Z.J. Pei and C. Treadwell, Rotary ultrasonic machining of titanium alloy: effects of machining variables, Machining Science and Technology 10 (2006) 301–321.
- [99] A. R. Machado and J. Wallbank, The effects of a high-pressure coolant jet on machining, Proceeding of the Institution of Mechanical Engineers, Part B: Journal of Engineering Manufacture 208 (1994) 29–38.

- [100] C. H. Che-Haron, Tool life and surface integrity in turning titanium alloy, *Journal of Material Processing Technology*, Vol. 118 (2001) 231-237.
- [101] N. Narutaki and A. Murakoshi, Study on machining of titanium alloys, *Annals CIRP* 32 (1) (1983) 65.
- [102] P.D. Hartung, B.M. Kramer, Tool wear in titanium machining, *Annals CIRP* 31 (1) (1982) 75.
- [103] X. Yang and C.R. Liu, machining titanium and its alloys, *Machining Science and Technology*, 3(1) (1999) 107-139.
- [104] E.O. Ezugwu, High speed machining of aero-engine alloys, *Journal of the Brazilian Society of Mechanical Sciences and Engineering* 26 (1) (2004).
- [105] N. Zlatin and M. Field, Procedures and precautions in machining titanium alloys, in: *Titanium Science and Technology. Proceedings of the 2nd International Conference*, (1972) 489-504.
- [106] H. Dong, *Surface engineering of light alloys: aluminum, magnesium and titanium alloys*, Woodhead Publishing, Oxford, UK (2010).
- [107] Pedro N. Sanchez, *Titanium alloys: preparation, properties, and applications*, Nova Science Publishers, New York (2010).

- [108] C. Leyens and M. Peters, Titanium and titanium alloys: fundamentals and applications, Weinheim: Wiley-VCH (2003).
- [109] M. J. Donachie. Titanium - A Technical Guide, 2nd Edition, ASM International, Ohio (2004).
- [110] E.O. Ezugwu and Z.M. Wang, Titanium alloys and their machinability – a review, Journal of Material Processing Technology, Vol. 68 (1997) 262-274.
- [111] K. Iwata, K. Osakada and Y. Terasaka, Process modeling of orthogonal cutting by the rigid-plastic finite element method, Journal of Engineering Materials Technology 106 (1984) 132-138.
- [112] J. Strenkowski, and J. Carroll, A finite element model of orthogonal metal cutting, Journal of Engineering for Industry 107 (1985) 347-354.
- [113] J.T Black, On the fundamental mechanism of large deformation: Electron microscopy of metal cutting chips, Journal of Engineering for Industry (1971) 507-526.
- [114] SandvikCoromant, Milling developments improve titanium machining. <<http://www.myyellowcoat.com/featured-articles/milling-titanium-machining/>>, 2011 (accessed 16th April 2011).

- [115] RTI International, Machining Titanium, <<http://rtiintl.com/machining-titanium.html>>, 2009 (accessed 3rd September 2010).
- [116] Supra Alloys Inc, technical information: increased productivity by special techniques, <<http://www.supraalloys.com/technical2.php>>, 2011 (accessed 12th December 2010).
- [117] AgieCharmilles, Don't let machining titanium become 'hard' work, <<http://www.gfac.com/uk/news-detail/article/dont-let-machining-titanium-become-hard-work.html?cHash=93892315c4ada525db5a5311a0616688>>, 2011 (accessed 5 July 2011).
- [118] American Machinist, Cool Tips for Cutting Titanium, <<http://www.americanmachinist.com/304/Issue/Article/False/77297/>>, 2007 (accessed 3 September 2010).
- [119] K.F. Ehmann, S.G. Kapoor, R.E. Devor and I. Lazoglu, Machining process modelling: a review, *Journal Manufacturing Science Engineering* 119 (1997) 655-663.
- [120] C.A. Van Luttervelt, T. Childs, I.S. Jawahir, F. Klocke and P.K. Venuvinod, Present situation and future trends in modelling of machining operations, Progress report of the CIRP working group 'modelling of machining operations'. *CIRP Ann* 48(2) (1998) 587-626.

- [121] Y. Jusheng and Y. Nan, A brief review of FEM software technique, *Advances in Engineering Software* 17(1993) 195-200.
- [122] T.D. Marusich, M. Ortiz, Modeling and simulation of high-speed machining, *International Journal for Numerical Methods in Engineering* 38(21) (1995) 3675–3694.
- [123] T.D. Marusich, S. Usui and K.J. Marusich, Finite element modelling of part distortion, *Intelligent Robotics and Applications, Lecture Notes in Computer Science* Vol. 5315 (2008) 329-338.
- [124] J.Q. Xie, A.E. Bayoumi and H.M. Zbib, FEA modelling and simulation of shear localized chip formation in metal cutting, *Journal of Materials Processing Technology* 38 (1998) 1067-1087.
- [125] C. Shet, Finite element analysis of the orthogonal metal cutting process, *Journal of Materials Processing Technology* 105 (2000) 95-109.
- [126] I.S Jawahir, An intermediary level short course on machining process modelling and optimization for improved productivity, *Machining Research Laboratory Center for Manufacturing, Department of Mechanical Engineering Lexington, USA, (2008).*

- [127] E. Ceretti, P. Fallböhmer, W.T. Wu and T. Altan, Application of 2-D FEM to chip formation in orthogonal cutting, *Journal of Materials Processing Technology* 59 (1996) 169-181.
- [128] E. Ceretti, M. Lucchi, and T. Altan, FEM simulation orthogonal cutting: serrated chip formation, *Journal of Materials Processing Technology* 95 (1999) 17-26.
- [129] T. Özel and T. Altan, Process simulation using finite element method prediction of cutting forces, tool stresses and temperatures in high-speed flat end milling process, *International Journal of Machine Tools and Manufacture* 40/5 (2000) 713-738.
- [130] T. Özel and T. Altan, Determination of workpiece flow stress and friction at the chip-tool contact for high-speed cutting, *International Journal of Machine Tools and Manufacture* 40/1 (2000) 133-152.
- [131] F. Klocke, H.W. Raedt and S. Hoppe, 2D-FEM simulation of the orthogonal high speed cutting process, *Machining Science and Technology* 5/3 (2001) 323-340.
- [132] A. Bareggi, G.E. O'Donnell and A. Torrance, Modelling thermal effects in machining by finite element methods, *Proceedings of the 24th International Manufacturing Conference Vol.1, Waterford* (2007) 263-272.

- [133] Y. B. Guo and C. R Liu, Mechanical properties of hardened AISI 52100 steel in hard machining processes, *ASME Journal of Manufacturing Science and Engineering* 124 (2002) 1-9.
- [134] Y. B. Guo and C. R Liu, 3D FEA modeling of hard turning, *Journal of Manufacturing Science and Engineering* 124 (2002) 189-199.
- [135] E. Ng and D.K. Aspinwall, Modeling of hard part machining, *Journal of Materials Processing Technology* 124 (2002) 1-8.
- [136] M. Baker, J. Rosler, and C. Siemers, A finite element model of high speed metal cutting with adiabatic shearing, *Computers & Structures* 80 (2002) 495-513.
- [137] L. Chuzhoy, R.E. DeVor, S.G. Kapoor, and D.J. Bammann, Microstructure-level modeling of ductile iron machining, *ASME Journal of Manufacturing Science and Engineering* 124 (2002) 162-169.
- [138] L. Chuzhoy, R.E. DeVor and S.G. Kapoor, Machining simulation of ductile iron and its constituents. Part 2: numerical simulation and experimental validation of machining, *ASME Journal of Manufacturing Science and Engineering* 125 (2003) 192-201.

- [139] A.H Adibi-Sedeh and V. Madhavan, Understanding of finite element analysis results under the framework of Oxley's machining model, 6th CIRP International Workshop on Modeling of Machining Operations (2003).
- [140] P.J. Arrazola, D. Ugarte, J. Montoya, A. Villar and S. Marya, Finite element modeling of chip formation process with Abaqus/Explicit 6.3, Proceedings of VII International Conference on Computational Plasticity (2005).
- [141] T. Mabrouki and J.F. Rigal, A contribution to a qualitative understanding of thermo-mechanical effects during chip formation in hard turning, Journal of Materials Processing Technology 176 (2006) 214–221.
- [142] A. Otieno and C. Mirman, Finite element analysis of cutting forces and temperatures on microtools in the micromachining of aluminum alloys, Proceedings of the IAJC-IJME International Conference (2008) 191.
- [143] R. Han and J. Wu, Finite element simulation of drilling based on Third Wave System Advantedge, Key Engineering Materials Vol. 431-432 (2010) 229-232.
- [144] T. D. Marusich, D.A. Stephenson, S. Usui and S. Lankalapalli, Modeling capabilities for part distortion management for machined components, <http://www.thirdwavesys.com/pdfs/tech/modeling_capabilities.pdf>, (access on 2 February 2010).

- [145] K. Kadirgama, M.M. Noor and M.M. Rahman, Finite element analysis and statistical method to determine temperature distribution on cutting tool in end-milling, *European Journal of Scientific Research* Vol.30 No.3 (2009) 451-463.
- [146] H. Xiao, W.G Wu and W.T Mei, Prediction of forces in micro-cutting and the study based simulation, *Key Engineering Materials* Vol. 467-469 (2011) 197-201.
- [147] J.D. Gardner, A. Vijayaraghavan and D.A. Dornfeld, Comparative study of finite element simulation software, eScholarship Repository, University of California, Copyright c 2005 by the authors.
- [148] DEFORM-3D V6.0 User's Manual, Scientific Forming Technologies Corporation.
- [149] J. Huang and J. Black, Evaluation of chip separation criteria for the fem simulation of machining, *ASME Transactions, Journal of Manufacturing Science and Engineering* Vol. 118 (1996) 545-554.
- [150] Y.B. Guo and D.A. Dornfeld, Finite element modeling of burr formation in drilling 304 stainless steel, *Transaction of the ASME, Journal of Manufacturing Science and Engineering* Vol. 122 (2000) 612-619.

- [151] J. S. Przemieniecki, Finite element structural analysis: new concepts, Reston, VA: American Institute of Aeronautics and Astronautics (2009).
- [152] T. O'Donovan, Fluid flow and heat transfer of an impinging air jet, PhD. Thesis, Mechanical & Manufacturing Engineering, Trinity College Dublin, (2005).
- [153] T. Ozel, I. Llanos, J. Soriano and J. Arrazola, 3D finite element modelling of chip formation process for machining inconel 718: comparison of FE software predictions, *Machining Science and Technology* 15 (2007) 21-46.
- [154] T. Ozel and E. Zeren, Finite element modelling the influence of edge roundness on the stress and temperature fields induced by high speed machining, *International Journal of Advanced Manufacturing Technology* 35 (2007) 255-267.
- [155] N.A. Abukhshim, P.T. Mativenga and M.A. Sheikh, Heat generation and temperature prediction in metal cutting: A review and implications for high speed machining, *International Journal of Machine Tools and Manufacture* 46 (2006) 782–800.
- [156] J.S. Tsai and C.L. Liao, Finite-element modeling of static surface errors in the peripheral milling of thin-walled workpieces, *Journal of Materials Processing Technology* 94 (1999) 235-246.

- [157] E. Budak and Y. Altintas, Peripheral milling conditions for improved dimensional accuracy, *International Journal of Machine Tools and Manufacture* 34 (1994) 907-918.
- [158] H.Z. Li, W.B. Zhang and X.P. Li, Modelling of cutting forces in helical end milling using a predictive machining theory, *International Journal of Mechanical Sciences* 43 (2001) 1711-1730.
- [159] E. Budak, Analytical models for high performance milling. Part 1: Cutting forces, structural deformations and tolerance integrity, *International Journal of Machine Tools and Manufacture* 46 (2006) 1478-1488.
- [160] M. Wan, W.H. Zhang, G. Tan and G.H. Qin, New cutting force modelling approach for flat end mill, *Chinese J. of Aeronautics* 20 (2007) 282-288.
- [161] J.W. Sutherland and R.E. DeVor, An improved method for cutting force and surface error prediction in flexible end milling system, *ASME Journal of Engineering for Industry* 108 (1986) 269-279.
- [162] D. Montgomery and Y. Altintas, Mechanism of cutting force and surface generation in dynamic milling, *ASME Journal of Engineering for Industry* 113 (1991) 160-168.

- [163] D. Spence and Y. Altintas, A solid modeller based milling simulation and process planning system, *ASME Journal of Engineering for Industry* 116 (1994) 61–69.
- [164] L. Zheng, Y. Chiou and S.Y. Liang, Three dimensional cutting force analysis in end mill, *International Journal of Mechanical Sciences* 38 (1996) 259–269.
- [165] M.E. Merchant, Mechanics of the metal cutting process, *Journal of Applied Physics* 16 (1945) 267–275.
- [166] E.J.A. Armarego and N.D. Deshpande, Force prediction models and CAD/CAM software for helical tooth milling processes. III. End-milling and slot operations, *International Journal of Product Research* 32 7 (1994) 1715-1738.
- [167] E.J.A. Armarego and N.D. Deshpande, Computerized predictive cutting models for forces in end milling including eccentricity effects, *Annals of CIRP* 38/1 (1989) 45–49.
- [168] E. Budak, Mechanics and dynamics of milling thin walled structures, PhD. thesis, University of British Columbia, (1994).

- [169] S. Smith and J. Tlustý, An overview of the modelling and simulation of the milling process, *ASME Journal of Engineering for Industry* 113 (1991) 169-175.
- [170] W.A. Kline, R.E. DeVor and J.R. Undberg, The prediction of cutting forces in end milling with application to cornering cut, *International Journal of Machine Tool Design and Research* 22 (1982) 7–22.
- [171] W. Skarka, Application of MOKA methodology in generative model creation using CATIA, *Engineering Applications of Artificial Intelligence*, Vol. 20 No. 5 (2007) 677-690.
- [172] G. Maria, P. Martinez and O. Francisco, Task automation for modelling solids with CATIA V5, *International Journal Aircraft Engineering and Aerospace Tech*, Vol. 79 (2007) 53-59.
- [173] PediaView.com, Regression Analysis, <http://pediaview.com/openpedia/Regression_analysis> (Access on 12th December 2010).
- [174] A. J. P. Sabberwal, Chip section and cutting force during the milling operation, *ANNALS of the CIRP* 10 (1961)197-203.

- [175] J. Tlustý and P. MacNeil, Dynamics of cutting forces in end milling, *ANNALS of the CIRP* 24 (1975) 21-25.
- [176] W.J. Endres, R.E. Devor and S.G. Kapoor, A dual-mechanism approach to the prediction of machining forces: Part 1 Model development and calibration. *Manufacturing Science and Engineering, ASME PED* 64 (1993) 563–576.
- [177] S.G. Kapoor, R.E. DeVor, R. Zhu, R. Gajjela, G. Parakkal and D. Smithey, Development of mechanistic models for the prediction of machining performance: model building methodology, *Machining Science and Technology* 2 (1998) 213–238.
- [178] B. Edes, Helical tool geometry in stability predictions and dynamic modelling of milling, Master's thesis, University of Missouri Columbia, 2007.
- [179] E. Budak, Y. Altintas and E.J.A. Armarego, Prediction of milling force coefficients from orthogonal cutting data, *Trans. ASME Journal of Manufacturing Science and Engineering* 118 (1996) 216–224.
- [180] T. L. Schmitz and K. S. Smith, 'Milling dynamics' *Machining Dynamics*, Springer Science & Business Media, NY, USA (2009).
- [181] E. Abele and B. Frohlich, High speed milling of titanium alloys. *Journal Advances in Production Engineering and Management* 3 (2008) 131-140.

- [182] X. W. Liu, K. Cheng, D. Webb and X. C. Luo, Prediction of cutting force distribution and its influence on dimensional accuracy in peripheral milling, *International Journal of Machine Tools Manufacture* 42 (2002) 791-800.
- [183] A. S. Antonialli, A. E. Diniz and R. Pederiva, Vibration analysis of cutting force in titanium alloy milling. *International Journal of Machine Tools Manufacture* 50 (2010) 65-74.
- [184] R. Izamshah R.A, John P.T Mo and Songlin D, Finite element analysis of machining thin-wall parts, *Journal of Key Engineering Materials* Vol. 458 (2011) 283-288.
- [185] D. W. Pepper and J. C. Heinrich, *The finite element method: basic concepts and applications*, Hemisphere Publ. Corp., USA (1992).
- [186] S. Shivaswamy, *Finite element analysis and programming: an introduction*, Alpha Science International Ltd. Oxford (2010).
- [187] M. R. Gosz, *The finite element method: applications in solids, structures and heat transfer*, Taylor and Francis, Florida (2006).
- [188] A. F. Bower, *Applied mechanics of solids*, Boca Raton, Fla.: CRC Press, (2010).

- [189] H. S. Valberg, Applied metal forming: including FEM analysis, Cambridge University Press, New York (2010).
- [190] S. S. RAO, The finite element method in engineering, Elsevier Science, Burlington (2010).
- [191] A. Berlioz and P. Trompette, Solid mechanics using the finite element method, Wiley London, Hoboken, NJ (2010).
- [192] J.S. Przemieniecki, Finite element structural analysis: new concepts, American Institute of Aeronautics and Astronautics, Reston, VA (2009).
- [193] MMSonline, Aerospace - Programming - Thin walls - Incremental pocketing, High speed machining electronic supplement, <<http://www.mmsonline.com/hsm/>> (Access on 12th December 2010).
- [194] S.N. Mukherjee and S.K. Basu, Multiple regression analysis in evaluation of tool wear, International Journal of Machine Tool Design and Research, Vol. 7 No. 1 (1967) 15-21.
- [195] A. Atkinson and M. Riani, Robust diagnostic regression analysis, Springer New York (2000).

- [196] R. Andersen, Modern methods for robust regression, Sage Publications, Los Angeles (2008).
- [197] D. C. Montgomery, E. A. Peck and G. Vining, Introduction to linear regression analysis, Wiley Interscience, N.J (2006).
- [198] P. J. Rousseeuw and A. M. Leroy, Robust regression and outlier detection, Wiley Interscience, N.J (2003).
- [199] N. R. Draper and H. Smith, Applied regression analysis, Wiley, New York (1998).
- [200] T. P. Ryan, Modern regression methods, Wiley, New York (1997).
- [201] W. A. Rosenkrantz, Introduction to probability and statistics for science, engineering, and finance, CRC Press, Boca Raton (2009).
- [202] I. Walker, Research methods and statistics, Palgrave, New York (2010).
- [203] J. Antony, Design of experiments for engineers and scientists [electronic resource], Butterworth-Heinemann Oxford (2003).

- [204] P. Depince and J. Y. Hascoet, Active integration of tool deflection effects in end milling. Part 1. Prediction of milled surface, *International Journal of Machine Tools and Manufacture* 46 (2006) 937–944.
- [205] P. Depince J. Y. Hascoet, Active integration of tool deflection effects in end milling. Part 2. Compensation of tool deflection, *International Journal of Machine Tools and Manufacture* 46 (2006) 945–956.
- [206] T. C. Bera, K. A. Desai and P. V. M. Rao, Error compensation in flexible end milling of tubular geometries, *Journal of Material Processing Technology*, Vol 211 (2011) 24-34.
- [207] *Electronic Machinery*, Factors affecting the precision machining <<http://www.iee.com.ru/factors-affecting-the-precision-machining>>, 2010 (accessed 10th May 2010).
- [208] D. A. Stephenson and J. S. Agapiou, *Metal cutting theory and practice*, CRC Taylor & Francis, 2nd ed., FL (2006).

Appendix

Appendix I

Chemical compositions of Ti-6Al-4V alloy (wt. %).

Chemistry	N	C	H	O	Fe	Al	V	Ti	Other elements
% w/w min.	-	-	-	-	-	5.50	3.50	-	-
% w/w max.	0.05	0.10	0.0125	0.20	0.30	6.75	4.50	Balance	0.40

Mechanical properties of Ti-6Al-4V alloy at room temperature.

Density	Young's modulus	Poisson ratio	Yield strength	Hardness	Elongation
[kg/m ³]	[GPa]		[MPa]	[HB]	[%]
4430	113.8	0.34	880	334	14

Cutting tool specification.

D	d	Ap	H	L	Flute	Ha°	Rd°	Shank	Ch
6.0	6.0	14.0	20.0	57.0	4	38.0	5.0	C	0.25x45